RECEIVED BY DTIE MAY 2? 1965

ALO-2661-12
AEC RESEARCH & DEVELOPMENT REPORT
UC-33, C-92A, C-92B (Composite)
TID-4500-48 Ed. and M-3679-48 Ed.

DEVELOPMENT OF 1800F-400F FIBROUS-TYPE INSULATION FOR RADIOISOTOPE POWER SYSTEMS

FINAL REPORT

REPORT NO. ALO-2661-12

LEGAL NOTICE

This report was prepared as an account of Government sponsored work. Neither the United States, nor the Commission, nor any person acting on behalf of the Commission:

A. Makes any warranty or representation, expressed or implied, with respect to the accuracy, completeness, or usefulness of the information contained in this report, or that the use of any information, apparatus, method, or process disclosed in this report may not infringe privately owned rights; or

B. Assumes any liabilities with respect to the use of, or for damages resulting from the use of any information, apparatus, method, or process disclosed in this report.

As used in the above, "person acting on behalf of the Commission" includes any employee or contractor of the Commission, or employee of such contractor, to the extent that such employee or contractor of the Commission, or employee of such contractor prepares, disseminates, or provides access to, any information pursuant to his employment or contract with the Commission, or his employment with such contractor.

by
J. O. Collins
K. L. Jaunarajs
D. R. Reid

JOHNS-MANVILLE RESEARCH & ENGINEERING CENTER
Manville, New Jersey

Prepared under
Contract AT(29-2)-2661

for the
Albuquerque Operations Office
U. S. ATOMIC ENERGY COMMISSION

DISCLAIMER

This report was prepared as an account of work sponsored by an agency of the United States Government. Neither the United States Government nor any agency Thereof, nor any of their employees, makes any warranty, express or implied, or assumes any legal liability or responsibility for the accuracy, completeness, or usefulness of any information, apparatus, product, or process disclosed, or represents that its use would not infringe privately owned rights. Reference herein to any specific commercial product, process, or service by trade name, trademark, manufacturer, or otherwise does not necessarily constitute or imply its endorsement, recommendation, or favoring by the United States Government or any agency thereof. The views and opinions of authors expressed herein do not necessarily state or reflect those of the United States Government or any agency thereof.

DISCLAIMER

Portions of this document may be illegible in electronic image products. Images are produced from the best available original document.

W. Kortier
Battelle Memorial Institute
505 King Avenue
Columbus, Ohio 43201 (1 cy)

J. Epstein
Goddard Space Flight Center
Greenbelt, Maryland (1 cy)

J. O. Collins
Johns-Manville Research &
Engineering Center
Post Office Box 159
Manville, New Jersey 08835 (2 cys)

W. DeWitt
Union Carbide Corporation
Linde Division
Post Office Box 44
Tonawanda, New York 14152 (2 cys)

R. Berlin, Manager
Technology Development
Radio Corporation of America
415 South Fifth Street
Building 18-2
Harrison, New Jersey 07029 (1 cy)

V. Trucillo
Jet Propulsion Laboratory
Pasadena, California (1 cy)

H. S. Potter, Chief
New York Patents Group
U. S. Atomic Energy Commission
Brookhaven Area Office
Upton, New York 11973 (1 cy)

J. Dunlay
Thermo Electron Engineering Corp.
Post Office Box 482
Waltham, Massachusetts 02154 (2 cys)

Harold Garber
NUMEC
609 North Warren Avenue
Apollo, Pennsylvania 15613 (1 cy)

U. S. Atomic Energy Commission
New York Operations Office
376 Hudson Street
New York, New York 10014
Attn: Reports Library (1 cy)

U. S. Atomic Energy Commission
Division of Technical Information
Extension
Post Office Box 62
Oak Ridge, Tennessee 37831 (3 cys &
1 reproductible copy)

H. Cameron
NASA/Lewis
Cleveland, Ohio (1 cy)

R. Poorman
NASA/Marshall Space Flight Center
Huntsville, Alabama (1 cy)

I. Jones
TRW Systems
Redondo Beach, California (1 cy)

ACKNOWLEDGEMENT

The author wishes to acknowledge the assistance, direction, and encouragement afforded him by P. A. O'Riordan and Major E. F. Redden of the Division of Space Nuclear Systems, AEC Germantown, and by D. L. Krenz, H. Gay and D. Mottern of Sandia Corporation, Albuquerque, during the performance of this contract.

ABSTRACT

by

J. O. Collins

This is the Final Report for AEC Contract Number AT(29-2)-2661 Mod #3 (formerly AT(30-1)-3633).

An extensive evaluation of submicron particles other than silica was undertaken to provide for a MIN-K product with long term service capability to 2200F. The mechanism of product failure at elevated temperatures was studied, and attempts were made to prevent or delay this failure.

A high density MIN-K formulation was developed and evaluated for 1400F service as a load-bearing insulation. The effect of product formulation on the thermal conductivity, modulus of elasticity, and load relaxation with time were the primary considerations.

GLASROCK 25 foam silica, a relatively low density, low thermal conductivity, high strength refractory was studied with the intent of adding opacifiers for further thermal efficiency. The primary areas of investigation included the effect of the opacifiers on the manufacturing procedure, strength, and thermal conductivity.

The thermal conductivity evaluation of the MIN-K formulations developed under Phase I of this Contract (Phase I Final Report No. ALO-3633-7) was completed.

TABLE OF CONTENTS

		Page
	LEGAL NOTICE	ii
	DISTRIBUTION	iii
	ABSTRACT	vi
I.	INTRODUCTION	1
II.	PHASE I, TASK 5 - DETAILED EVALUATION	3
	Introduction	3
	Exposure of the Thermal Conductivity Specimens	5
	Re-evaluation of the Thermal Conductivity Specimens	6
	Dynatech Thermal Conductivity Study	7
	Johns-Manville Thermal Conductivity Study	12
	Thermal Conductivity Results	13
	Summary of Results	15
	Analysis of Results	21
III.	PHASE II, TASK 2 - MATERIAL RESEARCH AND DEVELOPMENT	26
	Introduction	26
	Literature Survey on Sintering of Refractory Metallic Oxides	27
	Candidate Submicron Particles	38
	Thermal Stability and Thermal Conductivity	46
	Porosity and Pore Size Distribution	53
	Microstructure	65
	Shrinkage Inhibitors	84
IV.	TASK 3 - LOAD-BEARING INSULATION FOR 400 - 1800F SERVICE	113
	Introduction	113

TABLE OF CONTENTS (Cont'd)

Page

Subtask 3.1 - Load-Bearing Insulation for 400-1400F Service 113

Subtask 3.2 - Load-Bearing Insulation to 1800F 138

V. CONCLUSIONS 177

Phase I, Task 5 - Detailed Evaluation 177

Phase II, Task 2 - Material Research and Development 177

Phase II, Task 3 - Load-Bearing Insulation for 400-1800F Service. 178

Subtask 3.1 - Load-Bearing Insulations for 400 to 1400F Service. 178

Subtask 3.2 - Load-Bearing Insulations of Service up to 1800F 178

VI. REFERENCES 180

VII. APPENDIX A 185

APPENDIX B 187

LIST OF FIGURES

		Page
Figure 5-1.	Best Composite of Thermal Conductivity Data for MIN-K 1999, 2002, and 2020 Prior to Extended Thermal Exposure	4
Figure 5-2.	Thermal Conductivity of MIN-K 1999, 2002, and 2020 in Air After Extended Thermal Exposure	20
Figure 5-3.	Thermal Conductivity of MIN-K 2002 in Argon After Extended Thermal Exposure	22
Figure 5-4.	Apparent Thermal Conductivity of MIN-K 2002 and 2020 in Vacuum After Extended Thermal Exposure	23
Figure 2-1.	Migration of Grain Boundary by Atomic Diffusion	31
Figure 2-2.	Grain Growth and Secondary Recrystallization	32
Figure 2-3.	ALON-C Gamma - Mag: 27,500X	43
Figure 2-4.	ALON-C Alpha - Mag: 27,500X	44
Figure 2-5.	Schematic Diagram of High Temperature Vacuum Furnace	47A
Figure 2-6.	Cross-Section of Thermal Gradient Thermal Conductivity Apparatus	48
Figure 2-7.	MIN-K/ALON-C Gamma/TiO_2 Unfired Control Mag: 800X	54
Figure 2-8.	MIN-K/ALON-C Gamma/TiO_2 2000F for 5 hr in Air Mag: 800X	55
Figure 2-9.	MIN-K/ALON-C Gamma/TiO_2 2000F for 5 hr in Vacuum - Mag: 800X	56
Figure 2-10.	Total Porosity and Pore Size Distribution of MIN-K 1999	58
Figure 2-11.	Total Porosity and Pore Size Distribution of MIN-K/ALON-C Gamma/TiO_2 Formulation	59
Figure 2-12.	Pore Size Distribution and Total Porosity of Unfired ALON-C Specimens	60

LIST OF FIGURES (Cont'd)

Page

Figure 2-13. Pore Size and Total Porosity of MIN-K/ALON-C Alpha Specimens Exposed to 2000F for 5 hr 61

Figure 2-14. Pore Size and Total Porosity of MIN-K/ALON-C Gamma Specimens Exposed to 2000F for 5 hr 62

Figure 2-15. Pore Size and Total Porosity of MIN-K/ALON-C Alpha Specimens Exposed to 2200F for 5 hr 63

Figure 2-16. Pore Size and Total Porosity of MIN-K/ALON-C Gamma Specimens Exposed to 2200F for 5 hr 64

Figure 2-17. MIN-K/ALON-C Gamma/TiO_2 2000F for 5 hr in Vacuum Mag: 27,500X 66

Figure 2-18. MIN-K/CAB-O-SIL/TiO_2 (MIN-K 1999) Unfired Control - Mag: 800X 68

Figure 2-19. MIN-K/CAB-O-SIL/TiO_2 (MIN-K 1999) 2000F for 5 hr in Air - Mag: 800X 69

Figure 2-20. MIN-K/CAB-O-SIL/TiO_2 (MIN-K 1999) 2000F for 5 hr in Vacuum - Mag: 800X 70

Figure 2-21. MIN-K/ALON-C Gamma/TiO_2 Unfired Control Mag: 800X 71

Figure 2-22. MIN-K/ALON-C Gamma/TiO_2 2000F for 5 hr in Air Mag: 800X 72

Figure 2-23. MIN-K/ALON-C Gamma/TiO_2 2000F for 5 hr in Vacuum - Mag: 800X 73

Figure 2-24. MIN-K/CAB-O-SIL/TiO_2 (MIN-K 1999) Unfired Control - Mag: 27,500X 74

Figure 2-25. MIN-K/CAB-O-SIL/TiO_2 (MIN-K 1999) 2000F for 5 hr in Air - Mag: 27,500X 75

Figure 2-26. MIN-K/CAB-O-SIL/TiO_2 (MIN-K 1999) 2000F for 5 hr in Vacuum - Mag: 27,500X 76

Figure 2-27. MIN-K/ALON-C Gamma/TiO_2 Unfired Control Mag: 27,500X 77

Figure 2-28. MIN-K/ALON-C Gamma/TiO_2 2000F for 5 hr in Air - Mag: 27,500X 78

LIST OF FIGURES (Con'd)

Page

Figure 2-29. MIN-K/ALON-C Gamma/TiO_2 2000F for 5 hr in Vacuum - Mag: 27,500X^2 79

Figure 2-30. MIN-K/ALON-C Gamma Unfired Control Mag: 800X 80

Figure 2-31. MIN-K/ALON-C Gamma 2200F for 5 hr in Vacuum - Mag: 800X 81

Figure 2-32. MIN-K/ALON-C Alpha Unfired Control Mag: 800X 82

Figure 2-33. MIN-K/ALON-C Alpha 2200F for 5 hr in Air - Mag: 800X 83

Figure 2-34. Effect of Inhibitor Concentration on the Shrinkage of ALON-C Compositions 89

Figure 2-35. MIN-K/ALON-C Gamma/0.5 Mol % K_2CO_3 Following 2 hr at 2200F in Vacuum - Mag: 27,500X 97

Figure 2-36. MIN-K/ALON-C Gamma/5 Mol % K_2CO_3 Following 2 hr at 2200F in Vacuum - Mag: 27,500X 98

Figure 2-37. MIN-K Formulation 2041 After 2 hr in Vacuum @ 2200F 110

Figure 2-38. MIN-K Formulation 2041 After 168 hr in Vacuum at 2200F 111

Figure 3.1-1. Thermal Conductivity of MIN-K Formulations vs CAB-O-SIL M5 Density - 800F Mean Temperature 117

Figure 3.1-2. Thermal Conductivity of MIN-K Formulations vs TiO_2 Density 118

Figure 3.1-3. Effect of MIN-K Product Density and CAB-O-SIL M5 Density on Modulus of Elasticity 121

Figure 3.1-4. Typical Compression-Relaxation Apparatus 123

Figure 3.1-5. Stress-Strain Characteristics of MIN-K 2002 at 35 pcf 125

Figure 3.1-6. Effect of Constant Load on 35 pcf MIN-K 2002 at 1400F Hot Face 126

LIST OF FIGURES (Cont'd)

Page

Figure 3.1-7. Deflection vs Time for 35 pcf MIN-K 2002 Under Constant Loads - 1400F Hot Face. 129

Figure 3.1-8. Stress vs Time at Constant Deflection for Various Initial Loads - MIN-K 2002 at 35 pcf 1400F Hot Face 133

Figure 3.1-9. Load-Relaxation with Time for 35 pcf MIN-K 2002 - 1400F Hot Face 135

Figure 3.1-10. Thermal Conductivity of 35 pcf MIN-K 2002 in Air and Argon 136

Figure 3.2-1. Thermal Conductivity Versus SiO_2 Density of Glasrock at 15 Per Cent Opacification Level - Part 1 149

Figure 3.2-2. Thermal Conductivity - Product Density Relationship for Opacified and Unopacified Glasrock - Parts 1 and 2 161

Figure 3.2-3. Thermal Conductivity vs Silica Density for Opacified and Unopacified Glasrock - Parts 1 and 2 163

Figure 3.2-4. Thin Section of 10 Per Cent Titania Opacified Glasrock Having a Low Thermal Conductivity 164

Figure 3.2-5. Thin Section of 10 Per Cent Titania Opacified Glasrock Having a High Thermal Conductivity 165

Figure 3.2-6. Stress-Strain of Unopacified Glasrock at 25 and 30 pcf Density 170

Figure 3.2-7. Thermal Conductivity of Unopacified Glasrock 25 Silica Foam up to 1600F Mean Temperature 175

LIST OF TABLES

		Page
Table 5-1.	Effect of Specimen Edge Temperature On the Measured Thermal Conductivity of MIN-K 2002 in Air	8
Table 5-2.	Effect of Specimen Edge Temperature on the Measured Thermal Conductivity of MIN-K 2002 in Vacuum.	9
Table 5-3.	Effect of Specimen Edge Temperature on the Measured Thermal Conductivity of MIN-K 2020 in Air	10
Table 5-4.	Effect of Specimen Edge Temperature on the Measured Thermal Conductivity of 35 pcf Density MIN-K 2002 in Air	11
Table 5-5.	Thermal Conductivity in Air of MIN-K 1999 after 2000 hrs in Argon at 1000F	14
Table 5-6.	Thermal Conductivity of MIN-K 2002 in Air, Argon and Vacuum Following Extended Thermal Exposure	16
Table 5-7.	Thermal Conductivity of MIN-K 2002 in Air Following Extended Thermal Exposure.	17
Table 5-8.	Thermal Conductivity of MIN-K 2020 in Air and Vacuum Following Extended Thermal Exposure	18
Table 5-9.	Thermal Conductivity of MIN-K 2020 in Air After Extended Thermal Exposure in Air	19
Table 5-10.	Comparison of Predicted and Test Thermal Conductivity Values for MIN-K at 1100F Mean Temperature	25
Table 2-1.	Submicron Candidate Materials	40
Table 2-2.	Properties of ALON-C (Manufacturer's Data)	41
Table 2-3	Effect of Time and Temperature on the Conversion of ALON-C from Gamma to Alpha Form	45

LIST OF TABLES (Cont'd)

		Page
Table 2-4.	Thermal Stability and Thermal Conductivity of MIN-K Compositions	49
Table 2-5.	Additives and Their Effect on the Shrinkage of ALON-C Compositions	85
Table 2-6.	Shrinkage Inhibitors for ALON-C Compositions	86
Table 2-7.	Shrinkage Inhibitors for ALON-C Compositions Having Common Anion	87
Table 2-8.	Shrinkage Inhibitors for ALON-C Compositions Having Common Cation	88
Table 2-9.	Effect of Sizing Process on Inhibitor Particle Size	91
Table 2-10.	Summary of Variables in the Shrinkage Inhibitor Investigation	92
Table 2-11.	Results of Shrinkage Inhibitor Evaluation at 2200F in Air	93
Table 2-12.	Results of Shrinkage Inhibitor Evaluation at 2200F in Vacuum	94
Table 2-13.	Results of K_2CO_3 Shrinkage Inhibitor Evaluation at 2200F in Vacuum	96
Table 2-14.	Linear Shrinkage of MIN-K/ALON-C Containing Inhibitor and Opacifier After Exposure to 2200F (Isothermal)	100
Table 2-15.	Effect of Zirconia Content on Linear Shrinkage of MIN-K/ALON-C Gamma	101
Table 2-16.	MIN-K Formulation 2041	103
Table 2-17.	Linear Shrinkage of MIN-K Formulation 2041 in Air at 2200F Isothermal	104
Table 2-18.	Linear Shrinkage of MIN-K Formulation 2041 in Vacuum at 2200F Isothermal	105

LIST OF TABLES (Cont'd)

Page

Table 2-19. Linear Shrinkage of MIN-K Formulation 2041 at 2200F Following 400C Drying 107

Table 2-20. Estimated Linear Shrinkage of MIN-K Formulation 2041 in Air at 2200F Isothermal 108

Table 2-21. Qualitative X-Ray Diffraction Analysis of MIN-K Formulation 2041 Following 2200F Exposure 109

Table 3.1-1. MIN-K Formulations for High Density Thermal Conductivity Evaluations 115

Table 3.1-2. Thermal Conductivity and Partial Densities of High Density MIN-K Formulations 116

Table 3.1-3. Materials Evaluated for Modulus of Elasticity 120

Table 3.1-4. Equation Constants for each 35 pcf MIN-K 2002 Specimen Tested Under Constant Load and at 1400F Hot Face 128

Table 3.1-5. Maximum and Minimum Deflection Values for each Load Level at 10 and 10,000 hr 131

Table 3.1-6. Measured and Calculated Time Zero Intercepts (Deflections) MIN-K 2002 @ 35 pcf and 1400F Hot Face 132

Table 3.2-1. Particle Size Distribution of Candidate Opacifiers for Glasrock 25 Foamed Silica 140

Table 3.2-2. Particle Size Distribution of Candidate Opacifiers Presented in Terms of Optimum Size Range 141

Table 3.2-3. Density of Opacified Glasrock 25 Specimens - Part I 143

Table 3.2-4. Cold Crushing Strength of Opacified Glasrock 25 - Part I 144

Table 3.2-5. Thermal Stability of Opacified Glasrock 25 - Part I 145

LIST OF TABLES (Cont'd)

Page

Table 3.2-6. Chemical Analysis of Opacified Glasrock Specimens - Part 1 147

Table 3.2-7. Thermal Conductivity and Density of Opacified Glasrock Specimens - Part 1 148

Table 3.2-8. Permanent Set of Opacified Glasrock Specimens - Part 1 151

Table 3.2-9. Product Density of Opacified Glasrock Specimens - Part 2 153

Table 3.2-10. Cold Crushing Strength of Opacified Glasrock - Part 2 154

Table 3.2-11. Opacifier Content of Glasrock Specimens - Part 2 155

Table 3.2-12. Thermal Stability of Opacified Glasrock Specimens - Part 2 157

Table 3.2-13. Permanent Set of Opacified Glasrock Specimens - Part 2 158

Table 3.2-14. Thermal Conductivity and Density of All Opacified Glasrock Specimens - Parts 1 and 2 159

Table 3.2-15. Thermal Conductivity and Density of Unopacified Glasrock Specimens - Part 2 160

Table 3.2-16. Permanent Set of 25 and 30 pcf Unopacified Glasrock Silica Foam 168

Table 3.2-17. Moduli of Elasticity for Unopacified Glasrock Before and After Sustained 200 psi Loading 171

Table 3.2-18. Permanent Set of Unopacified Glasrock Specimens Following the Stress-Strain Evaluation 172

Table 3.2-19. Thermal Conductivity of Unopacified Glasrock as Determined by ASTM C-182. 174

I. INTRODUCTION

Phase I of Contract No. AT(29-2)-2661 (formerly AT(30-1)-3633) involved the development of MIN-K thermal insulations having minimum outgassing, and minimum chemical impurity characteristics. Other features of these insulations included a reduction in thermal conductivity, an improvement in machinability, and increased thermal stability over currently used insulations for radioisotope generators.

The objective of Phase II was to evaluate and develop non-metallic insulation technology for use in the 400F to 1800F temperature range for use in radioisotope power systems. In particular, a MIN-K insulation was to be investigated that could be used to extend the useful temperature range to 2200F. Also, insulations optimized for load-bearing service in the 400F to 1800F temperature range were to be developed.

To accomplish this objective, Johns-Manville conducted a program consisting of the following general areas of effort.

a. Perform a basic study of sintering phenomena in submicron silica particles and other similar systems.

b. Study materials other than silica which could be used to give the desirable physical structure of existing MIN-K products, but which would have higher temperature limits.

c. Determine the effect of additives, either surface or bulk, on the sintering of high temperature submicron particles such as pure oxides.

d. Formulate and evaluate base materials, opacifiers, and reinforcements found to be suitable for a MIN-K formulation in the 2200F temperature range.

e. Formulate and evaluate insulations consisting of base materials, opacifiers and reinforcements optimized for load-bearing in the 400F to 1800F temperature range.

In addition to the Phase II effort, thermal conductivity evaluations of the MIN-K products developed under Phase I were continued. These evaluations were made following 2000 hr of simulated service exposure to determine the effect of such exposure upon the efficiency of the insulations.

This document constitutes the Final Report for Contract No. AT(29-2)-2661. Specifically, it covers the Phase II effort initiated October 1967 and completed February 1969. Work previously conducted under this contract was reported in the Phase I Final Report (ALO-3633-7, dated October 2, 1967). Additionally, a portion of it constitutes the supplement referenced in the Phase I Final Report covering the thermal conductivity evaluations of the MIN-K products developed under Phase I.

II. PHASE I, TASK 5 - DETAILED EVALUATION

INTRODUCTION

Thermal Conductivity Program. The thermal conductivity program for MIN-K 1999, 2002, and 2020 which was initiated during Phase I of this contract was continued during Phase II (see Appendix A for formulations). The program may be summarized as follows:

MIN-K 1999 - Measure the thermal conductivity in air, argon, and vacuum at four mean temperatures between 500F and 1200F before and after a 2000-hr exposure to 1000F (isothermal) in 1 atm argon.

MIN-K 2002 - Measure the thermal conductivity in air, argon, and vacuum at four mean temperatures between 500F and 1200F before and after a 2000-hr exposure to 1200F (isothermal) in 1 atm argon.

MIN-K 2020 - Measure the thermal conductivity in air and vacuum at four mean temperatures between 500F and 1200F before and after a 2000-hr exposure to 1600F (isothermal) in vacuum ($< 2 \times 10^{-3}$ mm Hg). This program was subsequently modified so as to extend the upper mean temperature to 1600F (after exposure only).

Results Presented in Phase I Final Report. At the time the Phase I Final Report was issued [1], MIN-K 1999 and 2002 had been evaluated in air, argon, and vacuum ($< 10^{-4}$ mm Hg), and MIN-K 2020 in air, all tests being conducted prior to extended isothermal exposure. Although these results were presented individually for each product, the data were very close as anticipated. Figure 5-1 presents a composite set of curves for all three formulations, representing the best data available prior to extended exposure.

The average curve in air was considered to be correct since it included data from both the high temperature Guarded Hot Plate apparatus used for testing in various atmospheres, as well as the standard alundum Guarded Hot Plate unit both of which are designed and operated in accordance with ASTM C-177.

The argon data were thought to be slightly high (about 14 per cent) as compared with a theoretical analysis. However, this deviation of actual from theoretical (or theoretical from actual) was not considered serious.

(1) See Section VI References

FIGURE 5-1.

BEST COMPOSITE OF THERMAL CONDUCTIVITY
DATA FOR MIN-K 1999, 2002, AND 2020
PRIOR TO EXTENDED THERMAL EXPOSURE

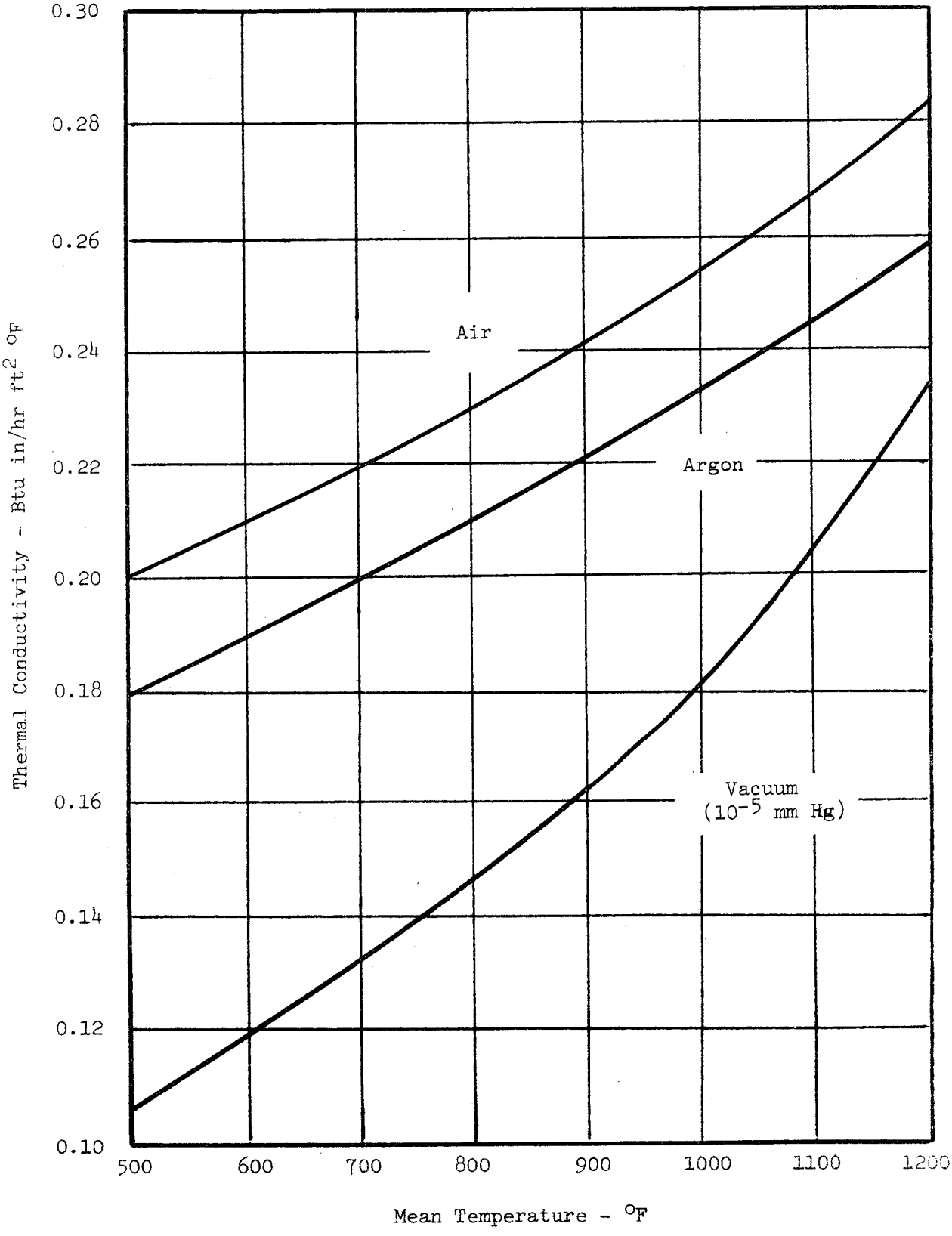

LEGAL NOTICE

This report was prepared as an account of Government sponsored work. Neither the United States, nor the Commission, nor any person acting on behalf of the Commission:

A. Makes any warranty or representation, expressed or implied, with respect to the accuracy, completeness, or usefulness of the information contained in this report, or that the use of any information, apparatus, method or process disclosed in this report may not infringe privately owned rights; or

B. Assumes any liabilities with respect to the use of, or for damages resulting from the use of any information, apparatus, method, or process disclosed in this report.

As used in the above "person acting on behalf of the Commission" includes any employee or contractor of the Commission, or employee of such contractor, to the extent that such employee or contractor of the Commission, or employee of such contractor prepares, disseminates, or provides access to, any information pursuant to his employment or contract with the Commission, or his employment or contract with the Commission, or his employment with such Contractor.

Printed in the United States of America
Available from
Clearinghouse for Federal Scientific and Technical Information
National Bureau of Standards, U. S. Department of Commerce
Springfield, Virginia 22151
Price: Printed Copy $3.00; Microfiche $0.65

DIRECT DISTRIBUTION

B. W. Colston, Director
Non-Weapons Activities Division
Albuquerque Operations Office
Post Office Box 5400
Albuquerque, New Mexico 87115 (2 cys)

G. J. Hildebrandt, Manager
Isotope Power Department
Department 9330
Sandia Corporation
Post Office Box 5800
Albuquerque, New Mexico 87115 (1 cy)

R. T. Carpenter, Chief
Isotopic Power Branch
Division of Space Nuclear Systems
U. S. Atomic Energy Commission
Washington, D. C. 20545 (1 cy)

S. J. Seiken
Division of Reactor Development & Technology
U. S. Atomic Energy Commission
Washington, D. C. 20545 (1 cy)

L. Sisler
Isotope Power Laboratory
Minnesota Mining & Manufacturing Co.
Space Center
2501 Walnut Street
Roseville, Minnesota 55119 (2 cys)

K. Dufrane
Isotopes Nuclear Division
Post Office Box 4937
Middle River, Maryland 21220 (1 cy)

A. Arker
General Electric Company
Missile & Space Development
Valley Forge Space Technology Center
Post Office Box 8555
Philadelphia, Pennsylvania 19101 (2 cys)

William Botts
Atomics International
Division of North American Aviation
Post Office Box 309
Canoga Park, California 91304 (2 cys)

P. Underhill, Project Manager
Large Milliwatt Program
Aeroject-General Nucleonics
Post Office Box 77
San Ramon, California (1 cy)

F. Hittman, General Manager
Hittman Associates, Inc.
4715 E. Wabash Avenue
Baltimore, Maryland 21215 (1 cy)

Zane Ardery
Union Carbide Corporation
Post Office Box Y
Department 27
Building 9202
Oak Ridge, Tennessee 37830 (1 cy)

J. Kenney, Program Manager
Compact Thermoelectric Converter
Westinghouse Electric Corporation
Post Office Box 10864
Pittsburgh, Pennsylvania 15213 (1 cy)

The vacuum data were considerably higher than anticipated, however, at the higher mean temperatures. The concern was the apparent tendency of the vacuum data to cross the air or argon data if the average rates of conductivity increase with temperature were extrapolated beyond 1200F mean temperature. This concern was deepened when two measured values in vacuum actually were higher than the air value at 1200F mean temperature, although these points were discarded when the final average vacuum curve was drawn,as shown in Figure 5-1.

This portion of the Phase II Final Report constitutes the supplement referenced in the Phase I Final Report. It covers the evaluation of the three products following their exposure to simulated service conditions, as well as a cursory evaluation of the thermal conductivity testing technique at elevated temperatures which has a significant effect upon the measured conductivity value.

EXPOSURE OF THE THERMAL CONDUCTIVITY SPECIMENS

The prolonged thermal exposure of the thermal conductivity specimens was conducted in 10" diameter ceramic tubes mounted vertically into 3 x 3 x 3 ft furnaces. The tubes extended about 12 in. above the top of the furnaces to permit the use of the Viton gasket sealing system associated with the vacuum equipment. A schematic diagram may be found in the Phase I Final Report, Figure 1 of Appendix A (Volume 2)[1]. The specimens were laid horizontally in the bottom of the tubes supported from the bottom and separated from each other by prefired ceramic furnace furniture. Temperature measurement and control was accomplished with couples placed directly opposite the specimens, but external to the tubes.

MIN-K 1999 was subjected to 2000 hr of isothermal heating between 993F and 998F in an atmosphere of argon which varied in pressure from 15.5 psia to 15.9 psia. (A slight positive pressure was maintained on the system to reduce diffusion of atmospheric gases into the system.) The specimens were subjected to a rigorous schedule of evacuation and argon backfill cycles at various temperature levels. At 400F, the chamber was actively evacuated to less than 2 microns for 24 hr, followed by an argon backfill to approximately 760 mm Hg. Two more short-term evacuation ($<$ 5 microns) and backfull cycles completed the 400F preconditioning. The system was heated to 600F in argon, and the evacuation and backfill cycles repeated (one 24-hr evacuation, plus two short-term evacuations). At 1000F, three more short cycles were conducted, for a total evacuation time of 15 min. The system was then pressurized to 15.5 - 16 psia argon during the last backfill and maintained at this pressure for the balance of the test.

MIN-K 2002 was subjected to 2004 hr of isothermal heating between 1197F and 1204F in an atmosphere of argon which also varied between 15.5 psia and 15.9 psia. These specimens were also subjected to the same evacuation and argon backfill cycles as the MIN-K 1999 specimens. However, following the final argon backfill at 1000F, the temperature was increased to 1200F, and the pressure adjusted accordingly.

DYNATECH THERMAL CONDUCTIVITY STUDY

Although it was not the purpose of this contract to study the test techniques for high temperature (800F-1800F mean temperatures) Guarded Hot Plate thermal conductivity measurements, the varying sets of data generated by these measurements under "similar" test conditions dictated that some investigation be initiated to determine their cause. As a result, Dynatech undertook the investigation described in the succeeding paragraphs at the same time as they were obtaining data on the MIN-K products.

Some years ago it was proposed, from theoretical considerations, that while testing at low to moderate mean temperatures in the Guarded Hot Plate, the temperature at the edge of the test specimen midway between its hot and cold face should not deviate greatly from the arithmetic mean temperature of the specimen. Specifically, it was concluded that:

$$\frac{T_M - T_E}{\Delta T} \leq 0.2 \qquad 1$$

where T_M = mean temperature

T_E = edge temperature of specimen midway between its hot and cold faces

ΔT = temperature drop across the specimen

This function has always been considered a reasonable criterion for test accuracy, although neither its experimental determination nor the monitoring of the edge temperature was ever required by the ASTM test procedure. To study this effect, Dynatech placed several thermocouples on the edge of the test specimens to monitor this edge temperature function. To change the function, the temperature of the heated guard ring surrounding the main stack was raised or lowered. This guard ring is a cylindrical heater which is approximately four inches larger in diameter than the main stack, and as tall as the stack. Standard operating procedure was to maintain the ring heater at the calculated mean temperature of the specimens.

A purposely abbreviated study by Dynatech Corp. of the effect of the edge temperature function upon the calculated thermal conductivity resulted in the relationships shown in Tables 5-1, 5-2, 5-3, and 5-4. It became evident that: the edge temperature function (formula #1) must be maintained at about 0.02 rather than 0.2, a deviation from this value would result in a large error in

TABLE 5-1.

EFFECT OF SPECIMEN EDGE TEMPERATURE
ON THE MEASURED THERMAL CONDUCTIVITY OF
MIN-K 2002 IN AIR

Mean Temperature = 1200F
Atmosphere = Air at 760 mm Hg.

$\frac{T_M - T_E}{\Delta T}$	Measured Thermal Conductivity Btu in/hr ft^2 °F
+ 0.464	0.373
+ 0.315	0.353
+ 0.047	0.265
+ 0.032	0.275

TABLE 5-1.

EFFECT OF SPECIMEN EDGE TEMPERATURE
ON THE MEASURED THERMAL CONDUCTIVITY OF
MIN-K 2002 IN AIR

Mean Temperature = 1200F
Atmosphere = Air at 760 mm Hg.

$\frac{T_M - T_E}{\Delta T}$	Measured Thermal Conductivity Btu in/hr ft^2 ^oF
+ 0.464	0.373
+ 0.315	0.353
+ 0.047	0.265
+ 0.032	0.275

TABLE 5-2.

EFFECT OF SPECIMEN EDGE TEMPERATURE
ON THE MEASURED THERMAL CONDUCTIVITY
OF MIN-K 2002 IN VACUUM

Mean Temperature = 1200F
Atmosphere = Vacuum ($< 10^{-5}$ torr)

$\frac{T_M - T_E}{\Delta T}$	Measured Thermal Conductivity Btu in/hr ft^2 ^oF
+ 0.020	0.284
+ 0.030	0.293
+ 0.075	0.321
+ 0.083	0.313

TABLE 5-3.

EFFECT OF SPECIMEN EDGE TEMPERATURE
ON THE MEASURED THERMAL CONDUCTIVITY
OF MIN-K 2020 IN AIR

Mean Temperature = 500F
Atmosphere = Air at 760 mm Hg.

$\frac{T_M - T_E}{\Delta T}$	Measured Thermal Conductivity Btu in/hr ft^2 ^oF
- 0.020	0.218
+ 0.030	0.216
+ 0.170	0.222
+ 0.440	0.230

TABLE 5-4.

EFFECT OF SPECIMEN EDGE TEMPERATURE ON THE MEASURED THERMAL CONDUCTIVITY OF 35 PCF DENSITY MIN-K 2002* IN AIR

Mean Temperature = 1200F
Atmosphere = Air at 760 mm Hg.

$\frac{T_M - T_E}{\Delta T}$	Measured Thermal Conductivity Btu in/hr ft^2 ^oF
- 0.085	0.374
+ 0.087	0.408
+ 0.284	0.440

* See Section IV, this report for Product Details

the calculated thermal conductivity, and the error was magnified by elevated mean temperatures and reduced thermal conductivity conditions (such as vacuum).

Since the ASTM Guarded Hot Plate C-177 test method was conducted with a temperature drop of about 200F across the 1" thick specimen, it is easily seen that an edge temperature function of 0.02 requires that the difference between the calculated mean temperature and the edge temperature be 4F. During this brief investigation, it has been assumed that the edge thermocouple was placed midway between the two faces of the specimen. However, every 0.005" displacement from this midpoint represented a 1°F error. Thus, even with normal care, a 2 to 3°F error would not be unexpected due to placement error. Similarly, it has been assumed that the calculated mean temperature of the specimen also fell midway between its two faces. However, a similar magnitude of error could also exist here. Consequently, a stacking of errors to their worst condition would result in an edge temperature function of 0.05 rather than 0.02. With normal materials, this may not present a problem. With MIN-K, in vacuum, at high mean temperatures, it could result in a significant measurement error.

JOHNS-MANVILLE THERMAL CONDUCTIVITY STUDY

Work was subsequently started at Johns-Manville to evaluate this problem in depth. The program was just initiated, however, prior to the conclusion of effort under the contract, and consequently no definitive results were obtained. (The program is continuing under Johns-Manville sponsorship.) However, the program is utilizing 4 - 1/2" specimens rather than 2 - 1" specimens. These specimens have been ground flat to accurately known (and equal) dimensions. Thermocouples were placed at the interface. A small, thin platinum foil tab was attached to the edge of the thermocouple bead used to measure the edge temperature. This tab was inserted between the two adjacent 1/2-in. thick specimens.

The first test point at about 560F mean temperature indicated that the midpoint of the top set of specimens (interface between the two 1/2" thick specimens) was 6°F hotter than the calculated mean temperature. Similarly, the edge temperature was 5°F cooler than the center temperature for the upper specimens. The interface of the lower specimens was also 6°F hotter than the calculated mean temperature, but the edge temperature of these specimens was 28°F cooler than the center temperature. The disparity between the two different edge temperature measurements was tentatively attributed to the design and placement of certain support rods within the unit. Thus, it became evident that factors which previously had been discounted or even unknown were significantly affecting the measurements. As noted above, this first set of data was taken at 560F mean temperature. The disparity is expected to increase as the test temperatures are increased.

The data presented herein with respect to the edge temperature function are tentative, and serve only to point out that a definite probelm in the measurement of low conductivity materials at elevated temperatures does exist, and further work on the problem must be conducted by qualified laboratories. The edge temperature function could have been the cause for the erratic data obtained by Johns-Manville and discussed earlier in this section.

THERMAL CONDUCTIVITY RESULTS

MIN-K 1999. Following their exposure to 1000F in argon for 2000 hrs., the MIN-K 1999 specimens (2 - 9" diameter x 1" thick) were placed in a Guarded Hot Plate unit (without special atmosphere capability) for re-evaluation in air. Only one point was obtained before a combination of water pump, heater cutoff, and emergency cooling water failures resulted in a water line leak and subsequent soaking of the samples. The samples were dried to constant weight at 800F and retested, although a significant loss in thermal efficiency was anticipated. Table 5-5 shows the results of this test.

The single point at 635F prior to soaking was less than 5 per cent above the average air regression shown in Figure 5-1. Past experience has shown that whenever a MIN-K product tests satisfactorily at one mean temperature, its regression over a temperature range would also match the established average regression. Consequently, it can be concluded with reasonable confidence that such would have been the case with these specimens. Additionally, it was concluded that the 2000-hr thermal exposure had no effect upon the conductivity of MIN-K 1999.

The results after water exposure were considerably lower than anticipated. A smooth relationship through the test points indicated an average increase of only 0.03 Btu in/hr ft^2 ^oF over the average regression shown in Figure 5-1. The amount of water adsorbed by the specimens was not determined, although it was estimated that they weighed about twice as much when wet than they did when dry. Similarly, the weight to which they were dried coincided with their original weight. Although soaking with water is not recommended under any circumstances, the relatively small change in conductivity lends further strength to the conclusion that no change occurred solely as a result of the thermal exposure.

MIN-K 2002. The thermal conductivity of MIN-K 2002 after extended thermal exposure was determined by Dynatech in air, argon, and vacuum. The data presented in this section was based upon an edge temperature function of zero to +0.03, as determined by the calculated mean temperature, and a thermocouple placed on the edge of the specimens midway between their hot and cold

TABLE 5-5.

THERMAL CONDUCTIVITY IN AIR OF MIN-K 1999
AFTER 2000 HRS IN ARGON AT 1000F

Mean Temperature °F	Thermal Conductivity* Btu in/hr ft^2 °F	
	Before Water Soak	After Water Soak
653	0.22(0)	
489		0.23(3)
748		0.26(6)
865		0.26(4)
1064		0.28(3)

* The third decimal place is presented in parenthesis for purposes of plotting the data. Because of accuracy limitations however, the third place is usually not quoted.

faces. Table 5-6 presents the data points. The most glaring problem was the apparent crossover of the vacuum data at the higher mean temperatures. From a theoretical standpoint, this crossover cannot be accepted by Johns-Manville, although it is conceded that radiation transmission might be altered somewhat by the absence of the air molecules. Rather, it is felt that the problem of balanced and uniform heat flow within the test apparatus constitutes the main source of error, even though an attempt was made to control these conditions. This opinion is not shared by Dynatech who, although they have no explanation for the phenomenon, feel that the data must be accepted at face value.

These same specimens were also evaluated in air by Johns-Manville in the Guarded Hot Plate apparatus (without special atmosphere capability). These data points are shown in Table 5-7. It will be noted that, with the exception of the value at 1066F mean temperature, the data fall closely to the data prior to exposure shown in Figure 5-1.

MIN-K 2020. MIN-K 2020 was also evaluated by Dynatech in air and vacuum following its extended thermal exposure in vacuum. The data are shown in Table 5-8. It will be noted that the mean temperature test range was increased to include a value at about 1600F. Again, the problem of a crossover arose, even though the edge temperature function was held between +0.02 and +0.04.

The MIN-K 2020 specimens which were thermally exposed in air were retested by Johns-Manville in the Guarded Hot Plate apparatus (without special atmosphere capability). These data points are presented in Table 5-9. A comparison of these values with Figure 5-1 would lead one to suspect that the thermal exposure in air did have an effect upon the conductivity. A check of the original control test data from the Rapid Heat Meter before exposure showed that these blocks were 0.25 Btu in/hr ft^2 °F at 800F mean. This was slightly higher than normal due to the 22.3 pcf density. Consequently, the values presented in Table 5-9 are not unreasonable, and probably do not represent any change in the thermal conductivity as a result of the thermal exposure in air.

SUMMARY OF RESULTS

Thermal Conductivity in Air. The thermal conductivity data for MIN-K 1999 Table 5-5, one point only), MIN-K 2002 (Tables 5-6 and 5-7), and MIN-K 2020 (Table 5-8) are plotted in Figure 5-2. Not included are the data for MIN-K 1999 due to the water soak, or the data for the 22.3 pcf MIN-K 2020 of Table 5-5 due to the high density of the specimens. Also shown in Figure 5-2 is the average regression for all of the data.

TABLE 5-6.

THERMAL CONDUCTIVITY OF MIN-K 2002
IN AIR, ARGON AND VACUUM FOLLOWING
EXTENDED THERMAL EXPOSURE

Mean Temperature °F	Thermal Conductivity * Btu in/hr ft^2 °F		
	Air	Argon	Vacuum
491	0.21(3)	0.15(7)	0.11(3)
797		0.19(3)	0.15(4)
1013		0.23(0)	0.18(9)
1211	0.27(4)	0.25(4)	0.28(4)

* The third decimal place is presented in parenthesis for purposes of plotting the data. Because of accuracy limitations however, the third place is usually not quoted.

TABLE 5-7.

THERMAL CONDUCTIVITY OF MIN-K 2002
IN AIR FOLLOWING EXTENDED THERMAL EXPOSURE

Mean Temperature °F	Thermal Conductivity* Btu in/hr ft^2 °F
670	0.20(9)
840	0.22(9)
940	0.24(3)
1066	0.28(6)

* The third decimal place is presented in parenthesis for purposes of plotting the data. Because of accuracy limitations however, the third place is usually not quoted.

TABLE 5-8.

THERMAL CONDUCTIVITY OF MIN-K 2020 IN AIR
AND VACUUM FOLLOWING EXTENDED THERMAL EXPOSURE

Mean Temperature °F	Thermal Conductivity* Btu in/hr ft^2 °F	
	Air	Vacuum
500	0.21(6)	0.12(0)
869	0.24(6)	0.22(8)
1220	0.30(3)	0.35(0)
1598	0.36(1)	0.54(7)

* The third decimal place is presented in parenthesis for purposes of plotting the data. Because of accuracy limitations however, the third place is usually not quoted.

TABLE 5-9.

THERMAL CONDUCTIVITY OF MIN-K 2020 IN AIR
AFTER EXTENDED THERMAL EXPOSURE IN AIR

Mean Temperature °F	Thermal Conductivity* Btu in/hr ft^2 °F
325	0.18(4)
550	0.23(0)
764	0.26(2)
1022	0.32(8)

* The third decimal place is presented in parenthesis for purposes of plotting the data. Because of accuracy limitations however, the third place is usually not quoted.

FIGURE 5-2

THERMAL CONDUCTIVITY OF MIN-K 1999, 2002, AND 2020
IN AIR AFTER EXTENDED THERMAL EXPOSURE

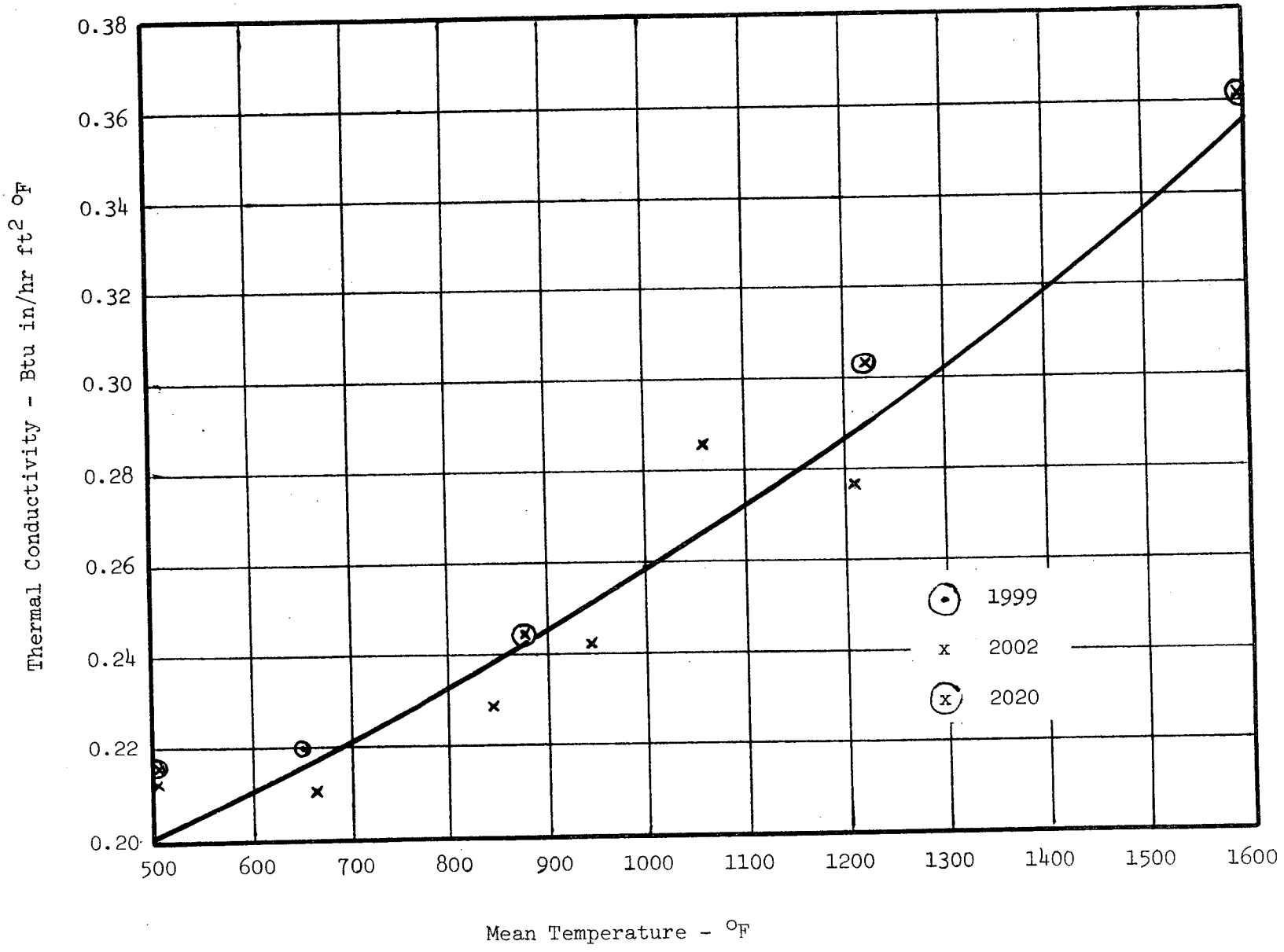

A comparison of this curve with the curve presented in Figure 5-1 representing the data before extended thermal exposures indicates no significant change as a result of the exposures. Similarly, Figure 5-2 also confirms that all three products are essentially the same with respect to thermal conductivity.

Thermal Conductivity in Argon. Due to the equipment failure during the testing of MIN-K 1999, this product could not be tested in argon as anticipated. Consequently, Figure 5-3 presents only the thermal conductivity of MIN-K 2002 in argon as previously shown in Table 5-6. A comparison of this regression with Figure 5-1 indicates that the conductivity was about 10 per cent lower after extended exposure in the 500F mean temperature range, but exactly the same in the 1200F mean temperature range. Considering the fact that the data in Figure 5-1 were obtained on the Johns-Manville equipment, while the data in Figure 5-2 were obtained on the Dynatech equipment, the agreement is satisfactory. Thus, it can be concluded that the extended exposure did not alter the thermal conductivity of MIN-K 2002 when tested in argon. Based upon the apparent similarity of MIN-K 1999 and 2002 when tested in air, it is reasonable to conclude that the conductivity in argon of MIN-K 1999 would also be unaffected.

Thermal Conductivity in Vacuum. Figure 5-4 is a plot of the vacuum conductivity data presented in Tables 5-6 and 5-8 for MIN-K 2002 and 2020 respectively. Also plotted are the data points (lower curve) obtained by Johns-Manville for MIN-K 2002 after extended exposure (the identical specimens which were subsequently tested by Dynatech), but which did not bear any relationship with the original Johns-Manville data plotted in Figure 5-1. Reference to these data was made earlier in this section. Based upon the discrepancy between the data, it is impossible at this time either to establish accurately the thermal conductivity of MIN-K in vacuum, or to determine the effect of extended exposure on the vacuum conductivity (although the latter is expected to be negligible). It would appear however, that at 500F mean temperature (and probably below), the cause of the divergent data is minimized or ceases to exist. Thus, a value of 0.11 Btu in/hr ft^2 ^oF at 500F mean temperature is probably accurate to within ± 10 per cent.

ANALYSIS OF RESULTS

It has become increasingly apparent that adherence to established test procedures for low temperature Guarded Hot Plate measurements may not yield accurate, or in many cases, reproducible results on the Guarded Hot Plate equipment above 800F mean temperature. As indicated previously, both Johns-Manville and Dynatech believe that a detailed evaluation of the thermal conductivity measurement technique for low conductivity materials such as MIN-K must be undertaken.

FIGURE 5-3.

THERMAL CONDUCTIVITY OF MIN-K 2002 IN ARGON
AFTER EXTENDED THERMAL EXPOSURE

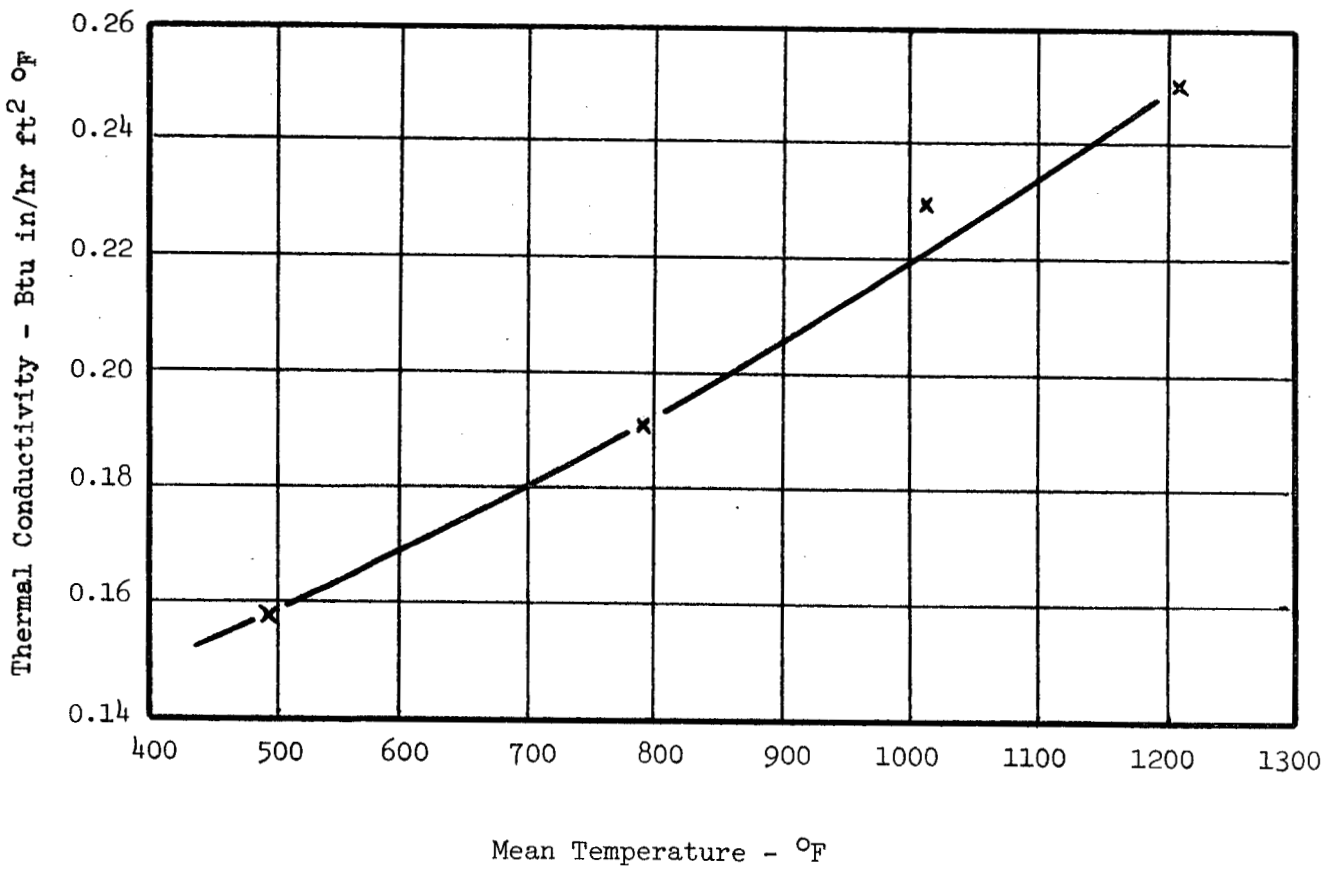

FIGURE 5-4.

APPARENT THERMAL CONDUCTIVITY OF
MIN-K 2002 AND 2020
IN VACUUM AFTER EXTENDED THERMAL EXPOSURE

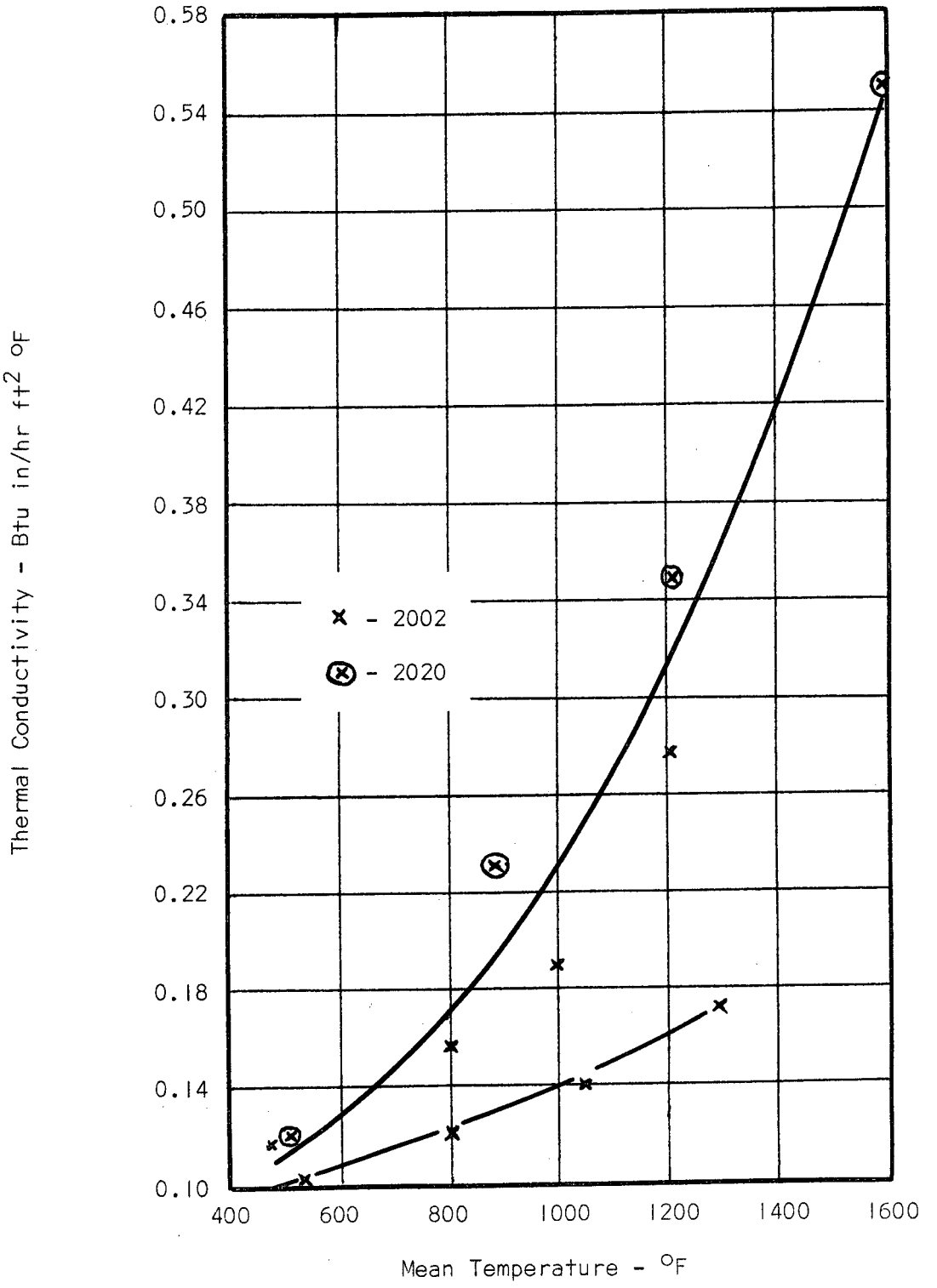

To summarize existing data, however, it can be concluded that:

1. MIN-K 1999, 2002, and 2020 have essentially the same thermal conductivity vs mean temperature relationship in air and argon, and

2. This relationship (in air or argon) is not altered by extended exposure to air, argon, or vacuum (10^{-3} mm Hg) at temperatures just below their respective temperature limits.

An interesting comparison can be made between the test data in all three atmospheres, and the theoretical analysis of heat transfer summarized in the Phase I Final Report [1]. Table 5-10 presents this comparison. The test values for air, argon, and the first vacuum comparison were taken from Figure 5-1 at 1100F mean temperature. Good agreement between the predicted and test values was obtained for air. The same might be said for the values in argon, although room for improvement does exist. The deviation between test and theory in vacuum however is very high, if one accepts the test data of Figure 5-1, or worse, the upper curve of Figure 5-4. In contrast, if the vacuum data generated by Johns-Manville for MIN-K 2002 (after extended exposure) as shown in the lower curve of Figure 5-4 is accepted, the agreement between test and theory is excellent.

TABLE 5-10.

COMPARISON OF PREDICTED AND TEST THERMAL CONDUCTIVITY VALUES FOR MIN-K AT 1100F MEAN TEMPERATURE

Condition	Test Value Btu in/hr ft^2 ^{o}F	Predicted Value Btu in/hr ft^2 ^{o}F	Deviation of Predicted From Test Value
Air	0.267	0.252	- 5.6%
Argon	0.244	0.210	-13.9%
Vacuum	0.208	0.138	-33.6%
Vacuum	0.144	0.138	- 4.2%

III. PHASE II, TASK 2 - MATERIAL RESEARCH AND DEVELOPMENT

INTRODUCTION

Task 2 was divided into four Subtasks:

Subtask 2.1 - Basic Studies

Subtask 2.2 - Materials

Subtask 2.3 - Additives

Subtask 2.4 - Product Development

These Subtasks may be described briefly as follows.

Subtask 2.1 - Basic Studies. This Subtask studied the sintering phenomena of submicron particles of silica and other materials in an effort to determine the mechanism by which the present and developmental MIN-K formulations fail due to shrinkage when exposed to elevated temperatures. This program was initiated with a literature survey summarizing the various mechanisms, and subsequently included a study of the effect of opacifiers, reinforcing materials, and test conditions upon the MIN-K matrix.

Subtask 2.1 utilized the electron microscope (both the scanning and rub-out types), the porosimeter, x-ray diffraction, and a comparative thermal conductivity test apparatus, together with conventional shrinkage and density change measurements to assist in defining the cause of failure.

Subtask 2.2 - Materials. This Subtask included a study of submicron particles other than silica which could be used to obtain a MIN-K product having a higher temperature capability (above 1800F). Dimensional shrinkage was the prime criterion for material behavior under various conditions of temperature, atmosphere, and time.

Subtask 2.3 - Additives. This Subtask covered the effect of bulk additives on the sintering or other failure mechanisms of the high temperature submicron particles and combinations of particles, opacifiers, and fiber reinforcement. As with Subtask 2.2, shrinkage was the primary guideline for material behavior.

Subtask 2.4 - Product Development. Although originally designed to develop and evaluate a product based upon the results of the first three Subtasks, Subtask 2.4 was later deleted from the contract effort.

Since most all of the work conducted under Task 2 related to the evaluation of certain individual materials, or combination of materials rather than products (although some product tests such as shrinkage and thermal conductivity were used as criteria of performance), formulation numbers were not assigned to the experimental compositions as in the Phase I effort. [1] Instead, sample content was spelled out in each case. For example, "ALON-C alpha/TiO_2" represented a sample made with ALON-C alpha submicron particles and titania opacifier. A sample designation beginning with "MIN-K," such as "MIN-K/ALON-C gamma" would indicate that a small amount of fiber - 5 per cent 1/4-in. ASTROQUARTZ and 4 per cent MICRO-QUARTZ - was included as reinforcement in the sample. Other additives are designated in a similar manner with notations in the text as to the amount.

Subtask 2.1 ran concurrently with, rather than preceded, Subtasks 2.2 and 2.3, and full communication was maintained between the researchers of each Subtask. Therefore, for the sake of clarity and continuity of this report, each Subtask will not be discussed separately in its entirety. Rather, each major section will be discussed in its proper order with respect to the entire Task 2 effort. It will become reasonably apparent, however, based upon the types of techniques employed, into which Subtask each section falls.

LITERATURE SURVEY ON SINTERING OF REFRACTORY METALLIC OXIDES

Definition of Sintering. Sintering may be defined as the coalescense and densification of a compact of particles by heat. The ideal end point of the sintering process is a homogeneous, non-porous, crystalline body.

Three broad stages of diffusion-controlled sintering have been distinguished in the literature[2]:

1. The initial stage in which only limited densification occurs (up to 10 per cent). During this stage the individual particles "neck" together and grain boundaries are confined to the small cross-sectional area of these necks.

2. The intermediate stage in which primary grain boundaries intersect but a continuous pore phase remains. This is a metastable structure with angular pores and it persists until about 90 per cent densification.

3. The final stage in which the pores are near-spherical and the pore phase is discontinuous. In this stage, ideally all the pores shrink continuously until finally eliminated and theoretical density is obtained. However, it is also possible during this stage for "discontinuous grain growth" to occur. Under these circumstances, certain grain boundaries migrate before their associated pores can be eliminated and theoretical density is never obtained.

Mechanisms of Sintering - General. The three stages of sintering mentioned above were in reference to solid state or diffusion-controlled sintering. Another quite different process which leads to densification is sintering in the presence of a reactive liquid. Under these conditions it is quite obvious that the liquid phase can fill interstics as well as facilitate particle rearrangements. However, the sintering mechanisms discussed here refer only to diffusion-controlled sintering.

Diffusion, as related to the sintering of metallic oxides, is the motion of atoms through the crystalline solid. Atoms can move through the solid by "jumping" from normal lattice positions to adjacent unoccupied lattice sites. Such motion is equivalent to the mobility of the unoccupied sites or vacancies in the opposite direction and is the reason for the term "vacancy diffusion" found frequently in the literature. Atoms may also diffuse to and from positions between the normal lattice sites of a crystalline lattice called interstitial sites. The primary diffusion-controlled mechanisms relating to sintering include surface diffusion, grain boundary diffusion, bulk diffusion, dislocation motion, and creep.

Surface Diffusion (3-5). Surface diffusion is the motion of atoms along the surfaces of a grain which are not in contact with other grains. For example, the diffusion of atoms along the surfaces of grains adjacent to the pore would be classified as surface diffusion. Because the atoms near the surface of a crystalline grain are not bound as tightly in the lattice as interior atoms, surface diffusion is more rapid than diffusion through the crystalline lattice. However, it is easy to see that although surface diffusion can cause changes in pore shape and increase the size of the "necks" between sintering particles, it cannot lead to pore shrinkage and densification. Therefore, surface diffusion by itself cannot be the only mechanism operating during the sintering process.

Grain Boundary Diffusion (6-9). Grain boundary diffusion is the movement of atoms or vacancies in the disordered structure of the grain boundaries. Like surface diffusion, grain boundary diffusion is more rapid than bulk diffusion because of the random nature of the grain boundary structure. Here again atoms

(3-5) Numbers in parentheses refer to Section VI References.

are not as tightly bound as they are in the crystalline lattice and many more vacancies exist. Shrinkage and densification may occur as the result of boundary diffusion because the grain boundaries act as vacancy channels to the surface of the powder compact. As vacancies are eliminated, the pores (vacancy sources) will shrink.

It has been shown experimentally, however, that sintering rates are faster than would be possible if pores were eliminated only by vacancy diffusion to the surface. Therefore, grain boundary diffusion also cannot be the only mechanism operating during the sintering process.

Bulk Diffusion (10-17). Bulk or volume diffusion is the movement of atoms directly through the crystalline lattice of a grain. Although surface diffusion and grain boundary diffusion tend to be important at relatively low temperatures, bulk diffusion becomes the most important diffusion mechanism at higher temperatures. In fact, the vast majority of recent articles in reference to solid state sintering of metallic oxides indicate that bulk diffusion has been established as a major mechanism in the sintering of powder compacts to complete densification.

In brief, the sintering mechanism for complete densification by bulk diffusion may be stated as follows. As the material to be sintered is compacted, the majority of large pores will, of course, be situated on the grain boundaries. As the temperature increases, atoms begin to diffuse from vacancy to vacancy in the crystalline lattice of the grains. The vacancies will wander until they reach a place which will least disturb the structure, namely the grain boundaries. As the vacancies accumulate on the grain boundaries, either the vacancies are discharged by grain boundary diffusion or a general "collapse" of the grains into the created grain boundary space takes place and the overall result is shrinkage.

As the temperature is increased, not only do the vacancies diffuse faster, but there is also an increase in the number of vacancies formed. Because of surface energy considerations, there is a greater tendency for the formation of vacancies at the highly curved contact areas or "necks" between the grains. Because of this difference in vacancy concentration, vacancies will tend to diffuse along the grain boundaries away from the neck areas. Conversely, the diffusion of atoms, or material transport, is from the grain boundaries to the neck areas. This process not only speeds the "collapse" or shrinkage but also enlarges the neck areas between grains and changes the size and shape of the included pores.

When densification has progressed to the point where the pore phase is no longer continuous, that is, to the final stage of sintering, the grain boundaries themselves are free to migrate by atomic diffusion. The boundaries will move to make some grains smaller and some grains larger. Hence, the term "grain growth" is used throughout the literature. The driving force for grain boundary movement is the difference in the free energies on the two sides of a grain boundary. A grain with positive curvature has a lower surface energy than one with negative curvature. In other words, atoms find it easier to escape from a surface of positive curvature than from one of no curvature or negative curvature where they are bound more tightly. Thus, the grain boundaries will move toward their centers of curvature. Note in Figure 2-1 that the grain boundary moves toward its center of curvature because it is easier for the atoms to diffuse from the convex surface to the concave surface of the grain boundary. Observations of polished sections of sintered compacts show that grains meet at points in groups of three and that the angle between the boundaries at these points is about 120°. If we consider a two-dimensional example for illustrative purposes, angles of 120° between grains with straight sides can occur only for six-sided grains. Those with fewer than six sides will have convex sides and become smaller. Those grains with more than six sides will have concave sides and become larger as shown in Figure 2-2.

Certain grain boundaries will not move until the pores associated with them have been eliminated by the diffusion process described earlier. This is because the driving force for boundary movement is not great enough to by-pass the pores. Ideally, grain boundary movement occurs only as the pores are removed, with the result that all the pores are "swept" out before the advancing grain boundaries and complete densification is obtained. However, if the curvature of a grain boundary is great enough, the free energy difference across it will be large enough for the boundary to by-pass some of the pores. This generally happens as a result of secondary crystallization or what is called discontinuous grain growth or exaggerated grain growth in the literature. Secondary crystallization occurs when certain large grains begin to grow at much faster rate than the average sized grains. This is possible because normally a large grain will have more sides which means that these sides must have a greater curvature if they are to meet the requirements of joining at 120° angles. Note the highly curved sides of the large grain in Figure 2-2.

As previously indicated, the amount of grain boundary curvature determines the amount of driving force for grain boundary movement and therefore boundaries with more curvature advance at a faster rate. The increased driving force can overcome the restraint offered by the pores to grain boundary advance and, as a result, many pores are permanently trapped within the new larger grains. Therefore, when secondary recrystallization occurs, complete densification is not obtained, and generally there is a deleterious effect upon the mechanical properties of the sintered body.

FIGURE 2-1.

MIGRATION OF GRAIN BOUNDARY BY ATOMIC DIFFUSION

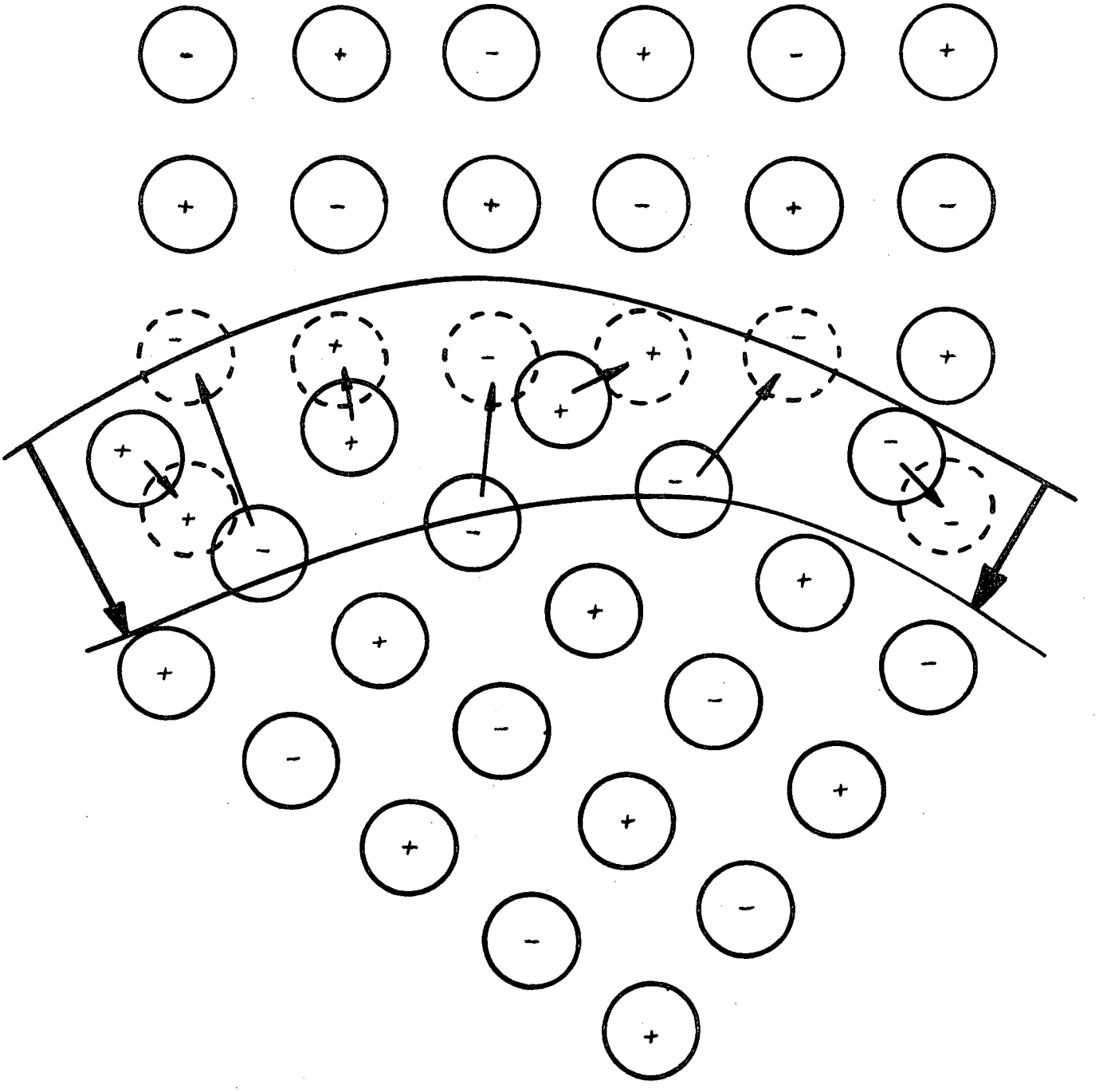

FIGURE 2-2.

GRAIN GROWTH AND SECONDARY RECRYSTALLIZATION

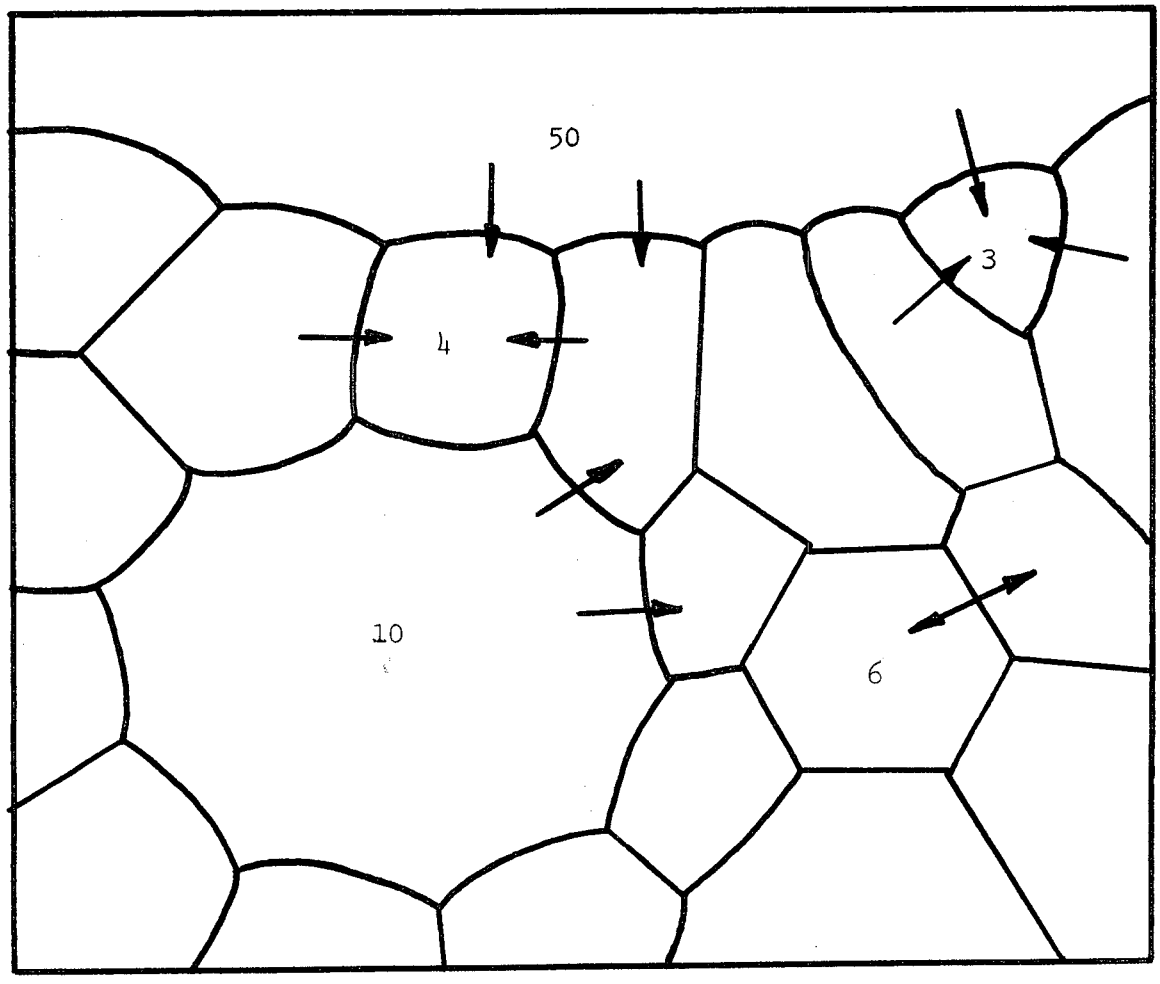

Dislocation Motion (18-21). Although most of the model studies in the literature indicate that bulk diffusion is the major material transporting mechanism, the recent work by Morgan and Hall gives evidence that dislocation motion may make a significant contribution to powder compact densification.

Densification by dislocation motion or plastic flow was originally proposed by Clark and White. They developed a theory in which the driving force for sintering and shrinkage was the capillary forces operating at the points of contact between particles in a powder compact. They developed formulas which fit the experimental shrinkage curves for compacts which contained reactive liquids and for those which did not. For the refractory exide compacts which contained no liquid during the sintering process, they proposed the diffusion-controlled movement of dislocations as a mechanism for densification.

Creep (22-27). The deformation of a crystalline body under constant stress at elevated temperatures is known as creep. Two types of creep which may contribute to the densification process during the sintering of metallic oxides are diffusional creep and grain boundary creep.

In diffusional or Nabarro-Herring creep, self-diffusion within the grains of a powder compact allows the body to yield to the stresses which were set up when the powder was pressed together, as well as the stresses set up from the weight of the body itself. Deformation and shrinkage result from diffusional flow within each crystalline grain away from those boundaries where there is a normal compressional force towards boundaries having a normal tensile stress.

Grain boundary creep is a diffusion-controlled rearrangement of particles within a powder compact. Because grain boundaries are areas of poor lattice fit, they can be thought of as areas of noncrystalline structure between the crystalline grains which behave viscously when a shear stress is applied. O'Hara postulates that grain boundary creep is largely responsible for the initial shrinkage behavior of powder compacts.

Equally as important in the study of the various mechanisms of sintering is the consideration of the factors which affect the sintering rate. These factors include temperature, pressure, particle size, atmosphere, and impurities.

Temperature (28, 29). The most obvious factor affecting the rate of solid state sintering is temperature. Both the concentration of structural defects and the movement of atoms through a crystalline lattice are temperature dependent. Structural defects include both interstitital ions and vacancies which are necessary for diffusion. The number of structural defects increases exponentially with increasing temperature.

The movement of an atom from one site to another in a crystalline lattice may be thought of as overcoming an energy barrier. That is, a certain amount of acquired energy is necessary for an atom to diffuse from vacancy to vacancy. As temperature is increased, the acquired thermal energy of the atoms is increased and more of them can cross the activation energy barriers between sites and thus the rate of diffusion is increased.

Pressure (30, 31). Another factor affecting the rate of diffusion-controlled sintering is the external pressure which is applied to powder compacts. In fact, at low temperatures, densification of single material powder compacts will occur only if some external pressure is applied. This is because of the force of repulsion between the particles which all have an electrical surface charge of the same sign.

External pressure assists in densification by removing many of the large pores caused by nonuniform mixing. In addition, there are stresses set up across grain boundaries so that particle surface energies are not the sole driving force for densification. These stresses permit diffusional creep and grain boundary creep to operate and assist in densification. It is from this standpoint that the relatively new techniques of hot pressing or pressure sintering are advantageous; that is, the additional driving force for solid state densification is obtained with the application of external pressure. In some cases of pressure sintering, it is possible to obtain complete densification at temperatures below those at which discontinuous grain growth occurs.

Particle Size (32-38). In the discussion of bulk diffusion, it was mentioned that there are energy differences between surfaces of different curvature. It is for this reason that fine particles with small radii of curvature and high surface energies will sinter together faster than large particles.

It might be worth mentioning at this point that the faster sintering rate of very fine particles does not automatically result in a denser sintered body. Neither does a mixture of particle sizes which might initially have a higher green density result in the densest body when sintered as is commonly thought. The reason for both of these facts is secondary recrystallization. That is,

with either very fine particles or a mixture of particle sizes, there is more chance for a few larger particles present to become the nucleation centers for the very large and undesirable grains during secondary recrystallization. To date, sintered polycrystalline metallic oxide bodies which have come closest to theoretical density have used a relatively large single particle size as a starting material.

When particles are submicron in size, Van der Waal's forces may play a significant role in granulation. Although these forces drop off according to a sixth-power distance law, they have been shown to be act over distances up to 1000 A^{o}.

Atmosphere (39-49). The atmosphere of the kiln during densification of powder compacts may effect the sintering rates in two ways: formation of reaction products, and creation of lattice defects.

Examples of reaction products would be the formation of carbides in a reducing atmosphere if carbon is present, or the formation of nitrides in the presence of excess nitrogen.

The presence of water vapor in the kiln atmosphere can also effect the sintering rate because of reaction products formed. For example, if a hydrate is formed which concentrates at the grain boundaries, it will generally impede the bulk diffusion across that boundary and thus lower the sintering rate. Green postulates that this is the case for beryllia and alumina. The formation of hydrates and reduced sintering rates are not the rule, however, for metallic oxides sintered in an atmosphere containing water vapor. The sintering rate of silica is increased if fired in the presence of water vapor. Both hydrogen and hydroxyl ions are able to diffuse into the silica structure and disrupt it. The result is a more amorphous or glassy type structure where bulk diffusion can take place much more rapidly.

Kiln atmosphere may also effect the rate of sintering by controlling the number of lattice defects. In the case of metallic oxides, the concentration of lattice defects is markedly influenced by the partial pressure of oxygen in the surrounding gas atmosphere. Some examples follow.

The sintering rate of aluminum oxide has been found to increase in a reducing atmosphere. The logical and most simple explanation is that the reduction of the partial pressure of oxygen results in oxygen vacancies which permit an increased rate of bulk diffusion. A further explanation, however, is offered

in the recent work by Kuczynski. Direct evidence was found that alumina particles which are sintered together in a hydrogen atmosphere lose their oxygen atoms in such a way that crystallographic facets develop and the geometry of the system changes. The growth of these crystallographic planes was noted particularly in the neck regions between particles. A neck surrounded by these crystalline planes will maintain its small radius of curvature even as the neck grows. The small radius of curvature means a faster rate of diffusion as pointed out in the previous discussion of bulk diffusion and solid-state sintering. No change in the geometry of particles was noted when sintering took place in an oxidizing atmosphere.

Another example of the influence of the partial pressure of oxygen in the kiln atmosphere is the sintering of uranium dioxide. In the case of oxygen-excess uranium dioxide, a reduced partial pressure of oxygen in the gas atmosphere would tend to eliminate the inherent excess interstitial oxygen and, therefore, retard sintering. On the other hand, in an initially oxygen deficient system, a reduced partial pressure of oxygen would augment the oxygen deficiency; and hence, it would enhance sintering.

It must be kept in mind that the partial pressure of oxygen is most important if oxygen atom diffusion is the rate determining step of the diffusion process. The rate of a diffusion process is controlled by its slowest diffusing component. In the case of metallic oxides, this may be the rate of oxygen atom diffusion, or it may be the rate of cation diffusion. Which it is depends on a number of factors including dissociation energies, activation energies for diffusion, ionic polarizabilities, and even grain size. For instance, in the case of aluminum oxide, oxygen atom diffusion is normally the rate controlling step. However, Paladino and Coble present evidence that in very fine grained compacts the rate of oxygen diffusion is significantly increased because of the grain boundary diffusion of oxygen. This increase can be to the extent where the aluminum atom diffusion becomes the slower rate controlling step of the sintering process.

The literature indicates that diffusion-controlled sintering rates of metallic oxides are generally enhanced in vacuum. This can be related to the increase in the number of oxygen vacancies because of the complete reduction of the oxygen partial pressure. However, there are a few cases where the sintering rates of metallic oxides are actually retarded in vacuum. One such case is silicon dioxide. It was previously mentioned that the sintering rate of silica was increased in the presence of water vapor which is generally found in the atmosphere of a kiln. Therefore, the complete absence of water vapor in vacuum inhibits the sintering rate of silica.

Impurities (50-70). Impurities or additives present in a powder compact may either enhance or inhibit diffusion-controlled sintering rates. Impurities may form a solid solution or a non-liquidus second phase with the host material. If an impurity does not form a second phase but goes into solid solution, it will generally change the number of cation or anion vacancies which, in turn, affects the rate of diffusion. Some examples follow.

When titanium dioxide is added to magnesium oxide in an oxidizing atmosphere, the quadrivalent titanium ions replace some of the divalent magnesium ions in the MgO lattice. The resulting excess positive charge is balanced by the creation of cation vacancies. With a greater number of cation vacancies available, the diffusion rate of the magnesium atoms, and thus the sintering rate, is increased. Even in a reducing atmosphere the addition of TiO_2 to MgO increases the rate of sintering although not to the same degree. The reason for this is that the titanium ions are now trivalent and do not promote the formation of cation vacancies to the extent that quadrivalent ions do.

Another example of enhanced sintering due to the formation of cation vacancies is the case of MgO or CaO fired in the presence of water vapor. In this case, the hydroxyl ions present act as impurity ions and replace some of the oxygen ions in the metallic oxide lattice. A monovalent negative ion replacing a divalent negative ion results in an overall positive charge. This permits the formation of cation vacancies and the associated increased diffusion of the magnesium or calcium atoms.

An example of increased diffusion by the creation of anion vacancies is the addition of manganese oxide to aluminum oxide. In this case, the divalent positive manganese ions replace some of the trivalent aluminum ions in the alumina lattice. The excess negative charge is balanced by the creation of anion vacancies which in turn increase the rate of the oxygen atom diffusion.

Some additives or impurities which go into solid solution with the host lattice do not result in the formation of lattice defects and do not affect the sintering rates. The addition of Fe_2O_3 under an oxygen atmosphere does not alter the sintering rate of Al_2O_3. The obvious explanation is that neither anion nor cation vacancies are produced because the trivalent iron ion is of the same valance as the trivalent aluminum ion of the host lattice.

The examples just cited illustrate the general principles involved in deciding how an impurity or additive in solid solution with the host material will affect the sintering rate. It should be kept in mind that not only can the kiln atmosphere change the effect of an impurity, but the amount of the additive is important also. Whereas minor additions may go into solid solution, larger

amounts may form second phases. In addition, the formation of complex groupings in solid solutions may play a more important role than the creation of lattice defects when an impurity is added. For example, it is thought that the addition of alkali ions to Al_2O_3 results in the formation of complex aluminate ions whose diffusion is difficult and therefore accounts for the observed retardation of the sintering rate.

If the impurity added does not form a solid solution with the host lattice, but instead forms a non-liquidus second phase, generally, the sintering rate is changed. The reason for this is that the reaction product is normally formed at the grain boundaries where it will change the diffusion coefficients of the host atoms as well as affect the migration of grain boundaries.

If the reaction product formed has a more open structure or a disrupted structure due to nonequilibrium stresses, diffusion rates may be increased. In addition, many of the reaction products formed evolve heat which further raises the temperature and accelerates the reaction and sintering process. On the other hand, the reaction product formed may be more stable and decrease the rate of diffusion of the host atoms through it as well as inhibit grain growth. In such cases, sintering is retarded.

A notable example of the metallic oxide whose sintering rate is retarded by the formation of a compound is the case of alumina with a minor addition of magnesia. The formation of spinel ($MgAl_2O_4$) at the grain boundaries not only reduces the diffusion rate of the host atoms across the boundaries, but also inhibits grain growth. This is the principle involved in the production of General Electric's translucent polycrystalline Al_2O_3 known as Lucalux. Diffusion and grain growth have been slowed down to the point where there is enough time for all the porosity to be eliminated at the grain boundaries by the diffusion process.

CANDIDATE SUBMICRON PARTICLES

Introduction. The primary concern of this portion of the effort was to locate a material with a submicron particle size having characteristics similar to CAB-O-SIL M5, but having a service temperature limit (in the product form) of about 2200F. The other characteristics believed to be essential were:

a. 0.01 to 0.03 micron particle size - to achieve the low thermal conductivity in a gaseous media typical of MIN-K.

b. high purity - to minimize undesired fluxing at high temperature and potential thermoelectric contamination, and

c. low bulk density - to permit a reasonably low product density, assuming a 5 or 6 to 1 compression ratio as experienced with MIN-K.

Candidate Particles. Candidates which were considered are listed in Table 2-1. These materials were chosen for their refractory nature and their resistance to sintering at 2200F by the mechanisms described earlier. As anticipated, all materials having a high bulk density resulted in a compressed or molded product of excessively high density. For example, a density of 80 pcf was necessary to achieve a handleable disc made from submicron zirconia. Although product density was not specified at the outset of this investigation, ultimate usage of the product for space applications dictated that density (or weight) be kept within reasonable limits. Similarly, insulations having densities of this order of magnitude generally have high thermal conductivities. Thus, most of the candidates were eliminated.

The remaining candidates (in the 3-10 pcf bulk density range) were evaluated for shrinkage at 2200F in air for 2 hr. This evaluation was conducted on discs approximately 1-1/8 in. in diameter and 1/2 in. thick compressed to a handleable density. These discs contained 5 per cent 1/4-in. ASTROQUARTZ staple fiber, and 4 per cent MICRO-QUARTZ fibers to provide structural reinforcement. A comparison of the diameter shrinkages indicated that the alumina discs were more stable than the titania discs (10 to 15 per cent compared with 20 per cent), and that the ALON-C was the most promising source of alumina. Thus, it became apparent that, as with silica, the mechanisms of sintering or agglomeration of other refractory materials are initiated at "lower-than-usual" temperatures due to the small particle size.

ALON-C Properties. The manufacturer's data for ALON-C are presented in Table 2-2. A preliminary comparison of the thermal stability of ALON-C vs CAB-O-SIL M5 at 2200F in air for 2 hr indicated that 1-1/8 in. diameter by 1/4-in. thick discs of pure CAB-O-SIL M5 had an average diameter shrinkage of 54 per cent, whereas the pure ALON-C discs had an average diameter shrinkage of 30 per cent. Similarly, specimens of MIN-K 1999[1] containing ALON-C in place of CAB-O-SIL M5 averaged 12 per cent shrinkage, whereas the regular MIN-K 2002[1] product averaged 35 per cent.

Although these tests were very preliminary, they showed that ALON-C was considerably more stable than CAB-O-SIL M5, and that fibrous reinforcement further enhanced the stability. It was evident, however, that further effort would be required to obtain still more thermal stability.

X-ray Diffraction and DTA of ALON-C. ALON-C was found by X-ray diffraction analysis to be the gamma form of Al_2O_3. This form is known to be unstable at high temperatures. All of the preliminary specimens which were subjected to 2200F for 2 hr, however, had converted from the gamma to the alpha structure. A Differential Thermal Analysis of ALON-C did not indicate any distinct gamma to alpha Al_2O_3 conversion peaks when heated at a 36F/min rate to 2183F. However, the appearance of a gradually increasing exothermic slope above 2030F

TABLE 2-1.

SUBMICRON CANDIDATE MATERIALS

Material	Manufacturer	Bulk Density pcf	Particle Size Microns
ALON-C (Al_2O_3)	G. L. Cabot	3	0.03
Baymal (AlO(OH))	du Pont	32	submicron
Baymal (Fired*)	du Pont	25	submicron
CAB-O-TI (TiO_2)	G. L. Cabot	6	0.03
Submicron Al_2O_3	Vitro Laboratories	16	---
Submicron Al_2O_3	Vitro Laboratories	10	0.03
Submicron MgO	Vitro Laboratories	8	0.02
Submicron TiO_2	Vitro Laboratories	31	---
Submicron Zr_2O_3	Vitro Laboratories	17	0.05
Ultrafine MgO	Vitro Laboratories	17	---
ZnO (Fired* $ZnCO_3$)	Vitro Laboratories	19	---

* by Johns-Manville

TABLE 2-2.

PROPERTIES OF ALON-C (MANUFACTURER'S DATA)

Color and Form	White powder
X-ray Structure	90% gamma Al_2O_3
Alumina Content	99% minimum
Moisture Content	2.5%
Ignition Loss	4.5%
Metallic Oxides (Excluding Al_2O_3)	1% maximum
Average Particle Diameter	0.03 microns
Surface Area	100 m^2/g
pH (10% aqueous suspension)	4.4
Specific Gravity	3.6
Loose Bulk Density	4 lb/cu ft

may have represented either a slow gamma to alpha Al_2O_3 conversion, or an increase in the thermal conductivity of the ALON-C.

ALON-C Conversion. Conversion of the ALON-C submicron alumina from the gamma form to the more stable alpha form would be desirable prior to formulation with the remaining ingredients. This conclusion was based on the fact that shrinkage of a molded MIN-K/ALON-C gamma disc was greater than that for a MIN-K/ALON-C alpha disc when exposed to 2200F for several hours. To this end, a series of tests was conducted to determine the time-temperature cycles required for the conversion of bulk ALON-C. The temperatures investigated ranged from 2000F to 2400F, and the exposure time between 1/4 and 3 hr. The firing was conducted by inserting several cubic centimeters of bulk ALON-C gamma into a small preheated platinum furnace, and subsequently removing the specimen after the prescribed time period and chilling to room temperature. After the firing, the bulk density of the ALON-C was estimated, and the degree of conversion to the alpha form determined by conventional X-ray diffraction techniques.

The results of this investigation are summarized in Table 2-3. It will be noted that within the exposure times investigated, a temperature of 2200F was required to affect any conversion. Equally as important, however, was the effect of time and temperature upon the bulk density of the ALON-C. If one can assume that the minimum bulk density which might be achieved under such conversion conditions was approximately 6 to 8 lb/cu ft, the resultant product density would be approximately 30 to 50 lb/cu ft. (This assumes that the compression ratio of 5 or 6 required to achieve adequate handling strength for a conventional formulation would also be required for a formulation containing ALON-C alpha.)

In contrast to the above results, samples of ALON-C gamma in molded form had been heated at 2200F for 2 hr, but permitted to heat up and cool down within the furnace, resulting in a total time of 5 hr above 1800F. (See previous section entitled, "Candidate Particles.") X-ray diffraction analyses of these specimens showed the conversion from gamma to alpha to be essentially complete. Figures 2-3 and 2-4 are "rub-out" electron micrographs of the ALON-C before and after this heat treatment. It is very apparent that a considerable amount of sintering and growth of the submicron alumina particles had taken place during the conversion process.

The apparent discrepancy between the time-temperature conditions required to achieve complete conversion of the bulk ALON-C material as shown in Table 2-3, and those required by the earlier molded specimens (depicted by Figures 2-3 and 2-4) could be attributed to two factors:

1. The additional elevated temperature exposure time afforded the molded discs, and/or

2. The greater particle-to-particle intimacy in the molded form.

FIGURE 2-3.

ALON-C GAMMA
MAG: 27,500X

1 micron

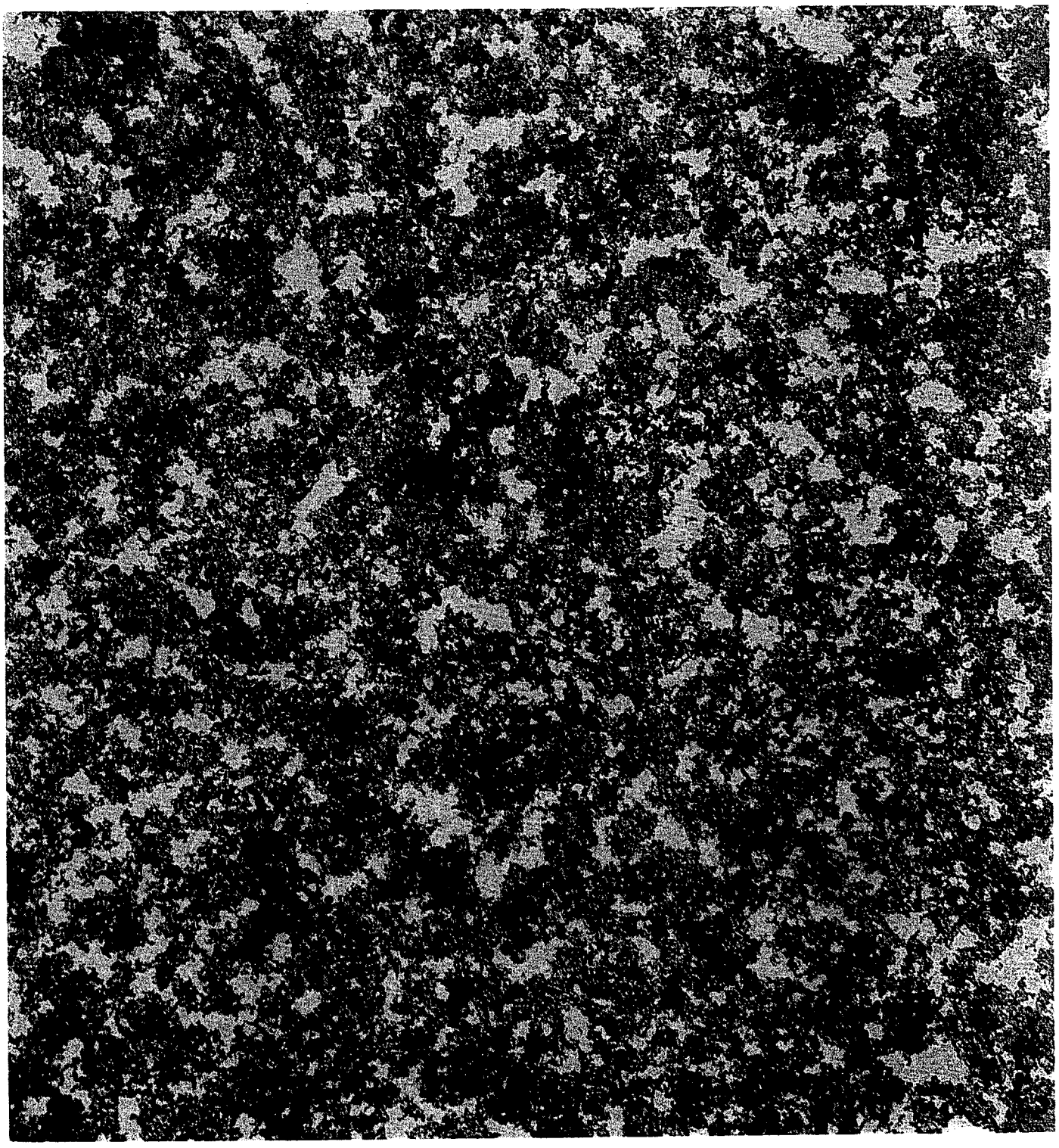

FIGURE 2-4.

ALON-C ALPHA
MAG: 27,500X

1 micron

TABLE 2-3.

EFFECT OF TIME AND TEMPERATURE ON THE CONVERSION OF ALON-C FROM GAMMA TO ALPHA FORM

Temperature °F	Exposure Time hr	Phase Present*	Bulk Density** lb/ft^3
2000	1/4	gamma	2
2000	1/2	gamma	2
2000	1	gamma	2
2000	1-1/2	gamma	2
2000	2	gamma	2
2000	3	gamma	3
2050	1/2	gamma	2
2050	1	gamma	3
2050	2-1/2	gamma	3
2100	1/2	gamma	2
2100	1	gamma	3
2100	2-1/2	gamma	3
2150	1/2	gamma	3
2150	1	gamma	3
2150	3	gamma	4
2200	1/2	not analyzed	3
2200	1	not analyzed	3
2200	3	50 per cent gamma, 50 per cent alpha	5
2250	1	not analyzed	4
2250	1-1/2	not analyzed	6
2250	2	25 per cent gamma, 75 per cent alpha	7
2300	1/2	85 per cent gamma, 15 per cent alpha	6
2300	1	not analyzed	7
2300	1-1/2	2 per cent gamma, 98 per cent alpha	11
2300	2	not analyzed	12
2300	2-1/2	not analyzed	13
2400	1/2	alpha	15
2400	1	alpha	16
2400	1-1/2	not analyzed	19

* The percentage quantities of the phases are based on estimates.

**The reported bulk densities are rough estimates, and therefore should be used only for comparison. The bulk density of the unfired ALON-C material, determined by the same technique, was 2 lb/ft^3.

Table 2-3 would tend to discount Item 1 as a factor by itself, since 3 hr at 2200, 2 hr at 2250F, and 1-1/2 hr at 2300F did not result in the same extent of conversion as noted in the molded specimen. Consequently, it is probable that Item 2 had a strong influence upon the results, with a possible assist from Item 1.

THERMAL STABILITY AND THERMAL CONDUCTIVITY

Specimen Preparation. Specimens used in these, and other evaluations, were prepared in the following manner. The fibers (1/4-in. ASTROQUARTZ staple fiber, and MICRO-QUARTZ) were opened and premixed by passing them twice through a willower (Tornado blower) and collected in a vacuum bag. The fiber mixture was then placed in a Waring Blendor along with the powdered ingredients and blended for 3-1/2 min at low speed (achieved by supplying only 30 volts to the Blendor through a variable transformer). Discs were then molded to approximately 1-1/8 in. diameter x 1/2-in. thick, using a steel die and a laboratory press. Those specimens made with ALON-C alpha required densities of about 30 pcf to achieve adequate handleability. In no case was binder used during any part of the Phase II program.

Furnace Equipment. The isothermal heat treatment of the specimens in both air and vacuum was carried out in two different furnaces depending upon the exposure temperature. Firings up to 2000F were conducted in the furnace system designed and built under Phase I of this contract [1]. This equipment consisted of a 3' x 3' x 3' resistance wire furnace (floor model) into which five 4-1/2 in. diameter mullite tubes (closed at one end) were inserted in an upright position. The tubes extended beyond the top of the furnace approximately 12 in. to afford sufficient cooling so as to permit a Vitron seal between the tubes and the vacuum system. A radiation shield of DYNAFLEX (2700F temperature limit) was inserted within the tube approximately even with the top of the furnace to reduce the radiation to the Vitron seal, and to limit the temperature gradient within the firing zone to 10 to 12F.

When testing in vacuum, the system was sealed and evacuated at room temperature, and subsequently heated to the desired temperature. During the period at temperature, the pressure within the system was below 2 microns, and generally averaged 1 micron. A typical time-temperature cycle for a 2000F firing was:

18 hr furnace heatup and overnight hold at 1500F

5 hr heatup from 1500F to 2000F

x hr at 2000F

18 hr (overnight) cooldown

Firings to 2200F were conducted in a 6-in. diameter alumina tube inserted horizontally into a glo-bar type furnace capable of 2400F. Figure 2-5 is a schematic of this system. The basic design was similar to the lower temperature furnace except that the vacuum flange at the cool end of the tube was fitted with a thermocouple feed-through to permit temperature measurements inside the tube as shown in the diagram. Although this furnace system had its own vacuum system, it was designed such that either or both of the vacuum systems (2000F and 2200F furnaces) could be activated for either furnace system.

The typical heating cycle for the 2200F firings was:

18 hr furnace heatup and overnight hold at 1000F

3 hr heatup from 1000F to 2200F

x hr at 2200F

6 hr cooling to 1000F

For the vacuum tests, the vacuum was drawn at room temperature, and active pumping was maintained throughout the test (including cooldown). After 18 hr at 1000F, the pressure was below 2 microns. Upon heatup to 2200F, the pressure averaged 15 microns. During the short test periods (2 hr), the pressure would decrease to about 4 microns before the cooldown cycle was initiated. During longer tests, however, pressures between 1 and 2 microns were achieved.

Thermal Conductivity Test Method. To eliminate the need for large (9 x 9 x 1 in.) thermal conductivity test specimens during the initial studies, a thermal gradient method was devised to accommodate the 1-1/8 in. diameter specimens both before and after thermal exposure. This method utilized a 1-in. thick sample of MIN-K 1999 (of known conductivity) as the comparative standard. The heat source was a Kanthal wound resistance hot plate which, when placed as shown in the schematic diagram in Figure 2-6, resulted in a mean temperature of 725F, and a temperature drop across the test specimen of 100 to 150F. The entire stack was placed in a vacuum bell for thermal conductivity measurements at pressures below 0.1 micron. Although this method of measurement gave only relative values, these values were shown to be reproducible, and gave an excellent indication of the effects of heat treatment and composition on thermal conductivity.

Thermal Stability. Table 2-4 presents the density change measurements of the various test specimens as a result of the heat treatments. The column labeled "Basis of Opacifier Addition" indicates whether the opacifiers were added on an equal weight basis or an equal mol basis. All compositions contained either 16 weight per cent of opacifier, or the mol equivalent of 16 weight per cent of titania. The "Heat Treatment" column gives the firing temperature and the atmospheric conditions during firing.

FIGURE 2-5.

SCHEMATIC DIAGRAM OF HIGH TEMPERATURE VACUUM FURNACE

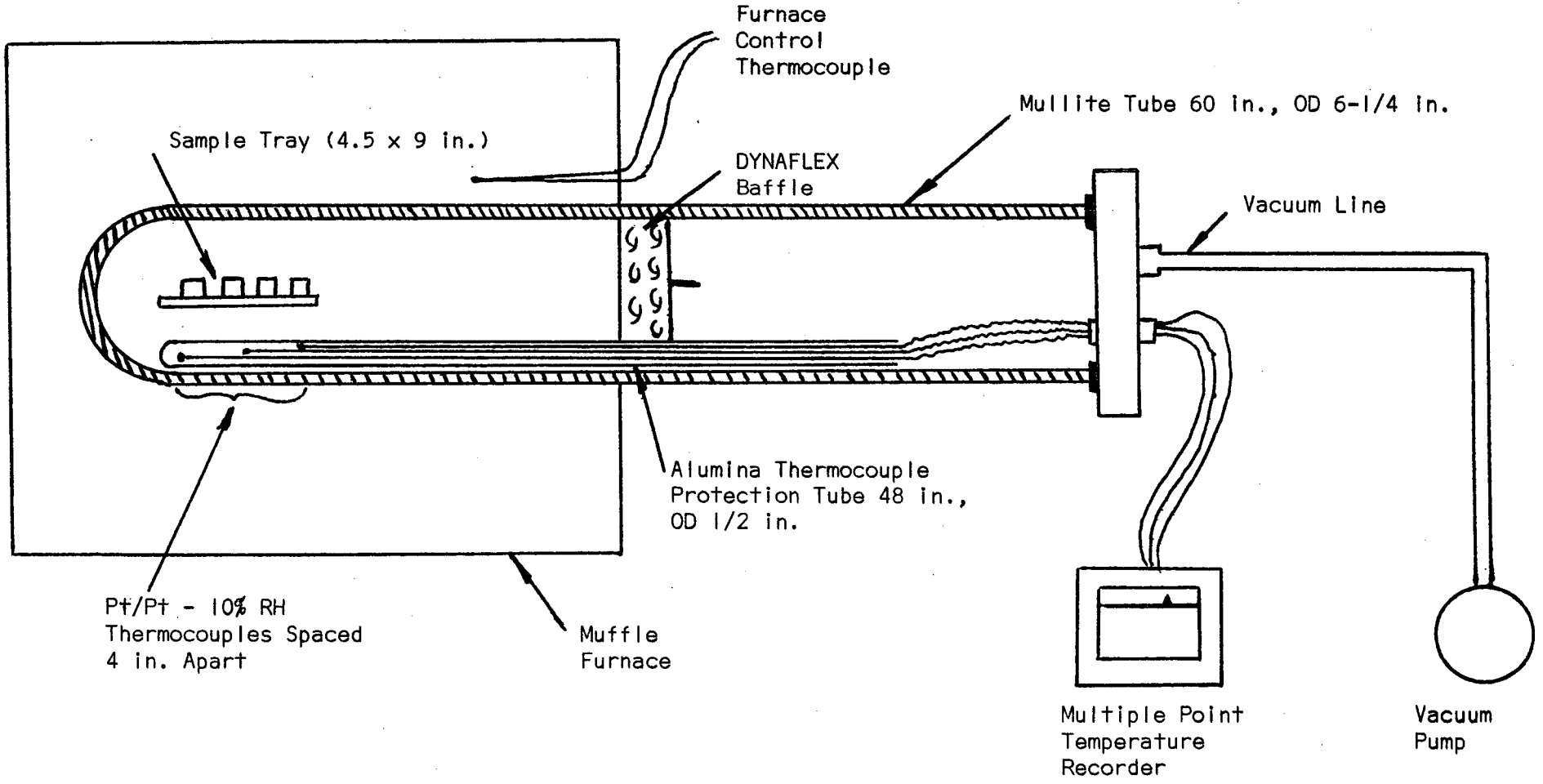

FIGURE 2-6.

CROSS SECTION OF THERMAL GRADIENT THERMAL CONDUCTIVITY APPARATUS

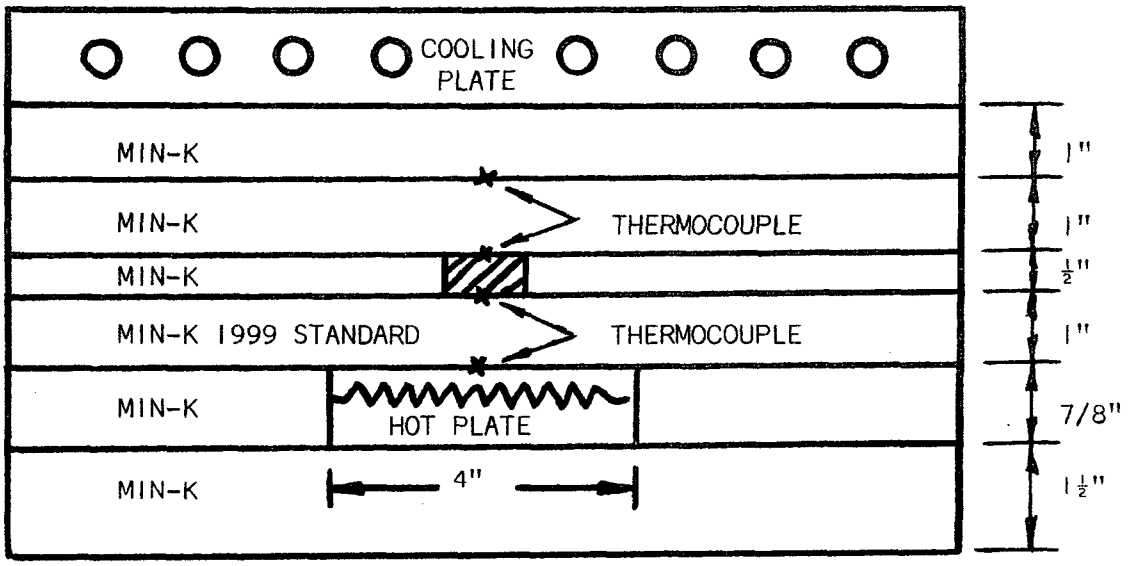

Each Layer is 12" x 12"

TABLE 2-4.

THERMAL STABILITY AND THERMAL CONDUCTIVITY OF MIN-K COMPOSITIONS

Sample	Number	Basis of Opacifier Addition	5hr Isothermal Heat Treatment	Density Before Heat Treatment pcf	Change in Density %	Thermal Conductivity @ 725F Mean Temp Btu in./hr ft^2 ^oF Air	Vacuum
MIN-K/CAB-O-SIL/TiO_2	1999	weight	none	19.2	----	0.24	0.16
	BS-12	weight	1400F, air	18.0	1.1	0.24	----
	BS-9	weight	1400F, vac	18.0	1.1	0.24	----
	H-1	weight	2000F, air	18.2	45.0	0.30	0.18
	F-G	weight	2000F, vac	17.8	18.5	0.27	0.17
MIN-K/ALON-C Gamma	88-2	----	none	21.4	----	0.40	0.27
	88-2A	----	2000F, air	19.6	10.7	0.43	0.28
	88-2B	----	2000F, vac	20.3	7.4	0.45	0.30
	BS-74	----	2200F, air	21.2	59.9	0.63	----
	BS-73	----	2200F, vac	17.7	66.7	0.64	0.29
MIN-K/ALON-C Gamma/TiO_2	88-1	weight	none	21.1	----	0.26	0.16
	BS-24	weight	1400F, air	17.5	0.0	0.26	----
	BS-21	weight	1400F, vac	21.4	0.0	0.28	----
	88-1A	weight	2000F, air	20.3	15.8	0.31	0.16
	88-1B	weight	2000F, vac	22.1	38.0	0.50	0.14
MIN-K/ALON-C Gamma/Cr_2O_3	BS-38	weight	2000F, air	19.0	6.3	0.38	0.26
	BS-37	weight	2000F, vac	17.5	5.1	0.31	0.19
MIN-K/ALON-C Gamma/$ZrSiO_4$	BS-40	weight	2000F, air	20.1	8.4	0.31	0.19
	BS-39	weight	2000F, vac	19.4	3.1	0.33	0.17
MIN-K/ALON-C Gamma/ZrO_2	BS-42	weight	2000F, air	19.9	8.5	0.26	0.20
	BS-41	weight	2000F, vac	19.6	4.1	0.30	0.20
MIN-K/ALON-C Alpha	112-5	----	none	30.6	----	0.45	0.19
	BS-62	----	2000F, air	30.2	6.0	0.49	0.18
	BS-61	----	2000F, vac	31.3	1.6	0.50	0.19
	BS-72	----	2200F, air	34.7	37.5	0.66	0.21
	BS-71	----	2200F, vac	32.6	25.5	0.65	0.20

TABLE 2-4. (CONTINUED)

Sample	Number	Basis of Opacifier Addition	5 hr Isothermal Heat Treatment	Density Before Heat Treatment pcf	Change in Density %	Thermal Conductivity @ 725F Mean Temp Btu in./hr ft^2 ^{o}F Air	Vacuum
MIN-K/ALON-C Alpha/TiO_2	112-1	weight	none	30.1	----	0.38	0.14
	BS-54	weight	2000F, air	32.1	1.2	0.38	0.14
	BS-53	weight	2000F, vac	29.9	2.3	0.42	0.14
	BS-64	weight	2200F, air	23.9	30.6	0.57	0.16
	BS-63	weight	2200F, vac	28.5	15.1	0.54	0.18
MIN-K/ALON-C Alpha/Cr_2O_3	112-2	weight	none	30.5	----	0.35	0.15
	BS-56	weight	2000F, air	30.8	1.0	0.35	0.15
	BS-55	weight	2000F, vac	26.0	3.1	0.40	0.15
	BS-66	weight	2200F, air	29.7	25.3	0.51	0.17
	BS-65	weight	2200F, vac	24.1	6.6	0.53	0.20
MIN-K/ALON-C Alpha/$ZrSiO_4$	112-3	weight	none	27.3	----	0.39	0.16
	BS-58	weight	2000F, air	29.8	2.3	0.40	0.16
	BS-57	weight	2000F, vac	31.9	3.1	0.39	0.15
	BS-68	weight	2200F, air	27.8	14.4	0.58	0.19
	BS-67	weight	2200F, vac	27.5	6.2	0.47	0.18
MIN-K/ALON-C Alpha/ZrO_2	112-4	weight	none	28.9	----	0.36	0.15
	BS-60	weight	2000F, air	28.6	2.1	0.40	0.15
	BS-59	weight	2000F, vac	27.7	3.6	0.39	0.15
	BS-70	weight	2200F, air	27.0	16.3	0.56	0.18
	BS-69	weight	2200F, vac	27.6	14.5	0.50	0.17
MIN-K/ALON-C Alpha/TiO_2	112-1	mol	none	30.1	----	0.38	0.14
	BS-54	mol	2000F, air	32.1	1.2	0.38	0.14
	BS-53	mol	2000F, vac	29.9	2.3	0.42	0.14
	BS-64	mol	2200F, air	23.9	30.6	0.57	0.16
	BS-63	mol	2200F, vac	28.5	15.1	0.54	0.18
MIN-K/ALON-C Alpha/Cr_2O_3	115-1	mol	none	36.4	----	0.36	0.12
	BS-82	mol	2000F, air	31.6	-2.8	0.41	0.15
	BS-81	mol	2000F, vac	32.5	-1.8	0.46	0.14
	BS-76	mol	2200F, air	33.2	13.0	0.44	0.13
	BS-75	mol	2200F, vac	33.8	9.2	0.47	[illegible]

TABLE 2-4. (CONTINUED)

Sample	Number	Basis of Opacifier Addition	5 hr Isothermal Heat Treatment	Density Before Heat Treatment pcf	Change in Density %	Thermal Conductivity @ 725F Mean Temp Btu in./hr ft^2 ^oF Air	Vacuum
MIN-K/ALON-C Alpha/$ZrSiO_4$	115-3	mol	none	34.8	----	0.40	0.13
	BS-86	mol	2000F, air	27.4	-0.4	0.44	0.15
	BS-85	mol	2000F, vac	34.8	-0.3	0.48	0.15
	BS-80	mol	2200F, air	37.6	10.1	0.49	0.14
	BS-79	mol	2200F, vac	34.6	2.9	0.50	0.19
MIN-K/ALON-C Alpha/ZrO_2	115-2	mol	none	31.6	----	0.36	0.12
	BS-84	mol	2000F, air	34.9	-0.3	0.45	0.14
	BS-83	mol	2000F, vac	36.2	0.8	0.45	0.14
	BS-78	mol	2200F, air	30.3	3.3	0.54	0.15
	BS-77	mol	2200F, vac	39.5	11.1	0.60	0.19

It can be seen from Table 2-4 that at 1400F, the MIN-K structure using ALON-C gamma in place of CAB-O-SIL M5 was more stable in an atmosphere of either air or vacuum (BS-12 & 9 vs BS 24 & 21). However, at 2000F, a significant density change was observed for these ALON-C gamma samples under both air and vacuum conditions (88-1A & 1B). This density change appeared to be tied up with the TiO_2 opacifier in the samples. Those samples containing no opacifier, or different opacifiers, did not show this amount of change (88-2A & 2B, BS-38 & 37, BS-40 & 39, and BS-42 & 41).

It can be further seen from Table 2-4 that samples containing the converted ALON-C alpha were significantly more stable (less density change) than those containing ALON-C gamma. This was true of both the 2000F (88-1A & 1B vs BS-54 & 53; 88-2A & 2B vs BS-62 & 61) and 2200F heat treatments (BS-74 & 73 vs BS-72 & 71). It should be kept in mind when comparing ALON-C alpha specimens with ALON-C gamma specimens that the specimens containing ALON-C alpha were approximately 30 pcf instead of the normal 20 pcf in order to obtain sufficient handling strength.

Specimens containing ALON-C alpha alumina and opacifiers other than TiO_2 similarly exhibited a greater thermal stability than their counterpart specimens containing ALON-C gamma (BS-38 & 77, BS-40 & 39, BS-42 & 41 vs BS-56 & 55, BS-58 & 57, BS-60 & 59). It is of particular significance that the ALON-C alpha samples containing opacifiers showed greater thermal stability than those ALON-C alpha samples without opacification. In other words, the opacifiers themselves acted as sintering inhibitors.

For a better comparison of the effect of different opacifiers on thermal stability, the opacifiers were also added to specimens on an equal mol basis. It can be seen from Table 2-4 that there was a definite improvement in the thermal stability of the samples containing the heavier opacifiers (Cr_2O_3, $ZrSiO_4$, ZrO_2) added on an equal mol basis with the standard TiO_2. This increased stability was probably the result of the additional amount of the more stable opacifier material in the sample composition. The small negative changes in density resulted because of a slight increase in sample thickness after heat treatment.

Thermal Conductivity. Also shown in Table 2-4 are the thermal conductivity values for each specimen. From a thermal conductivity standpoint, the ALON-C gamma bodies compared favorably with the MIN-K body containing CAB-O-SIL M5 (Sample #1999 vs 88-1). However, as the heat treatment temperature increased, a marked increase in conductivity in air of the MIN-K/ALON-C gamma/TiO_2 specimens was noted, while the conductivity in vacuum remained essentially constant. Two conclusions could be drawn from this phenomenon: (1) the pore size between ALON-C particles was increasing, thus increasing the air conduction component within the specimen, and (2) the particles were not sintering to a sufficient density to increase the solid conduction component.

The first conclusion was supported by the scanning electron micrographs shown in Figures 2-7, 2-8, and 2-9. This technique permits the examination of a freshly fractured surface of the specimen, and at moderate mignification yields a three-dimensional view of the undisturbed surface. It can be seen in Figure 2-7 that local particle agglomeration (before heat treatment) is minimized. Following the exposure to 2000F in air (Figure 2-8), agglomerates were more pronounced, while at 2000F in vacuum (Figure 2-9), the ALON-C had formed definite "islands" of agglomerates, with an accompanying increase in pore size. The cause of this agglomeration was undoubtedly the conversion of the ALON-C from the gamma to the alpha structure, the effect of which was shown previously in Figures 2-3 and 2-4 taken by the "rub-out" electron microscope technique.

In contrast, the MIN-K/ALON-C alpha/TiO_2 specimens (#112-1, BS-54, BS-53, BS-64, and BS-63) had a higher thermal conductivity in air prior to heat treatment, but showed less of a change than the ALON-C gamma specimens even when fired to 2200F. As before, however, the conductivity in vacuum was unaffected up to 2000F, but showed some increase following the 2200F heat treatments.

The advantage of an opacifier for blocking radiation under both vacuum and air conditions is clearly evident in Table 2-4. Opacifiers Cr_2O_3, $ZrSiO_4$, and ZrO_2 all appear to have merit as substitutes for TiO_2 in bodies containing ALON-C. In fact, there was good evidence that TiO_2 acted to some degree as a sintering flux, expecially in the case of specimens containing ALON-C gamma and fired at 2000F. It was less evident, however, when ALON-C alpha specimens were fired to 2200F. However, the tendency of the TiO_2 to act as a sintering flux would lead to the speculation that with significantly longer exposures to elevated temperature, the effect would become more apparent.

From a strictly thermal conductivity standpoint, there was no significant overall advantage to adding the heavier opacifiers (Cr_2O_3, $ZrSiO_4$, ZrO_2) on an equal mol basis with TiO_2. This applies not only when comparing weight and mol additions of the same opacifier, but also when comparing TiO_2 and the other opacifiers on a mol basis. Only samples in the unfired condition, and samples heat treated at 2200F in air appeared to show an improvement when measured under vacuum conditions (comparing equal weight and equal mol additions of the same opacifier).

POROSITY AND PORE SIZE DISTRIBUTION

Test Procedure. After the thermal conductivity determination, the samples were cut for porosity measurements. Both total porosity and pore size distribution values were obtained using an Aminco-Winslow Porosimeter. This apparatus uses mercury penetration under pressure to determine pore sizes ranging from 0.035 to 100 microns. Samples for porosity measurements were approximately 1/4 in. cubes cut from the interior of the experimental samples. Care was taken not to include the skin of any specimen. An average of five porosimeter tests was used to obtain the values reported for each sample.

FIGURE 2-7.

MIN-K/ALON-C GAMMA/TiO_2
UNFIRED CONTROL
MAG: 800X

10 microns

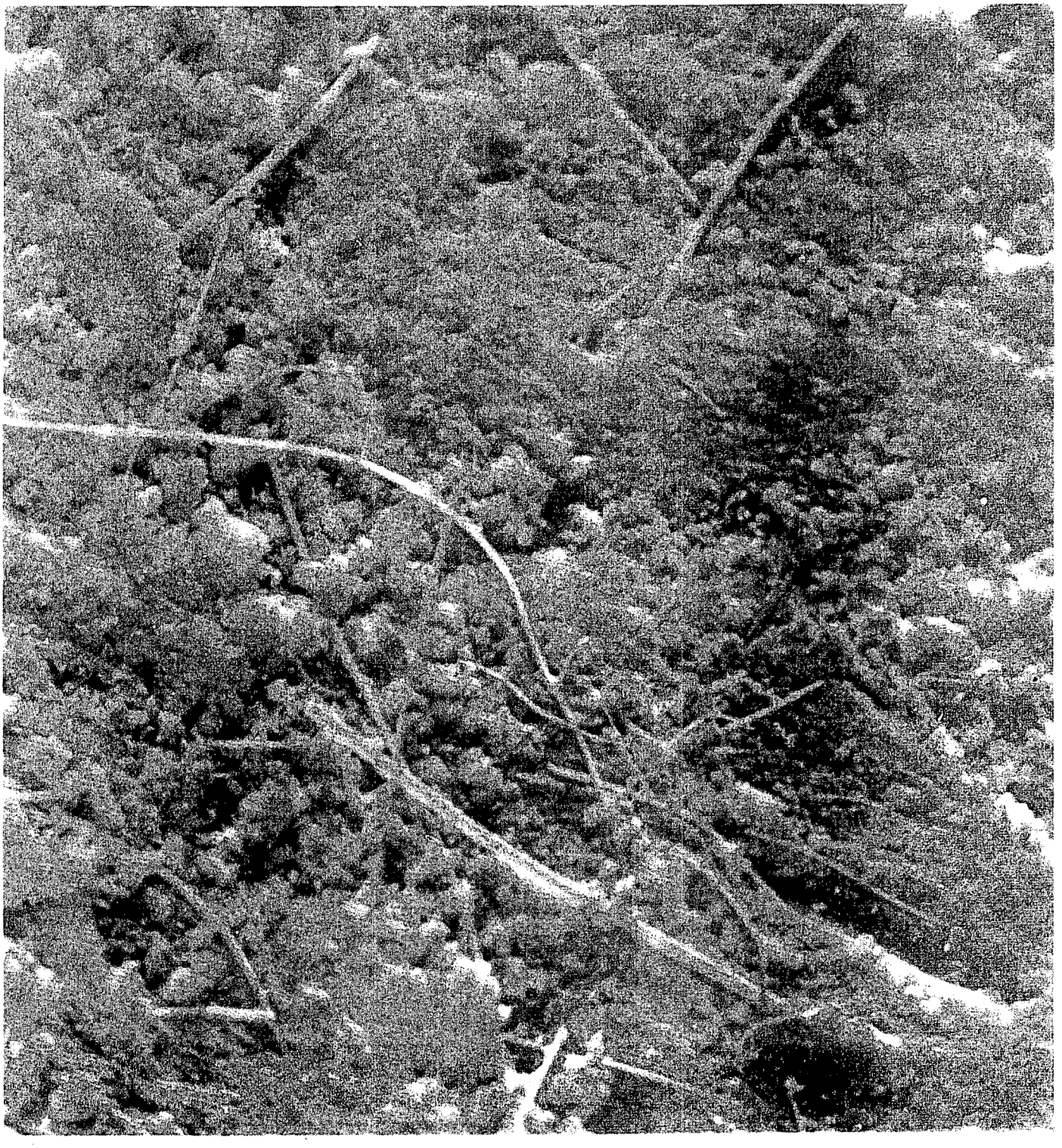

NEG 3582-1

FIGURE 2-8.

MIN-K/ALON-C GAMMA/TiO_2
2000F FOR 5 HR IN AIR
MAG: 800X

10 microns

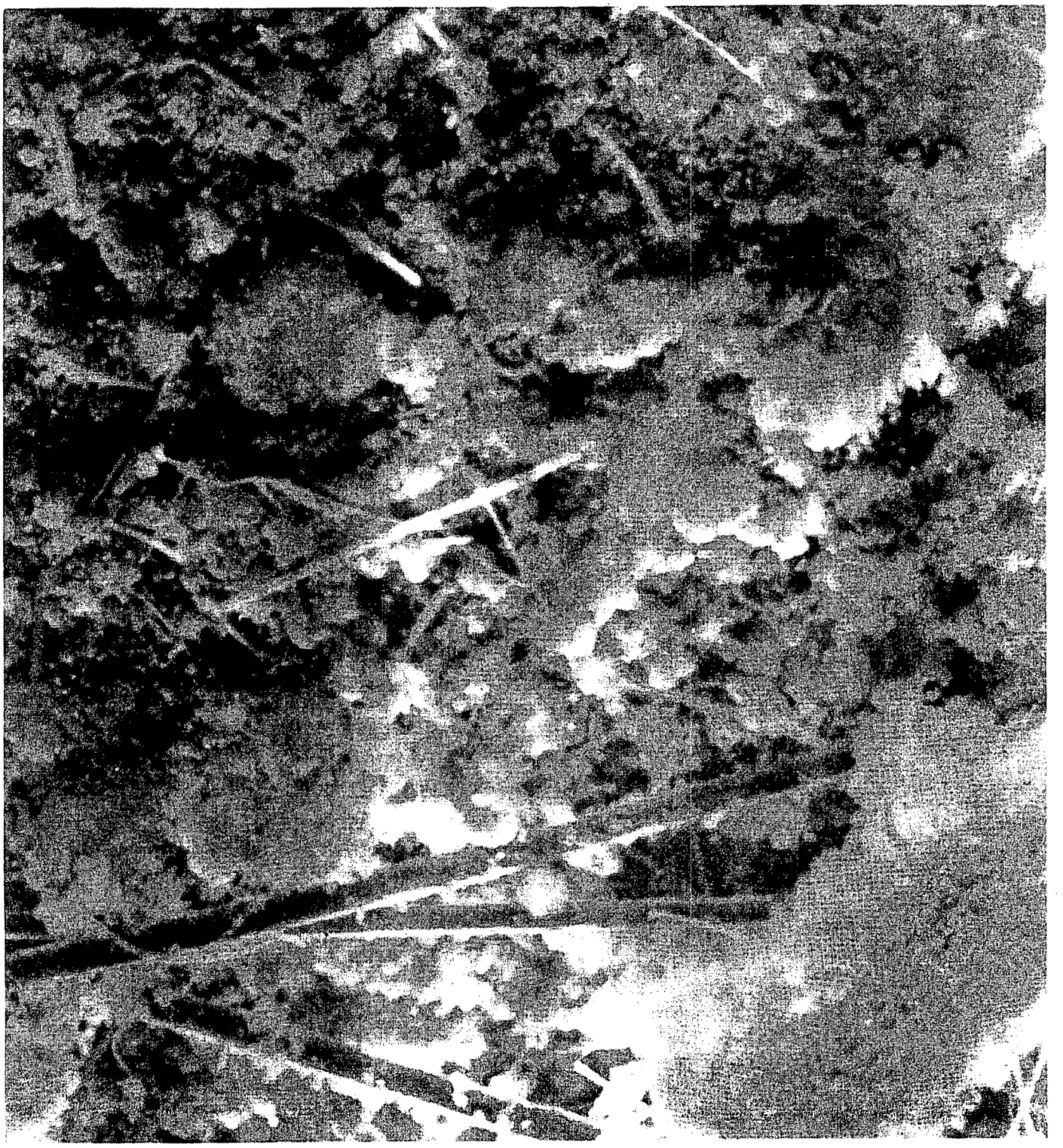

NEG 9582-4

FIGURE 2-9.

MIN-K/ALON-C GAMMA/TiO_2
2000F FOR 5 HR IN VACUUM
MAG: 800X

10 microns

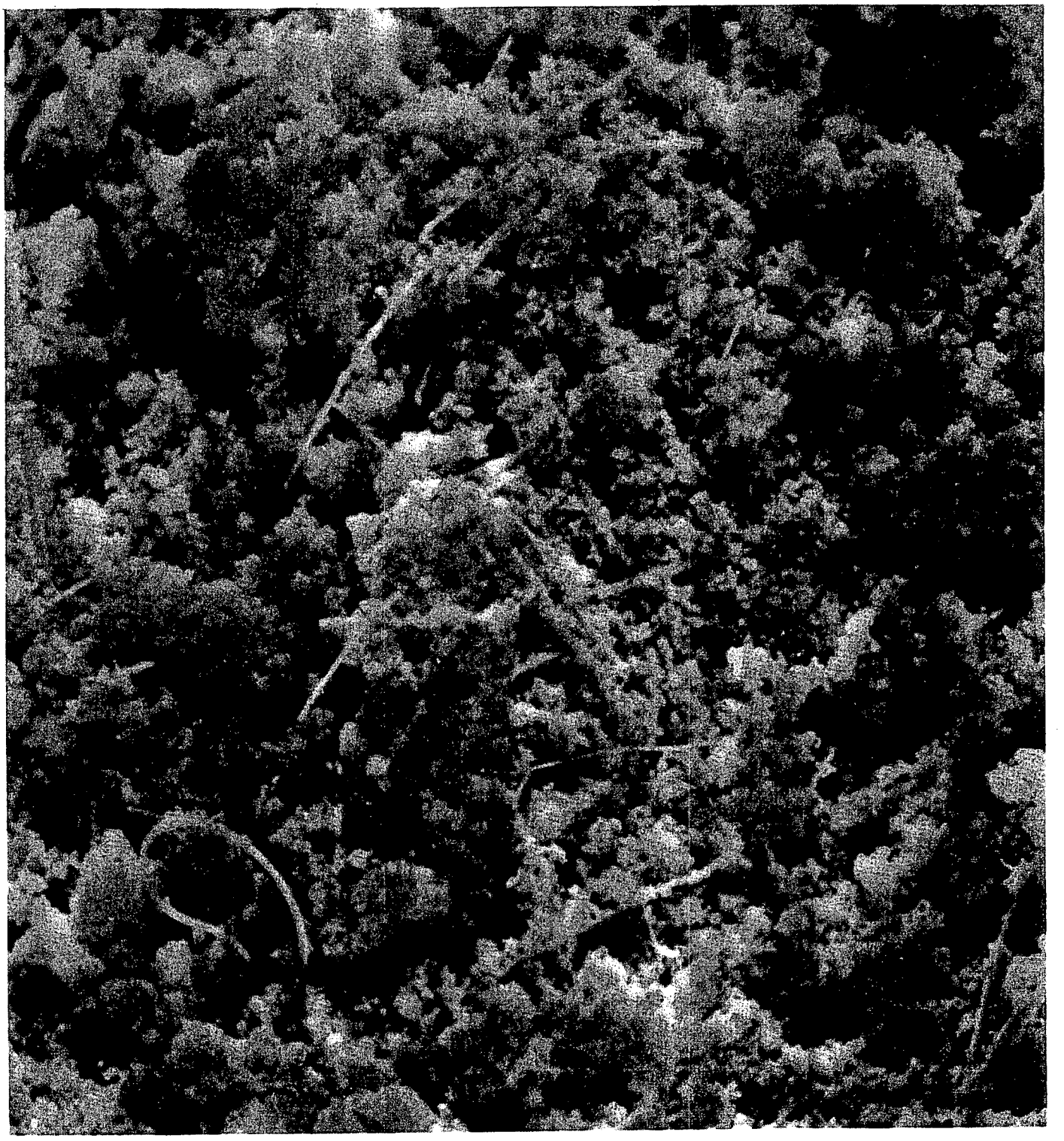

NEG 9582-17

Results. Figures 2-10 through 2-16 present in bar graph form the results of the porosity tests. All graphs are drawn to the same scale to permit a direct comparison of the pore size distribution between different specimens and heat treatments.

It can be seen from Figure 2-10 that there was less change in the total porosity and pore size distribution in the MIN-K/CAB-O-SIL/TiO_2 (MIN-K 1999) specimens which were heat treated in vacuum than in those heat treated in air. The literature points out that the presence of moisture in an air atmosphere accounts for a higher sintering rate of SiO_2 in air than in vacuum because the OH^- ions disrupt the silica lattice structure and promote atomic diffusion. This fact was also in evidence in the electron micrographs of Figures 2-7, 2-8, and 2-9 (presented during the discussion on thermal conductivity). These electron micrographs showed pure CAB-O-SIL discs (prepared by a modified "rub-out" technique) before and after exposure to 2000F in air and vacuum. (Particles were dispersed in water, and a dilute droplet was allowed to dry on the carbon coated electron grid of the electron microscope.) The CAB-O-SIL particles exposed to 2000F in air definitely showed a greater amount of sintering than those exposed to 2000F under vacuum conditions. Note from Figure 2-10 that during sintering, the pores became smaller so that the percentage of fine pores was actually increased. The fact that the thermal conductivity in air increased (samples H-1 and F-G of Table 2-4) in spite of this greater percentage of fine pores would indicate that the solid conductivity component was increased.

In the case of MIN-K/ALON-C gamma/TiO_2 samples (Figure 2-11), there was a greater change in total porosity and pore size distribution in the samples heat treated in vacuum than in those heat treated in air. In fact, the significant shift in pore size distribution was only noted for samples containing ALON-C gamma and TiO_2. This again was further evidence that TiO_2 acts as a fluxing agent in the presence of ALON-C gamma, particularly under vacuum conditions.

Porosimeter data showed that unfired formulations containing ALON-C gamma had a greater number of fine pores needed for the MIN-K conductivity effect than formulations containing ALON-C alpha (compare Figures 2-12a and 2-12b with Figures 2-12c and 2-12d). Note that these fine pores still remained in samples heat treated in either air or vacuum up to 2000F (see Figures 2-13 and 2-14). This differed from the porosimeter results of Figure 2-11 discussed above. However, the present samples did not contain the TiO_2 opacifier with its associated fluxing action.

The effect of exposure to 2200F in air and vacuum on the MIN-K/ALON-C alpha and MIN-K/ALON-C gamma specimens is shown in Figures 2-15 and 2-16, respectively. The almost total loss of fine pore structure confirmed the fact that these specimens no longer acted as a MIN-K body when evaluated for thermal conductivity in air (see Table 2-4).

FIGURE 2-10.

TOTAL POROSITY AND PORE SIZE DISTRIBUTION
OF MIN-K 1999

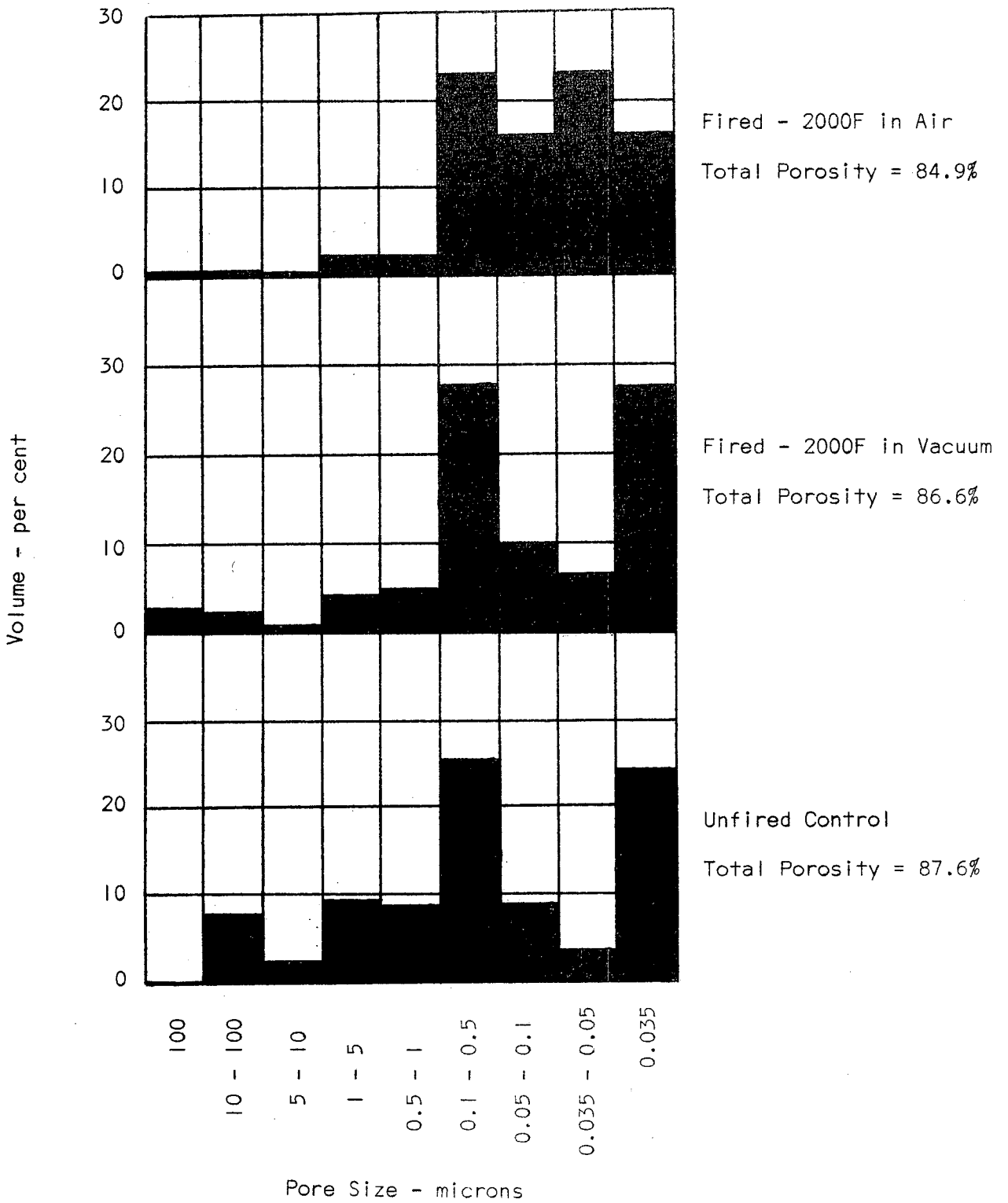

FIGURE 2-11.

TOTAL POROSITY AND PORE SIZE DISTRIBUTION
OF MIN-K/ALON-C GAMMA/TiO_2 FORMULATION

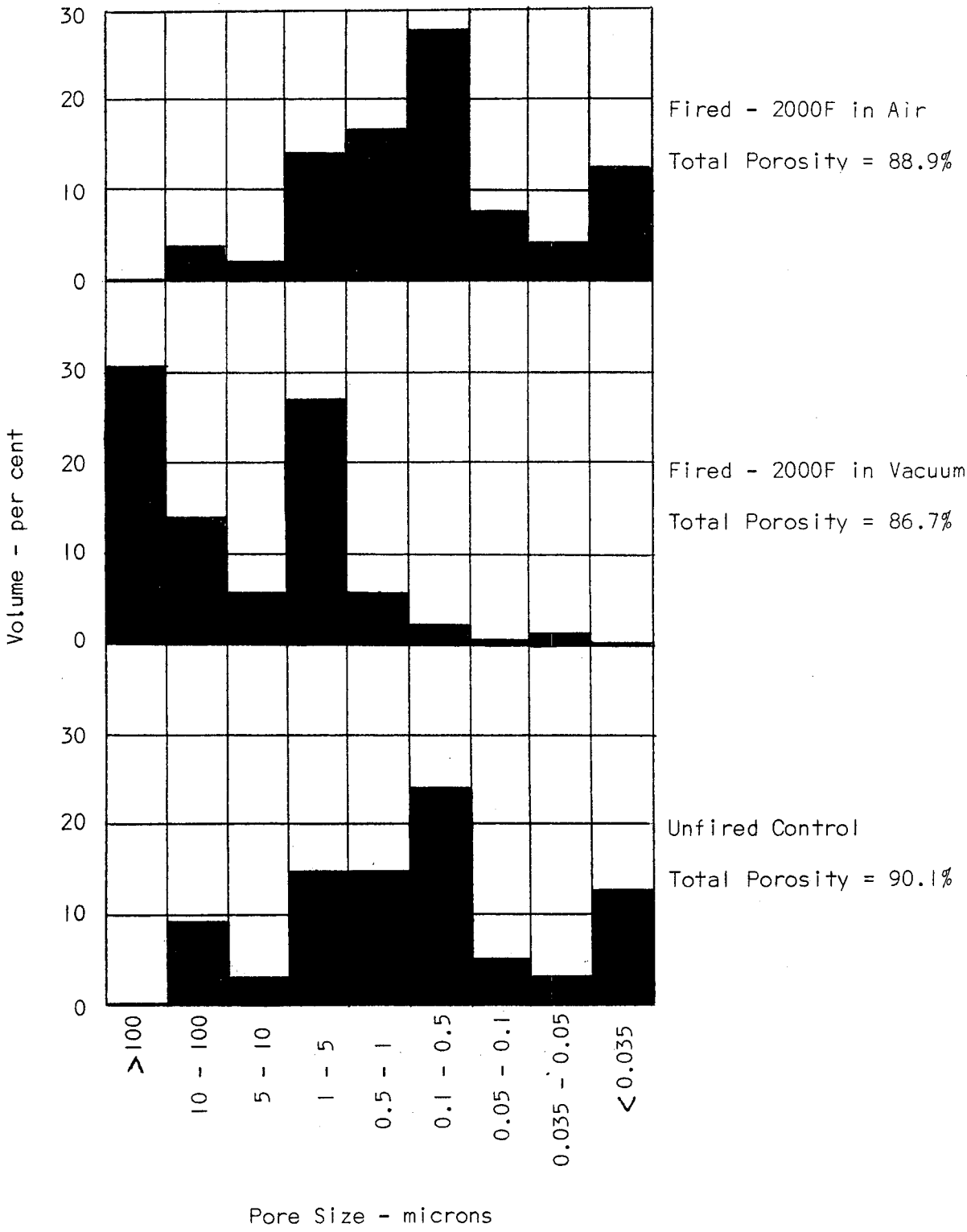

FIGURE 2-12.

PORE SIZE DISTRIBUTION AND TOTAL POROSITY OF UNFIRED ALON-C SPECIMENS

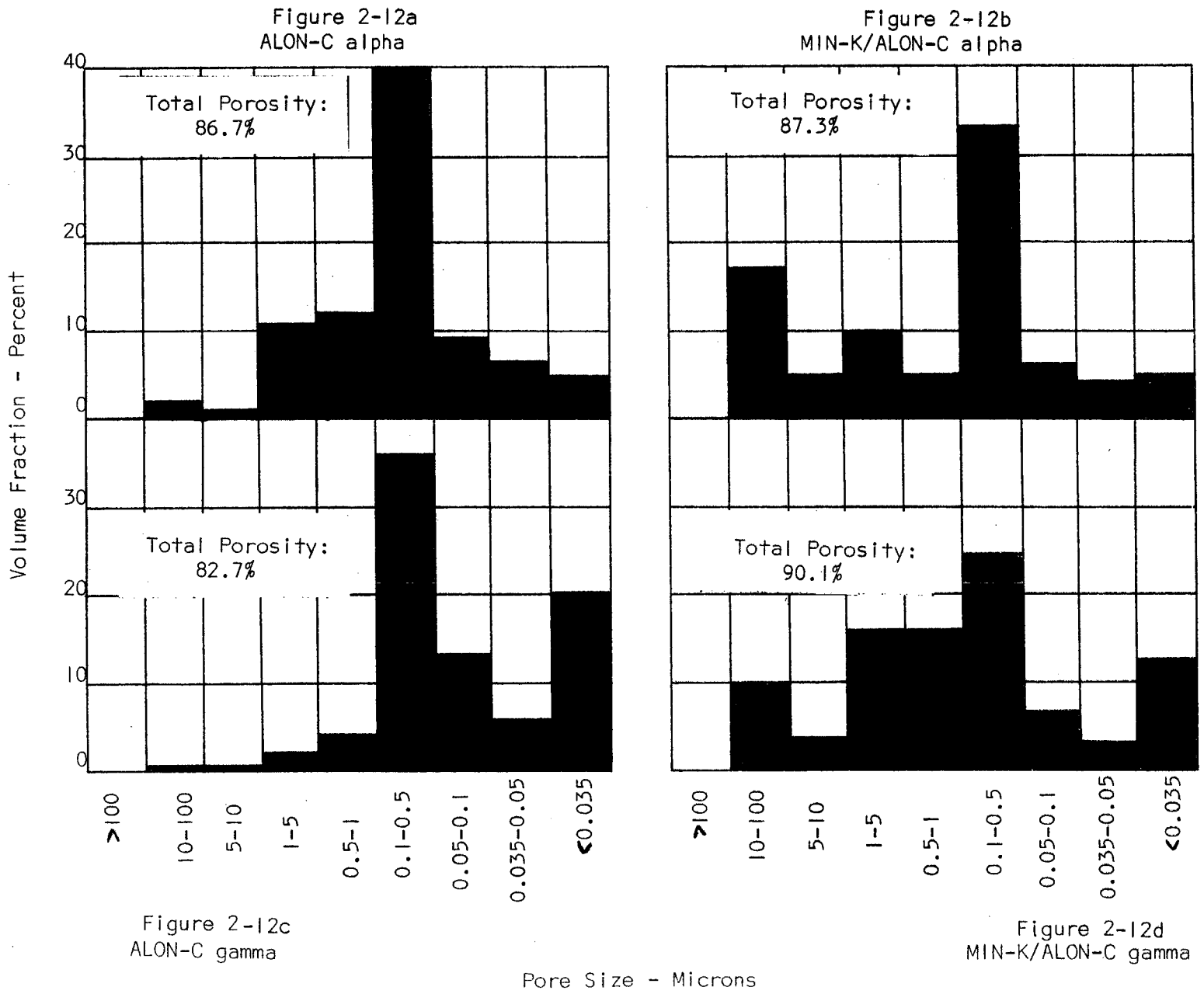

FIGURE 2-13.

PORE SIZE AND TOTAL POROSITY OF
MIN-K/ALON-C ALPHA SPECIMENS EXPOSED TO 2000F FOR 5 HR

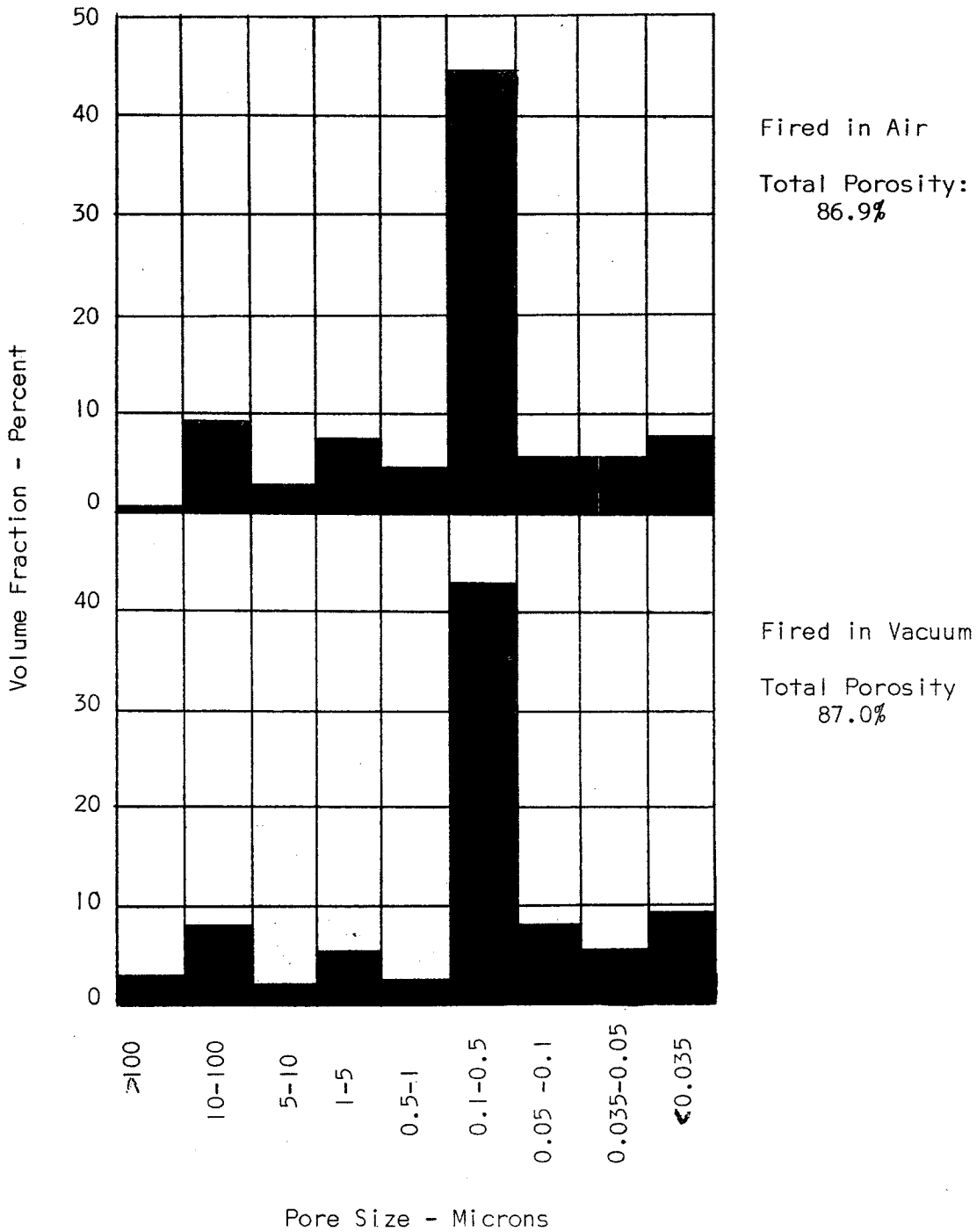

FIGURE 2-14.

PORE SIZE AND TOTAL PROOSITY OF
MIN-K/ALON-C GAMMA SPECIMENS EXPOSED TO 2000F FOR 5 HR

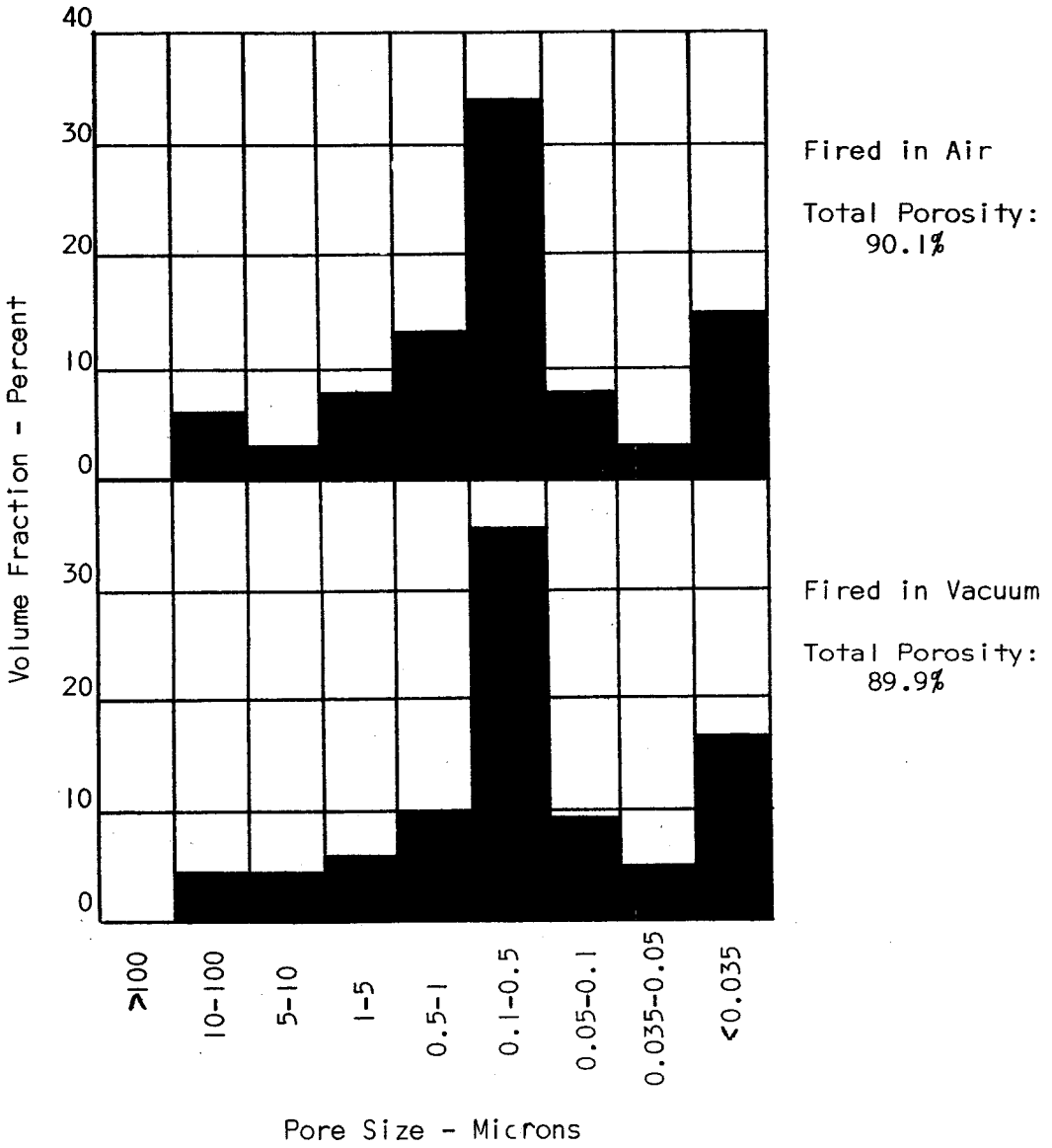

FIGURE 2-15.

PORE SIZE AND TOTAL POROSITY OF MIN-K/ALON-C " PHA SPECIMENS
EXPOSED TO 2200F FOR 5 HR

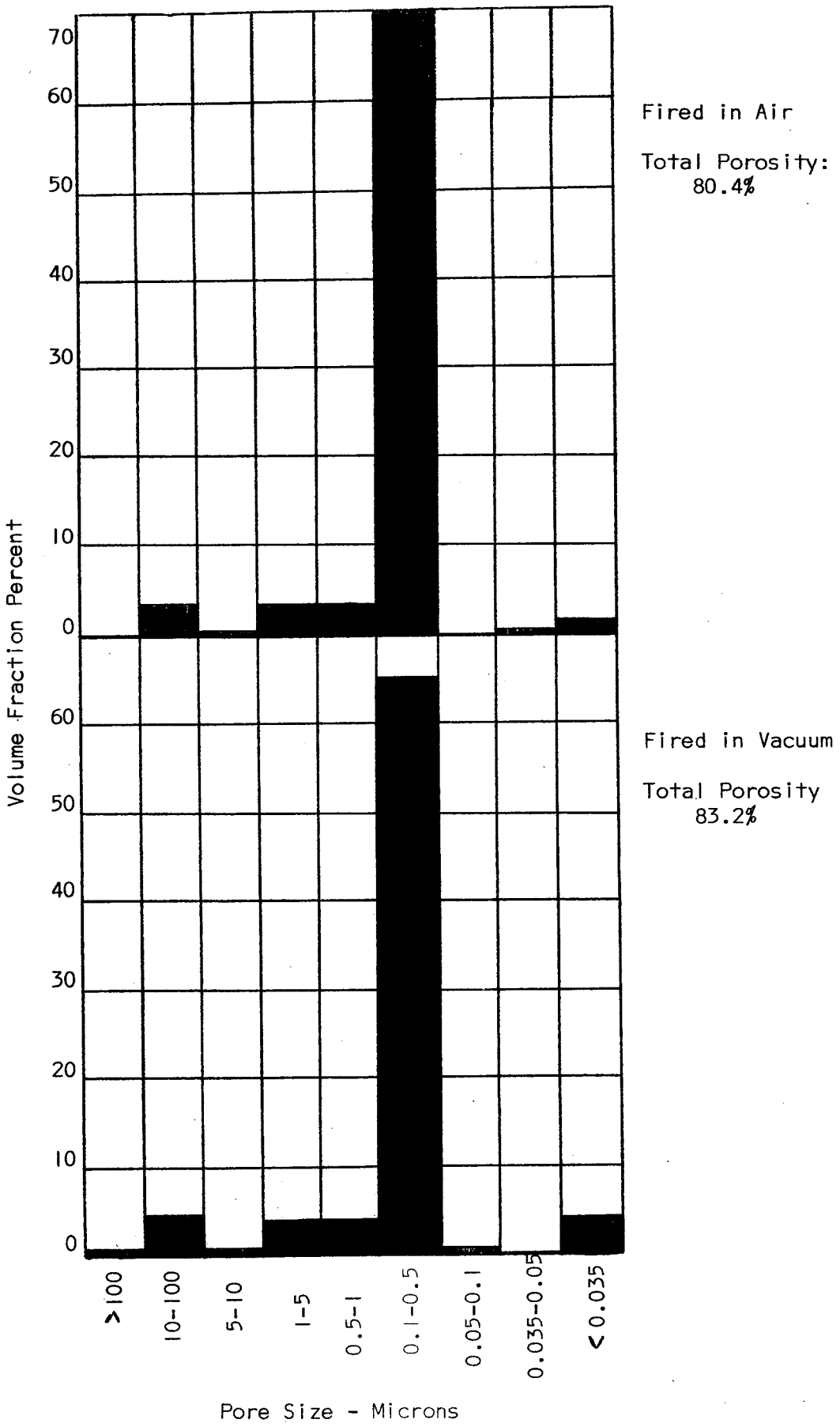

FIGURE 2-16.

PORE SIZE AND TOTAL POROSITY OF MIN-K/ALON-C GAMMA SPECIMENS
EXPOSED TO 2200F FOR 5 HOURS

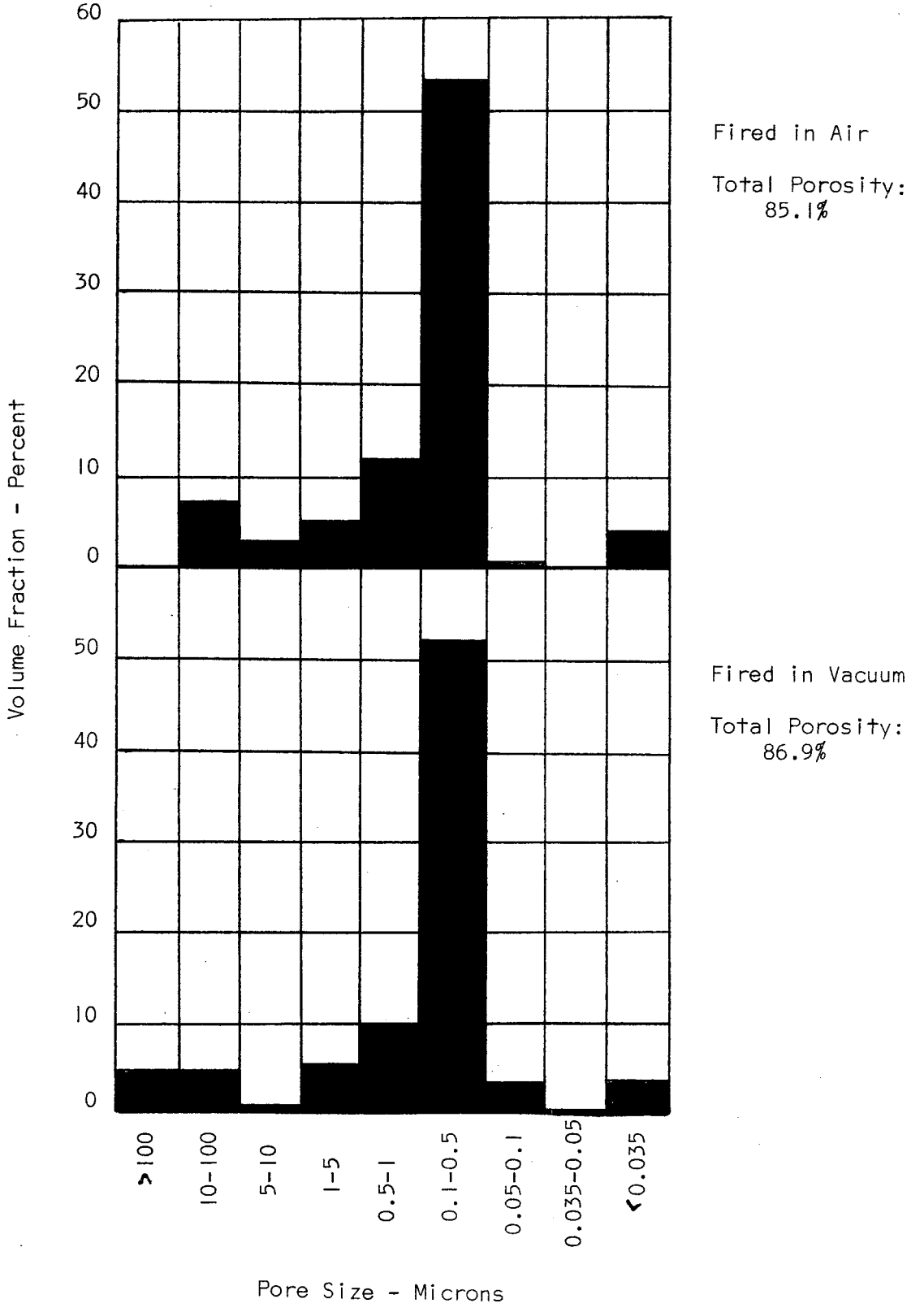

It is also of particular interest that the pore size tended to center around 0.1 to 0.5 microns regardless of the type of specimen or exposure condition. It has been suggested (see Literature Survey) that submicron size particles will agglomerate or sinter to a specific size at some temperature below the normal sintering temperature, and maintain this size until the normal sintering temperature is attained. This initial sintering has been attributed to Van der Waal's forces. The current porosimeter data supported this hypothesis with respect to the ALON-C particles.

Electron micrographs of heat treated ALON-C also appeared to support this hypothesis. Figures 2-3 and 2-4 presented earlier are "rub-out" electron micrographs of ALON-C before and after heat treatment, respectively. Before exposure to 2200F (Figure 2-3), the ALON-C was primarily gamma alumina with an average particle size of 0.03 microns. Note, however, that there were a number of considerably larger particles which account for the wide distribution of pore sizes even in unfired ALON-C. After exposure to 2200F, much of the ALON-C was converted to the alpha form. However, the alpha agglomerates or crystals did take on what appeared to be a certain limiting size as observed in Figure 2-4.

The only deviation from the apparent tendency toward the 0.1 to 0.5 micron pore size occurred when the MIN-K/ALON-C gamma/TiO_2 specimens were heated to 2000F in vacuum for 5 hr (Figure 2-11). In this instance, the pore size increased significantly, indicating that the particles were also significantly larger, due to a fluxing action of the titania. This was substantiated by an electron micrograph (Figure 2-17) which shows the enlarged crystals, as well as some which apparently had not been affected by the titania.

MICROSTRUCTURE

The changes in overall microstructure of the specimens as a result of the various heat treatments was best detected by scanning electron micrographs, some of which have already been presented. These, together with the electron micrograph specimens prepared by the "rub-out" technique resulted in a relatively complete story as to the changes undergone by these specimens.

Although the scanning electron micrographs were taken at magnifications as high as 10,000X, excessive magnification did not give a satisfactory overall view of the microstructure. Consequently, all those presented in this report were taken at 100X and subsequently blown up to 800X. The "rub-out" micrographs are all at 27,500X magnification, since the purpose of these was to study the individual particles or agglomerates.

FIGURE 2-17.

MIN-K/ALON-C GAMMA/TiO_2
2000F FOR 5 HR IN VACUUM
MAG: 27,500X

1 micron

EMS 735-A

Effect of Temperature and Atmosphere. Fugures 2-18 to 2-23 are scanning electron micrographs of two MIN-K type bodies before and after heat treatment under both air and vacuum conditions. It will be noted that the MIN-K 1999 specimens (Figures 2-18, 2-19, and 2-20) appear to be more compacted, from an overall structural viewpoint, as a result of the heat treatment. In contrast, the structure of the MIN-K/ALON-C gamma/TiO_2 specimens (Figures 2-21, 2-22, and 2-23) appears to become more open with heat treatment as previously mentioned in the discussion under thermal conductivity. (Figures 2-21, 2-22, and 2-23 are identical with Figures 2-7, 2-8, and 2-9). In the presence of titania, the ALON-C gamma sintered significantly even at 2000F, and in so doing, eliminated the submicron pores, but increased the number of larger pores. This effect was far more evident following the vacuum exposure than the air exposure, and confirmed the earlier porosimeter measurements (Figure 2-11). As a result of this sintering, the thermal conductivity of these specimens increased significantly when measured in air. However, when measured in vacuum where gas conductivity was not a factor, the thermal conductivity showed no appreciable increase, indicating no significant increase in solid conduction.

Figures 2-24 through 2-29 are electron micrographs by the "rub-out" technique of the same bodies as shown in Figures 2-18 through 2-23. It can be seen from Figures 2-24 through 2-26 that in the case of the MIN-K/CAB-O-SIL/TiO_2 specimens, there was more sintering of the submicron SiO_2 particles after heat treatment in air than after heat treatment in vacuum. As noted in the discussion of the porosimeter results, this was because of the increased sintering rate of SiO_2 in the presence of water vapor which was not present in the vacuum firing. It is interesting to note in Figure 2-24 the presence of a single fiber and two titania particles.

In the case of MIN-K/ALON-C gamma/TiO_2, it can be seen from Figures 2-27 through 2-29 that a significant amount of sintering took place during the vacuum heat treatment. The hexagonal nature of the resulting crystals can easily be distinguished in Figure 2-29, in contrast to the irregularly shaped, rough surfaced opacifier particle shown in Figure 2-24. Less sintering is noted in the heat treatment of Figure 2-28. Again, these electron micrographs are further confirmation of data which were presented in the discussion of Porosity.

Effect of Titania Opacifier. Further evidence of the effect of the fluxing action of titania on ALON-C is shown in the scanning electron micrographs (Figures 2-30 through 2-33). These specimens contained no titania opacifier.

Figures 2-30 and 2-31 may be compared directly with Figures 2-21 and 2-23, respectively, taken of specimens which contained the opacifier. Even though the specimen in Figure 2-31 was exposed to 2200F rather than 2000F as was the Figure 2-23 specimen, the large pores visible in Figure 2-23 are noticeably absent in Figure 2-31. In general, there was no significant macro changes between the two specimens depicted in Figures 2-30 and 2-31 other than an increase in density. The same conclusion was reached for the specimens made with ALON-C alpha shown in Figure 2-32 and 2-33.

FIGURE 2-18.

MIN-K/CAB-O-SIL/TiO_2 (MIN-K 1999)
UNFIRED CONTROL
MAG: 800X

10 microns

NEG 9582-8

FIGURE 2-19.

MIN-K/CAB-O-SIL/TiO_2 (MIN-K 1999)
2000F FOR 5 HR IN AIR
MAG: 800X

10 microns

NEG 9582-20

FIGURE 2-20.

MIN-K/CAB-O-SIL/TiO_2 (MIN-K 1999)
2000F FOR 5 HR IN VACUUM
MAG: 800X

10 microns

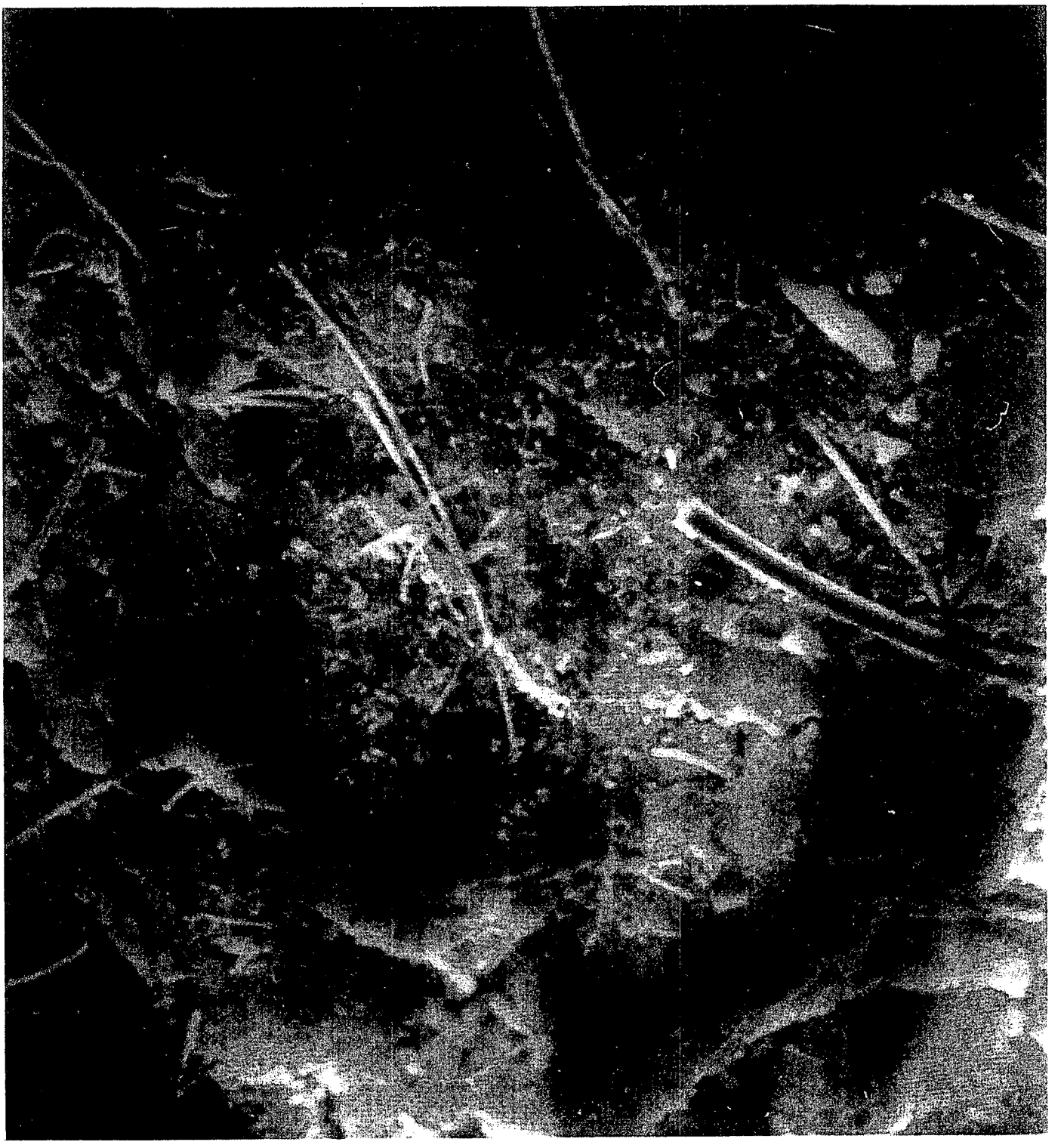

NEG 9582-14

FIGURE 2-21.

MIN-K/ALON-C GAMMA/TiO_2
UNFIRED CONTROL
MAG: 800X

10 microns

NEG 9582-11

FIGURE 2-22.

MIN-K/ALON-C GAMMA/TiO_2
2000F FOR 5 HR IN AIR
MAG: 800X

10 microns

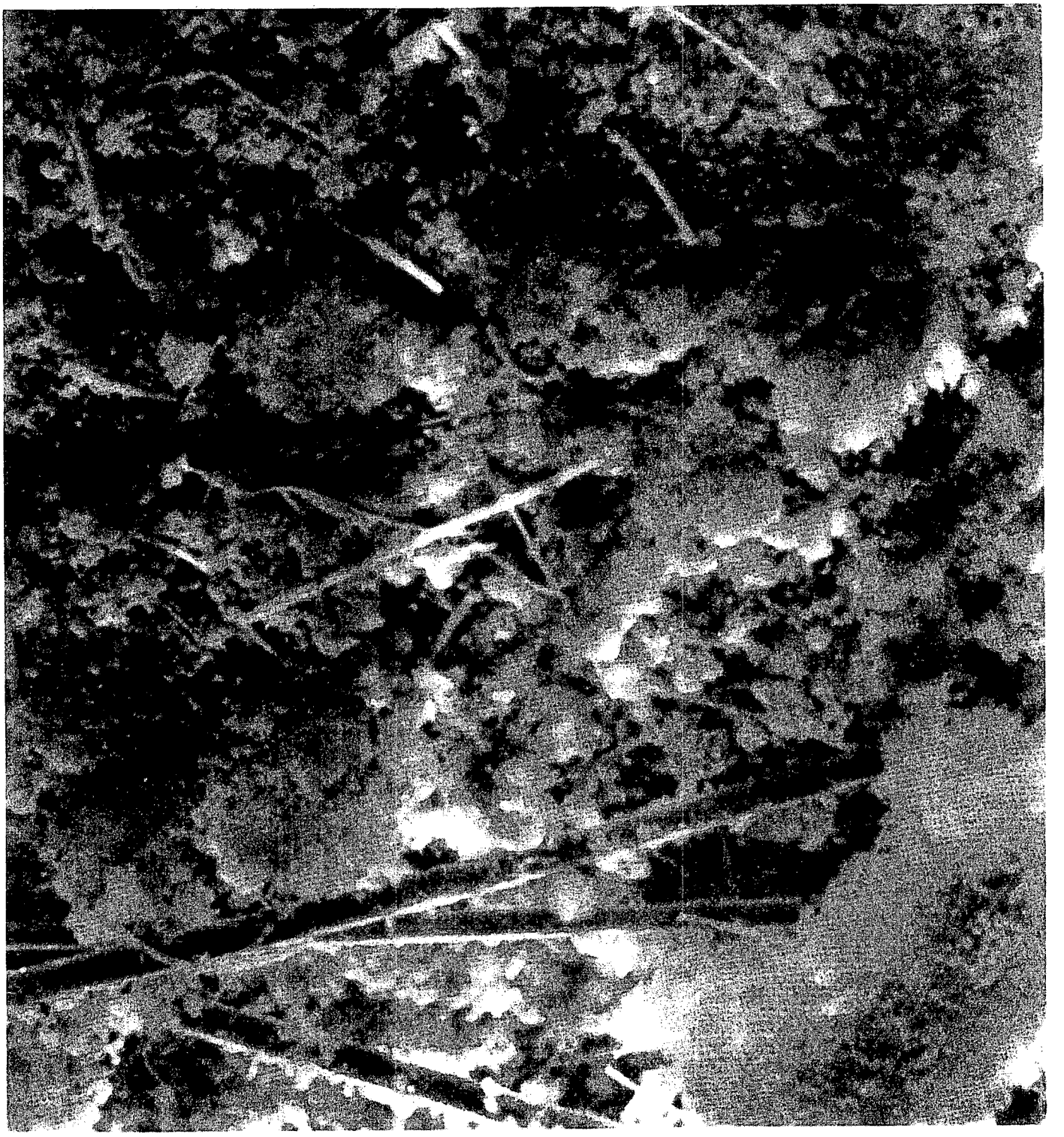

NEG 9582-4

FIGURE 2-23.

MIN-K/ALON-C GAMMA/TiO_2
2000F FOR 5 HR IN VACUUM
MAG: 800X

10 microns

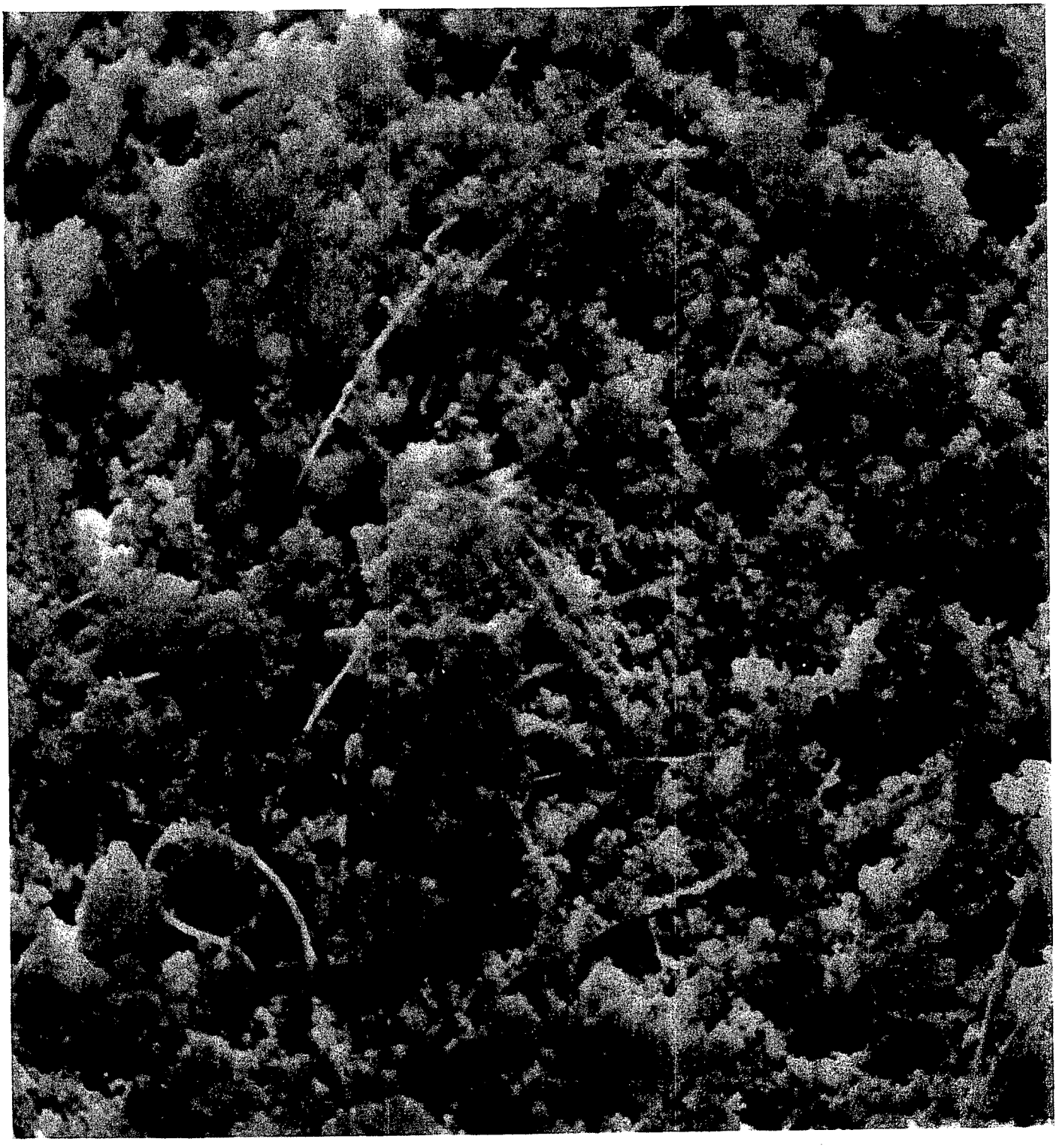

NEG 9582-17

FIGURE 2-24.

MIN-K/CAB-O-SIL/TiO_2 (MIN-K 1999)
UNFIRED CONTROL
MAG: 27,500X

1 micron

FIGURE 2-25.

MIN-K/CAB-O-SIL/TiO_2 (MIN-K 1999)
2000F FOR 5 HR IN AIR
MAG: 27,500X

1 micron

FIGURE 2-27.

MIN-K/ALON-C GAMMA/TiO_2
UNFIRED CONTROL
MAG: 27,500X

1 micron

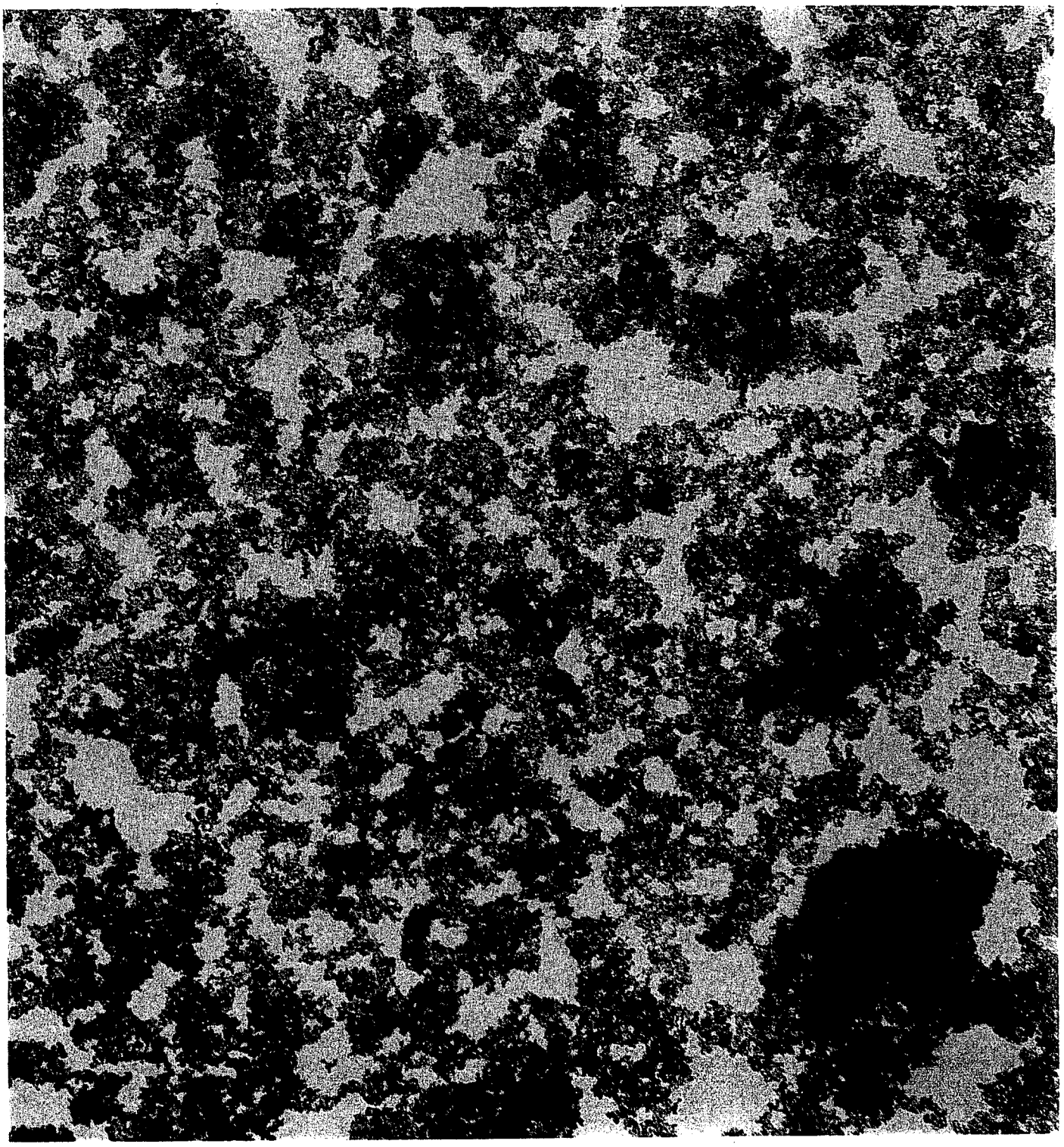

FIGURE 2-28.

MIN-K/ALON-C GAMMA/TiO_2
2000F FOR 5 HR IN AIR
MAG: 27,500X

1 micron

FIGURE 2-29.

MIN-K/ALON-C GAMMA/TiO_2
2000F FOR 5 HR IN VACUUM
MAG: 27,500X

1 micron

EMS 735-A

FIGURE 2-30.

MIN-K/ALON-C GAMMA
UNFIRED CONTROL
MAG: 800X

10 microns

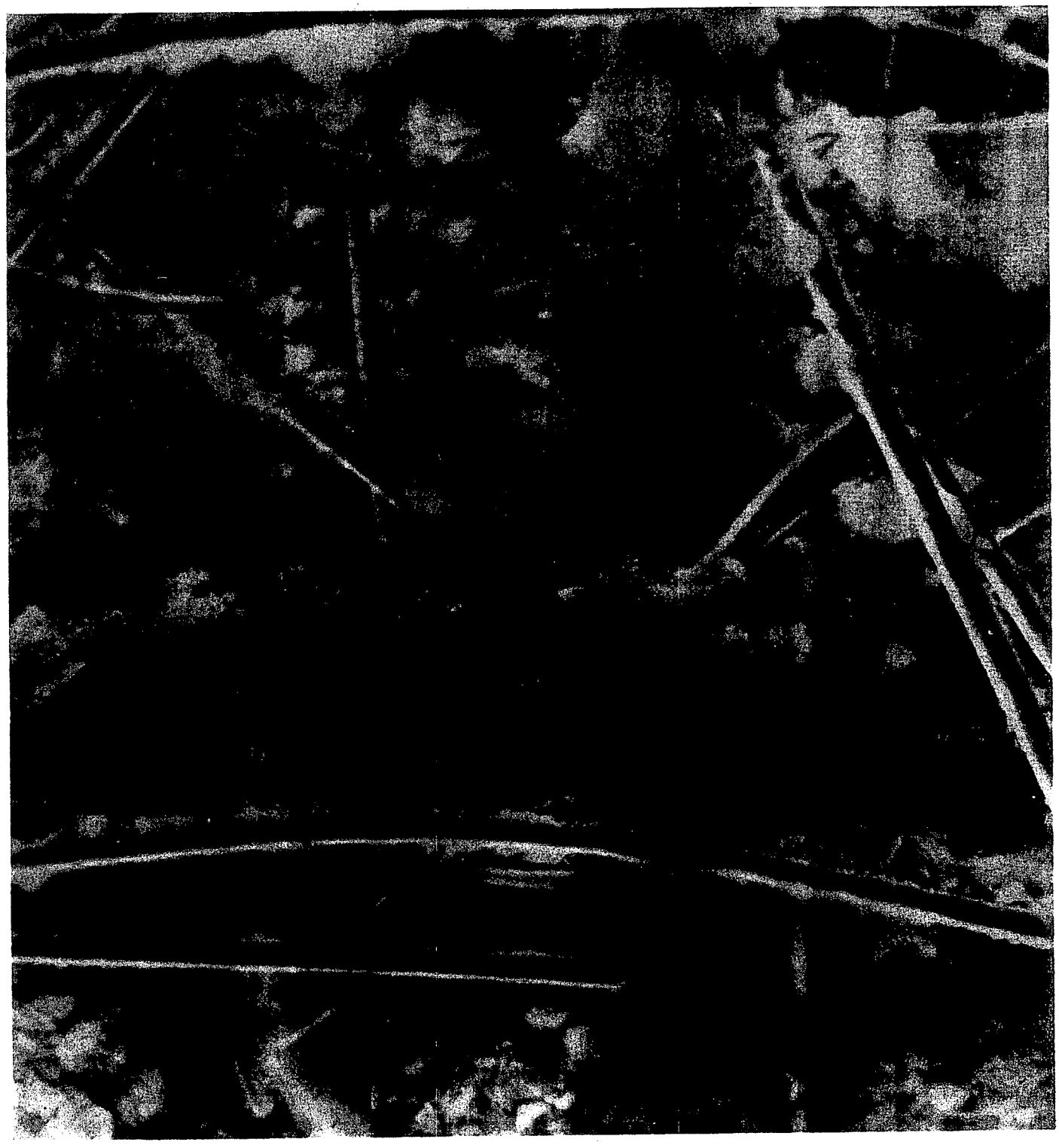

NEG 8-30-68-2-12

FIGURE 2-31.

MIN-K/ALON-C GAMMA
2200F FOR 5 HR IN VACUUM
MAG: 800X

10 microns

NEG 9-14-68-1-11

FIGURE 2-32.

MIN-K/ALON-C ALPHA
UNFIRED CONTROL
MAG: 800X

10 microns

NEG 9-14-68-1-14

FIGURE 2-33.

MIN-K/ALON-C ALPHA
2200F FOR 5 HR IN AIR
MAG: 800X

10 microns

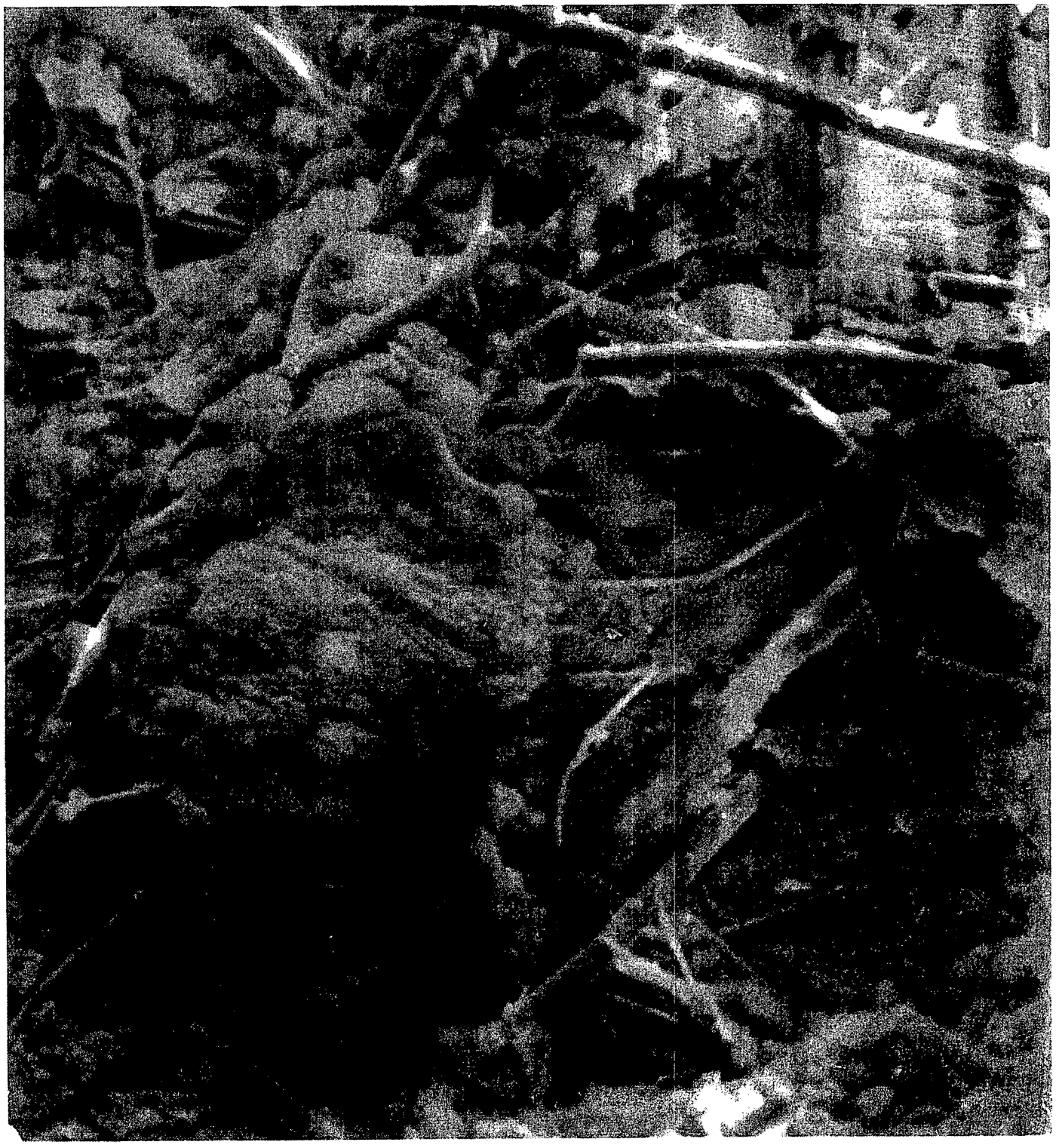

NEG 9-14-68-1-23

The same comparison was also made between opacified and unopacified specimens subjected to lower temperatures and air and vacuum conditions. In all instances, the scanning electron micrographs appeared essentially the same as those presented in Figures 2-30 through 2-33.

SHRINKAGE INHIBITORS

Introduction. From the results of the thermal conductivity and porosimeter tests, and from the electron micrographs, it became apparent that ALON-C gamma would convert to ALON-C alpha when exposed to elevated temperatures with the resultant increase in pore size. Although the increase in pore size was apparently not harmful to the thermal conductivity of the material in vacuum (long-term exposure may result in an increase due to solid conductivity), the material would no longer have the MIN-K effect in a gaseous media. Under such circumstances, the proposed 2200F product would have a limited usefulness. Consequently, it was apparent that some means of preventing this agglomeration should be investigated.

Shrinkage of a product consisting primarily of particles can be attributed in part to the agglomeration of the individual particles as a result of surface interaction or diffusion. Frequently, this interaction can be retarded through the use of small quantities of a foreign ion which interrupt this process and act as agglomerating inhibitors. Thus, an investigation was undertaken to determine what ions might act as shrinkage inhibitors for ALON-C. To accomplish this, samples were prepared with various additives which were known to have an effect on the sintering of high density alumina.

Shrinkage Inhibitor Candidates. The samples were prepared by compressing 1.3 g of powdered sample mixtures into 1/4-in. thick discs using a laboratory press (Carver) with a 1-1/8-in. diameter die. The density of the finished samples was 20 pcf nominal. In order to facilitate the screening of the inhibitors, no opacifiers or reinforcing fibers were used. The particle size of the inhibitors generally ranged between 20 and 70 microns, with a few particles in the 100 to 170 micron range. The firings were carried out in air at 2200F for 2 hr, and the effectiveness of the inhibitor was determined by the diameter shrinkage of the disc. Table 2-5 summarizes the results of the inhibitor evaluation. All comparisons were based on the shrinkage of pure ALON-C. Thus, the symbol "0" indicates that the inhibitor did not alter the amount of shrinkage of the ALON-C, the symbol "+" indicates that the inhibitor resulted in greater shrinkage, and the symbol "-" indicates that the inhibitor resulted in less shrinkage.

Potassium sulphate and sodium floride appeared to act as the best shrinkage inhibitors for ALON-C. These materials were investigated further with respect in the amount of inhibitor, the associated anion ($SO^{=}_{4}$ and F^{-}), and the cation (K^{+} and Na^{+}). These results are tabulated in Tables 2-6, 2-7, and 2-8. The effect of inhibitor quantity is also shown in Figure 2-34.

TABLE 2-5.

ADDITIVES AND THEIR EFFECT ON THE SHRINKAGE OF ALON-C COMPOSITIONS

Additive	Amount (Weight, %)	Effect on Shrinkage*
TiO_2 (submicron)	2.3	0
TiO_2 (submicron)	6.9	+
Cr_2O_3 (pigment grade)	2.3	0
Cr_2O_3 (pigment grade)	7.7	-
ZnO	2.3	+
ZnO	7.7	-
MgO	2.3	0
MgO	7.7	-
CaO	2.3	0
CaO	7.7	-
SiO_2	2.3	-
Nb_2O_3	2.3	+
V_2O_5	2.3	-
$VOSO_4$	2.3	0
La_2O_3	2.3	0
ZrO_2 (submicron)	2.3	0
CaF_2	2.3	-
Al (metal powder)	2.3	-
Si (metal powder)	2.3	0
Mo (metal powder)	2.3	-
Zn (metal powder)	2.3	-
Sn (metal powder)	2.3	-
LiCl	2.3	-
Li_2CO_3	2.3	-
Sb_2O_3	2.3	-
K_2SO_4	2.3	-
NaF	2.3	-

* + = increased shrinkage

0 = no effect on shrinkage

- = decreased shrinkage

TABLE 2-6.

SHRINKAGE INHIBITORS FOR ALON-C COMPOSITIONS

Inhibitor	Particle Size (mesh)	Amount Added Weight, %	Amount Added Mol, %	Linear Shrinkage, %
K_2SO_4	-200	1.0	0.6	14.7
K_2SO_4	-200	2.3	1.3	8.5
K_2SO_4	-325	1.0	0.6	15.8
K_2SO_4	-325	2.0	1.2	10.2
K_2SO_4	-325	4.0	2.4	7.0
K_2SO_4	-325	6.0	3.6	6.7
K_2SO_4	-325	8.0	4.9	6.7
K_2SO_4	-325	10.0	6.6	8.8
K_2SO_4	-325	15.0	9.4	17.5
NaF	-200	0.5	1.2	19.2
NaF	-200	1.0	2.4	11.2
NaF	-200	2.3	5.3	8.8
NaF	-325	1.0	2.4	10.5

TABLE 2-7.

SHRINKAGE INHIBITORS FOR ALON-C COMPOSITIONS HAVING COMMON ANION

Inhibitor	Particle Size (mesh)	Amount Added		Linear Shrinkage, %
		Weight, %	Mol, %	
NaF	-200	2.3	5.3	8.8
KF	-200	2.3	3.9	8.8
LiF	-200	2.3	8.4	19.3
MgF_2	-200	2.3	3.7	22.7
KCl	-200	2.3	3.1	9.5
NaCl	-200	2.3	3.9	9.5
CsCl	-200	2.3	1.4	16.5
K_2SO_4	-200	2.3	1.3	8.5
Na_2SO_4	-200	2.3	1.6	15.7
K_2SO_4	-325	4.0	2.4	7.0
Na_2SO_4	-325	4.6	3.2	8.8

TABLE 2-8.

SHRINKAGE INHIBITORS FOR ALON-C COMPOSITIONS HAVING COMMON CATION

Inhibitor	Particle Size (mesh)	Amount Added Weight, %	Amount Added Mol, %	Linear Shrinkage, %
KF	-200	2.3	3.9	8.8
KCl	-200	2.3	3.1	9.5
K_2SO_4	-200	2.3	1.3	8.5
K_2CO_3	-200	2.3	1.7	12.3
K_2HPO_4	-200	2.3	1.3	15.1
NaF	-200	2.3	5.3	8.8
NaCl	-200	2.3	3.9	9.5
Na_2SO_4	-200	2.3	1.6	15.7
Na_2SO_4	-325	2.3	1.6	12.3
Na_2SO_4	-325	4.6	3.2	8.8
Na_3PO_3	-325	2.3	2.3	17.5

FIGURE 2-34.

EFFECT OF INHIBITOR CONCENTRATION ON THE SHRINKAGE OF ALON-C COMPOSITIONS

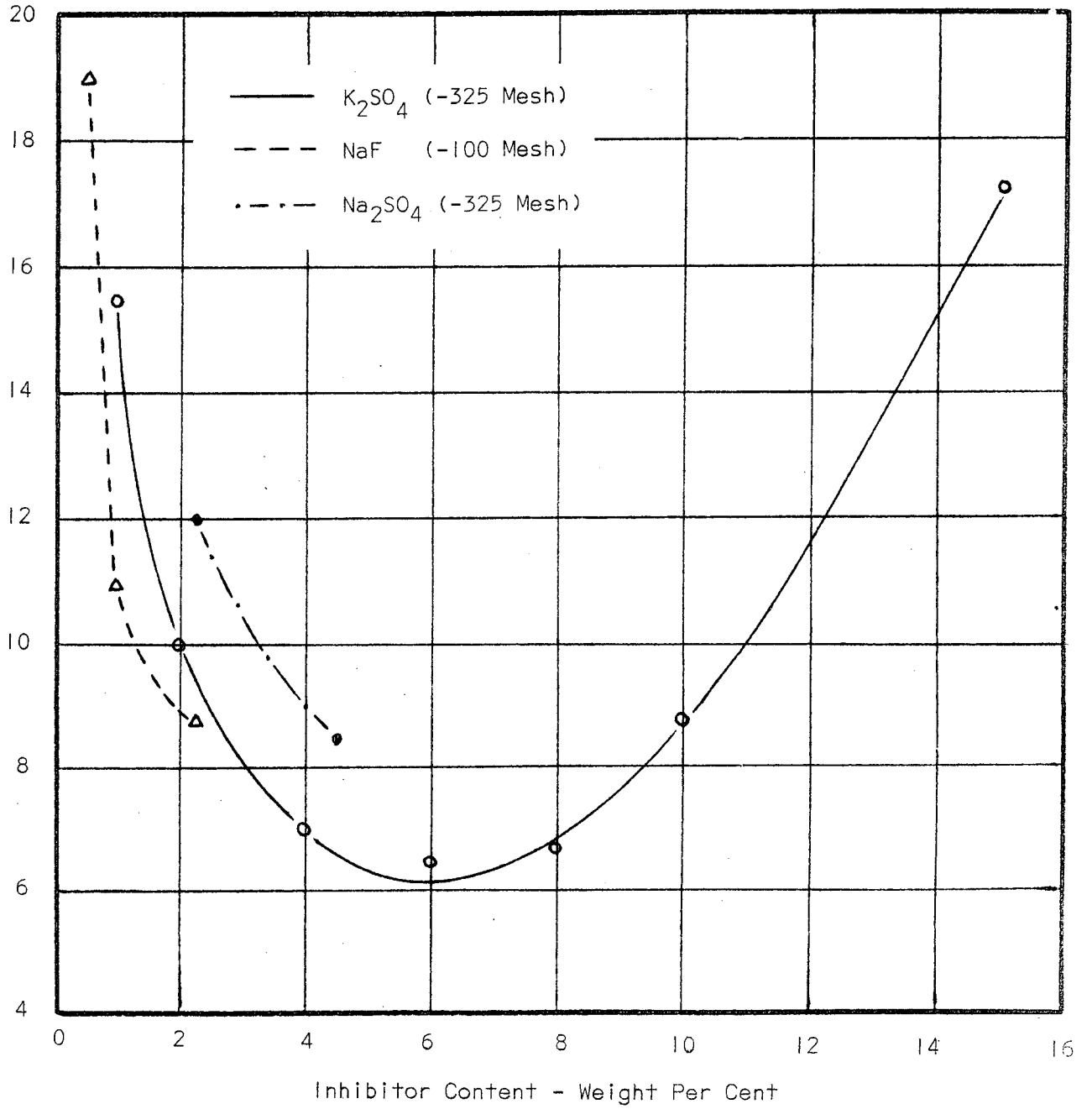

Based on these preliminary tests, it appeared that the potassium compounds were, in general, better than the sodium compounds, and that the cation, rather than the anion was the controlling factor. Potassium sulphate in the amounts of approximately 6 per cent by weight appeared to be the best.

Evaluation of Potassium Compounds. A designed experiment was carried out to establish by statistical analysis the best inhibitor, optimum concentration and particle size of inhibitors, and compatibility of the inhibitor with titania opacifier. The thermal stability of the experimental compositions in air and vacuum at 2200F for 2 hr was the criterion for evaluation.

Three potassium inhibitor compounds (K_2SO_4, K_2CO_3, and KCL) were subjected to various milling processes. The average particle size range resulting from these processes is shown in Table 2-9.

The MIN-K/ALON-C gamma mixtures containing ALON-C gamma, fiber, inhibitor, and opacifier, were prepared in the following manner. The fibers (1/4-in. ASTROQUARTZ staple, and MICRO-QUARTZ) were premixed by passing them twice through a willower (Tornado blower). The fiber mixture was then placed into a Waring Blendor along with the powdered ingredients (ALON-C gamma, inhibitor, and opacifier) and blended for 3-1/2 min at a low speed (achieved by supplying only 30 volts to the Blendor through a variable transformer). Samples were prepared by compressing the dry mixtures into discs having a diameter of 1-1/8 in. and a thickness of 1/2 in. The density of the discs was 20 pcf nominal.

The entire experiment consisted of 215 specimens. Half of these specimens were fired in air and half in vacuum. All of the specimens were made with ALON-C gamma, and half contained TiO_2 opacifier, while the others contained no opacifier. The amount of inhibitor used was 0.5 mol per cent, 1.5 mol per cent, and 5 mol per cent. Duplicate specimens were tested for each formulation. The performance of each specimen was based upon the change in diameter as a result of the isothermal exposure. Due to the small size of the specimens, the measurement accuracy was estimated to be approximately ± 2 per cent. Table 2-10 summarizes the variables investigated.

The experimental data were subjected to an analysis of variance with the aid of a time-shared computer system. The analysis indicated that the particle size of the inhibitor had no effect on the shrinkage inhibiting action. This was somewhat surprising since it was anticipated that maximum inhibitor efficiency would be achieved as its particle size more nearly approached that of the ALON-C. It is entirely possible, however, that such is still the case, since the smallest particle size range which could be evaluated (2 to 6 microns) was still approximately 100 times larger than the ALON-C particle. The effects of the other three variables, type of inhibitor, inhibitor content, and presence of TiO_2 opacifier each were found to be statistically significant. Tables 2-11 and 2-12 present the average shrinkages of the specimens in air and vacuum,

TABLE 2-9.

EFFECT OF SIZING PROCESS ON INHIBITOR PARTICLE SIZE

Inhibitor	Average Particle Size Range, microns		
	Screened (-325 Mesh)	Ball Milled	Air Jet Milled
K_2SO_4	25 - 37	12	3 - 6
K_2CO_3	25 - 37	6 - 12	2 - 3
KCl	37 - 61	12 - 25	3 - 6

TABLE 2-10.

SUMMARY OF VARIABLES IN THE SHRINKAGE INHIBITOR INVESTIGATION

Variable	Levels of Variation
Inhibitor	K_2SO_4, K_2CO_3, KCl
Inhibitor Particle Size	25-60 microns, 6-25 microns, 2-6 microns
Inhibitor Quantity	0.5, 1.5, 5 mol per cent (based on ALON-C gamma content)
Opacifier	TiO_2 @ 16 per cent by weight, and no opacifier

TABLE 2-11.

RESULTS OF SHRINKAGE INHIBITOR EVALUATION AT 2200F IN AIR

		Shrinkage, Per Cent		
		Mol Per Cent of Inhibitor		
		0.5	1.5	5
TiO_2 Opacifier	K_2SO_4	27.2	29.6	23.7
	KCl	27.2	27.3	27.9
	K_2CO_3	27.0	26.5	18.2
No Opacifier	K_2SO_4	18.2	16.6	16.2
	KCl	19.4	17.9	17.2
	K_2CO_3	16.5	16.9	12.2

TABLE 2-12.

RESULTS OF SHRINKAGE INHIBITOR EVALUATION AT 2200F IN VACUUM

		Shrinkage, Per Cent		
		Mol Per Cent of Inhibitor		
		0.5	1.5	5
TiO_2 Opacifier	K_2SO_4	25.3	18.2	9.7
	KCl	24.5	25.8	28.1
	K_2CO_3	24.4	26.0	13.6
No Opacifier	K_2SO_4	21.5	15.8	8.7
	KCl	22.5	22.2	22.7
	K_2CO_3	22.6	22.4	7.8

respectively, as a function of these three variables. Each value represents the average of the three different inhibitor particle size specimens together with their duplicates, thus representing a total of six specimens.

Considering only those specimens containing no opacifier, it was apparent that the K_2CO_3 was the most efficient inhibitor when fired in air. Similarly, a concentration level of 5 mol per cent was required to achieve this efficiency. In vacuum, K_2CO_3 and K_2SO_4 were considered equivalent in efficiency at the 5 mol per cent level. Considering both air and vacuum conditions, K_2CO_3 was selected as the best shrinkage inhibitor.

Several additional specimens were evaluated in vacuum to determine if the 5 mol per cent concentration level was in fact optimum. Duplicate specimens, with no opacifier, containing K_2CO_3 (-325 mesh) at the 3.0, 4.0, and 7.0 mol per cent concentration levels were fired at 2200F in vacuum. These results are presented in Table 2-13, together with the results of the other concentrations shown in Table 2-12. It will be noted that the optimum concentration spans a relatively broad range from at least 3 to 7 mol per cent. The slight discrepancy at the 5 mol per cent level should be attributed to the accuracy of sample measurement.

Samples of the 0.5 mol per cent and 5 mol per cent K_2CO_3 specimens were examined under the electron microscope (rub-out sample preparation technique). The electron micrographs are presented in Figures 2-35 and 2-36, respectively. After 2 hr, 15 min at 2200F (isothermal) in vacuum, the effect of the K_2CO_3 inhibitor on the ALON-C gamma particles was striking. The ALON-C particles in the 0.5 mol per cent specimen (Figure 2-35) showed extensive sintering with only small pockets of unagglomerated particles. X-ray diffraction analysis indicated the presence of well-developed alpha alumina. In contrast, the ALON-C particles in the 5 mol per cent specimen (Figure 2-36) showed only scattered areas of agglomeration, with most of the particles remaining in their original form. X-ray diffraction analysis showed both weak alpha and weak gamma formation, the balance being unknown - probably amorphous alumina.

It was concluded therefore that 5 mol per cent of K_2CO_3 was probably the most efficient shrinkage inhibitor for ALON-C gamma in both air and vacuum at 2200F, and that this efficiency was independent of particle size between 2 and 60 microns. It was also concluded that TiO_2 should not be employed as an opacifier in combination with ALON-C gamma at 2200F.

Zirconia Opacifier. All tests had shown that titania was not the opacifier to use in combination with the ALON-C gamma submicron particles due to the extensive fluxing created by the titania. Previous experience with MIN-K had shown that Cr_2O_3, $ZrSiO_4$, and ZrO_2 were reasonably good opacifiers.

TABLE 2-13.

RESULTS OF K_2CO_3 SHRINKAGE INHIBITOR EVALUATION AT 2200F IN VACUUM*

Mol % of K_2CO_3	Average Shrinkage, %
0.5	22.6**
1.5	22.4**
3.0	5.3***
4.0	5.0***
5.0	7.8**
7.0	5.3***

* Specimens contained no opacifier
** Average of 6 specimens
***Average of 2 specimens

FIGURE 2-35.

MIN-K/ALON-C GAMMA/0.5 MOL % K_2CO_3
FOLLOWING 2 HR AT 2200F IN VACUUM
MAG: 27,500X

1 micron

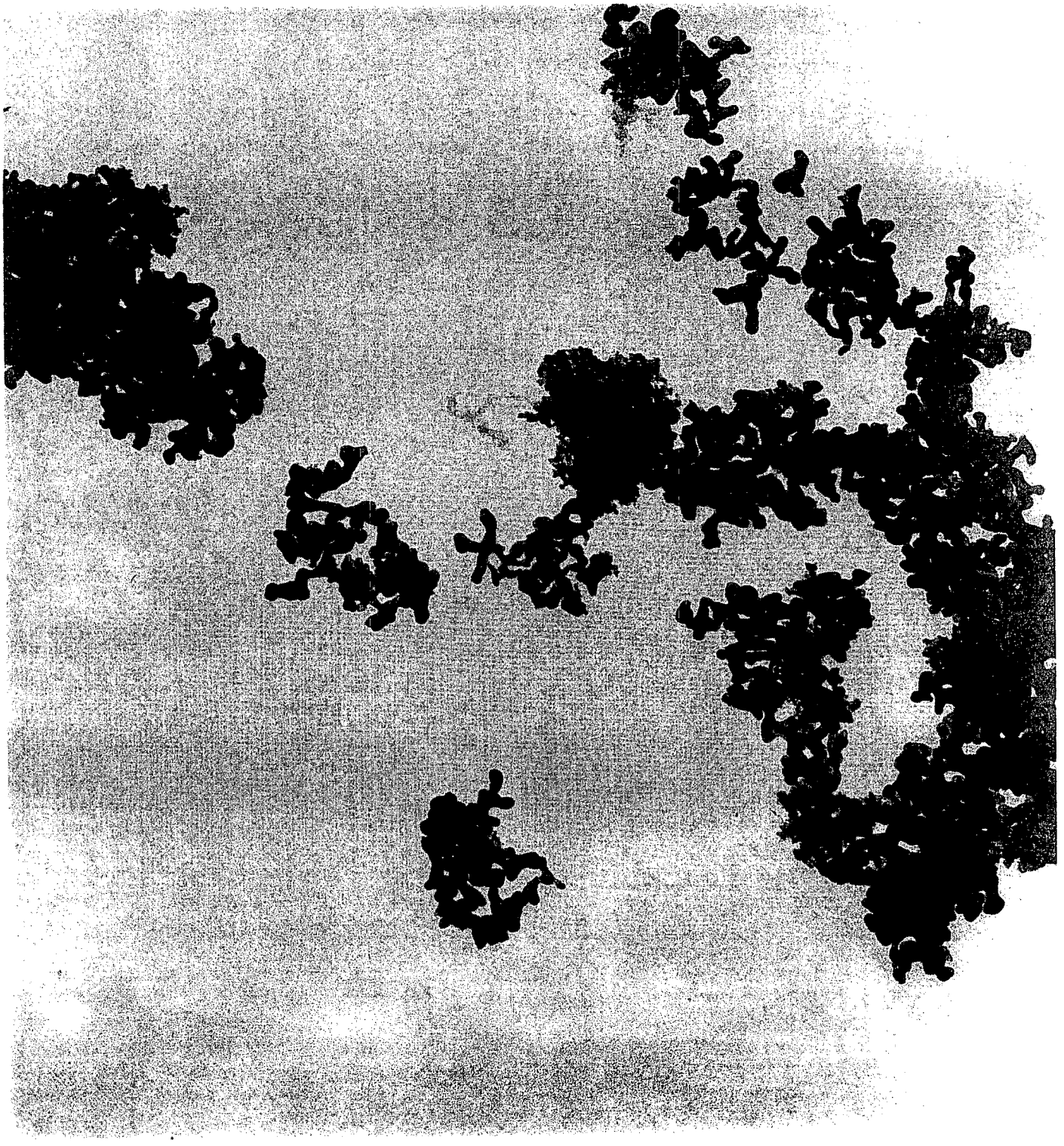

EMS 774-A

FIGURE 2-36.

MIN-K/ALON-C GAMMA/5 MOL % K_2CO_3
FOLLOWING 2 HR AT 2200F IN VACUUM
MAG: 27,500X

1 micron

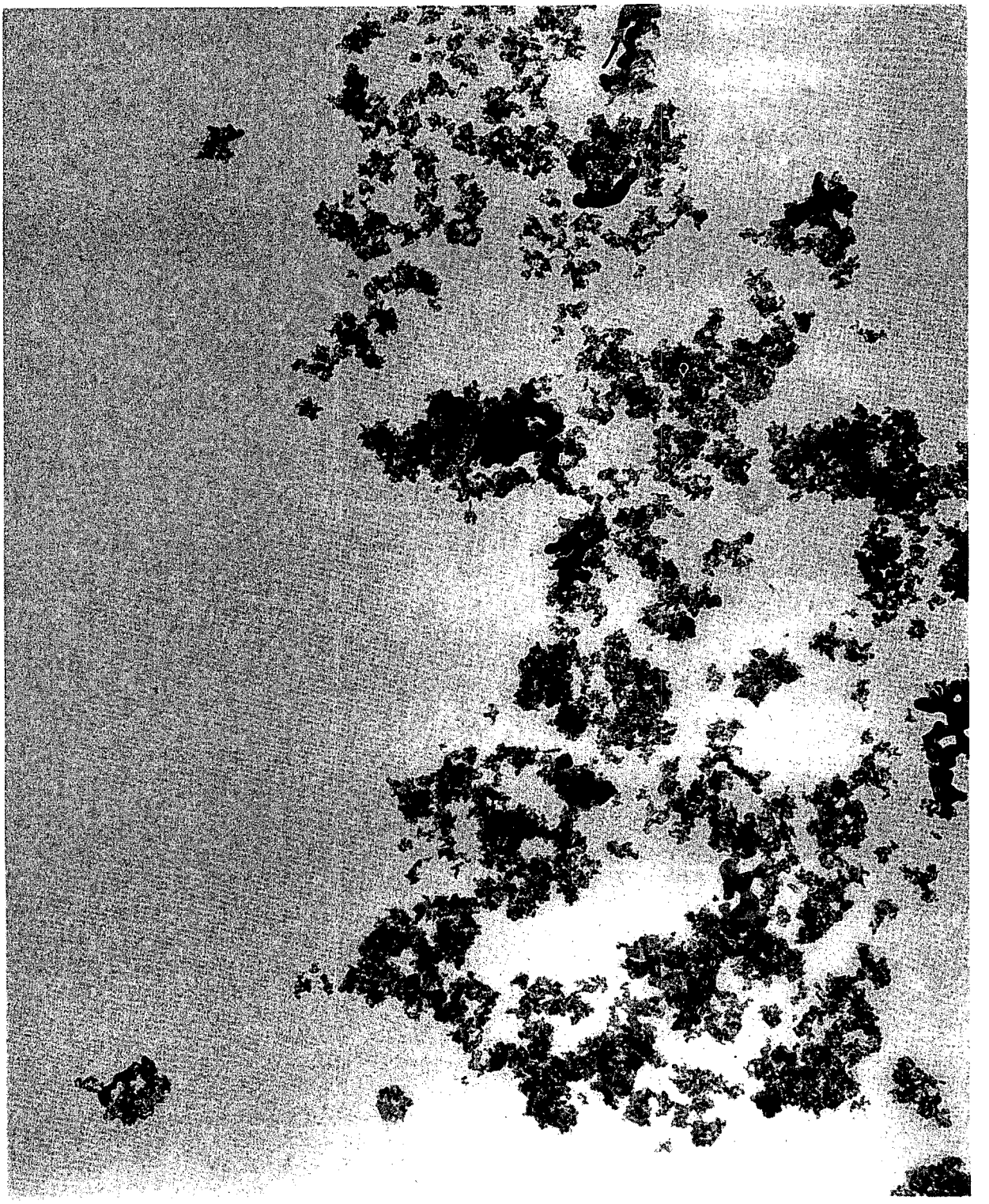

EMS 775-A

However, the work under Subtask 3.2 (to be discussed later) which was being conducted concurrently showed that at 1800F and under vacuum, Cr_2O_3 and $ZrSiO_4$ had strong outgassing tendencies. Consequently, these opacifiers were eliminated from consideration, both under Subtask 3.2 and Task 2.

Tests were then conducted to determine the effect of 16 per cent by weight of ZrO_2 opacifier and K_2CO_3 inhibitor on the shrinkage of similar sized discs made with both gamma and alpha ALON-C, and pressed to 30 pcf density. This increase in density was considered desirable from a handling standpoint in the case of the gamma ALON-C specimens, and a necessity in the case of the specimens made from the more dense alpha ALON-C. ASTROQUARTZ and MICRO-QUARTZ fibers were also incorporated into the specimens at the same weight per cent amounts indicated for the earlier experiments. The test time at 2200F in air and vacuum was extended to include a 24-hr exposure, as well as a 2-hr exposure. Table 2-14 presents the average diameter shrinkage of these specimens.

For this series, it was apparent that the inhibitor was more effective than the opacifier in preventing shrinkage. Similarly, the effect of both the inhibitor and zirconia opacifier, together, was not noticeably different from that of the inhibitor alone. This was significant in that it showed that the combination of all of these materials did not result in a catastrophic shrinkage.

Table 2-14 also points out, as expected, that the ALON-C alpha specimens were more stable than the ALON-C gamma specimens. It has been shown previously, however, that ALON-C alpha no longer had the desirable pore size distribution to yield the low thermal conductivity values in a gaseous media characteristic of MIN-K.

The effect of ZrO_2 opacifier content on the thermal stability of MIN-K/ALON-C gamma discs after 2 hr at 2200F in air and vacuum was then determined. The opacifier content ranged from 16 weight per cent to 28.3 weight per cent, the latter content representing the mol per cent equivalent to 16 weight per cent of TiO_2 opacifier used in the lower temperature MIN-K formulations. No shrinkage inhibitor was used to mask the effect of the zirconia. All specimens were 30 pcf nominal density. Table 2-15 summarizes these results.

It appeared that greater amounts of zirconia helped to stabilize the composition in air, but was slightly detrimental to the stability in vacuum. Comparison of the shrinkage values for the 16 weight per cent specimens tested in air as shown in Tables 2-15 and 2-14 (15.7 vs 15.8 per cent) indicated excellent agreement, and hence, the trend in air may be real. A similar comparison of the shrinkage values of similar specimens tested in vacuum (17.5 per cent vs 18.4 per cent), although still considered in good

TABLE 2-14.

LINEAR SHRINKAGE OF MIN-K/ALON-C
CONTAINING INHIBITOR AND OPACIFIER
AFTER EXPOSURE TO 2200F (ISOTHERMAL)

Type of ALON-C	16 Wt % Opacifier	Inhibitor	Per Cent Linear Shrinkage* in air 2hr	in air 24 hr	in vacuum 2 hr	in vacuum 24 hr
gamma	ZrO_2	----	15.8	15.4	18.4	19.3
gamma	----	K_2CO_3	4.6	11.0	7.9	14.4
gamma	ZrO_2	K_2CO_3	4.4	11.0	8.8	13.2
alpha	ZrO_2	----	4.9	11.7	8.8	10.5
alpha	----	K_2CO_3	2.1	6.5	5.3	7.4
alpha	ZrO_2	K_2CO_3	4.4	9.6	6.5	8.5

* Average of two specimens

TABLE 2-15.

EFFECT OF ZIRCONIA CONTENT ON LINEAR SHRINKAGE
OF MIN-K/ALON-C GAMMA

(2200F Isothermal, 2 hr)

Weight, % ZrO_2	Average Linear Shrinkage* in air	in vacuum
16.0	15.7	17.5
20.0	15.6	17.3
21.2	14.2	18.0
24.2	13.2	18.6
25.6	12.3	18.0
28.3	12.3	19.0

* Average of two specimens

agreement, tended to negate what appeared at first glance to be a trend. Since the effect of zirconia content on the shrinkage was minor, if at all, 16 weight per cent was chosen as the preferred amount of opacifier.

MIN-K Formulation 2041. To this point, all work on the thermal stability of the ALON-C - fiber - opacifier - inhibitor combinations had been conducted on small (1-1/8 in. diameter x 1/2 in. thick) specimens. Although gross effects due to composition changes could be established, minor effects - differences of several per cent - could not be considered significant due to the potential error involved in measuring these small samples. Consequently, a test series was conducted with larger specimens molded from a formulation which was processed in the same manner as that used for the other pilot plant formulations studied under both phases of this contract (see Phase I Final Report No. ALO-3633-7, dated October 7, 1967, for process details).

MIN-K Formulation 2041, shown in Table 2-16 was chosen as the optimum combination of ingredients for this larger scale thermal stability evaluation. The most obvious difference between this formulation and previous formulations (not only those devised for the small scale materials evaluation discs, but also the lower temperature "standard" formulations such as MIN-K 1999, 2002, and 2020), was the elimination of the MICRO-QUARTZ fiber. MICRO-QUARTZ was shown to have an adverse effect on the thermal stability of MIN-K 2020 unless it was prefired prior to batching. At 2200F, this effect would have been magnified still further.

Blocks 9 x 9 x 1 in. were pressed from the pilot plant mix to 20 and 30 pcf nominal densities. They were then cut to 3 x 2 x 1 in. specimens and measured to the nearest 0.001 in. Unlike the small disc specimens, they were not stored in dessicators until tested, but remained at the 72F, 40% RH room condition. These specimens were subjected to 2, 24, and 168 (1 wk) hr exposures to 2200F (isothermal) in air and vacuum. Tables 2-17 and 2-18 summarize the shrinkage results.

The first observation from both tables of data was that the 30 pcf density specimens were more stable than the 20 pcf density specimens. A second, and probably more important observation was that the shrinkage rate appeared to lessen considerably (on the average) in air after 24 hr, whereas it showed less indication of slowing down up to 168 hr in vacuum. Thus, the original hypothesis that submicron alumina particles shrink more in vacuum than in air (although subsequently tied to the TiO_2 opacifier as the prime cause for this phenomenon), may in fact hold true, given sufficient time at temperature.

During the tests in air, a considerable amount of moisture was noted within the furnace system. As previously noted, these specimens were not stored in

TABLE 2-16.

MIN-K FORMULATION 2041

Constituent	Weight, %
ALON-C gamma	74
ASTROQUARTZ 1/4-in. staple	5
ZrO_2	16
K_2CO_3	5*

* Represents 5 mol per cent based upon ALON-C gamma content

TABLE 2-17.

LINEAR SHRINKAGE OF MIN-K FORMULATION 2041 IN AIR
AT 2200F ISOTHERMAL

Nominal Density pcf	Firing Time hr	Average Shrinkage, %*		
		Length	Width	Thickness
20	2	6.5	6.6	7.6
20	24	12.1	12.3	15.8
20	168	12.8	13.4	28.4
30	2	5.3	5.3	4.8
30	24	10.2	9.7	12.3
30	168	10.2	10.7	17.6

* Average of four specimens.

TABLE 2-18.

LINEAR SHRINKAGE OF MIN-K FORMULATION 2041 IN VACUUM
AT 2200F ISOTHERMAL

Nominal Density pcf	Firing Time hr	Average Shrinkage, %*		
		Length	Width	Thickness
20	2	3.8	4.0	3.8
20	24	7.1	7.3	7.8
20	168	15.1	15.2	18.5
30	2	3.2	3.4	3.4
30	24	6.7	7.0	6.5
30	168	13.2	13.3	15.5

*Average of four specimens.

a dessicator prior to test, and hence, absorbed considerable quantities of moisture due to the hydroscopic nature of the K_2CO_3 inhibitor. Four specimens of Formulation 2041 at 20 pcf density and four specimens at 30 pcf density were dried at 400C (725F) in air for 18 hr, and subsequently retested for shrinkage at 2200F for 24 hr in air. The weight loss as a result of drying was 7 per cent, and an additional 3 per cent (both based upon the undried weight) was driven off as a result of the 2200F firing. The results of this shrinkage test are given in Table 2-19.

On the average, the shrinkage in air after drying was about 75 to 78 per cent of that shown in Table 2-17, although the effect was more pronounced on the thickness shrinkage than the length and width shrinkage. This would indicate that the moisture either contributed directly to the shrinkage, or prevented the K_2CO_3 from inhibiting the agglomeration of the ALON-C particles. It would not be unreasonable to assume also that had the specimens been completely dry prior to test, an additional improvement in thermal stability may have been realized.

Based upon the known effect of drying upon the shrinkage after 24 hr at 2200F, Table 2-20 was prepared. All numbers in italics represent estimates based on the 24-hr exposure data (Table 2-19). This "adjustment", shown in Table 2-20 does not alter the basic conclusion that, over prolonged exposure, MIN-K Formulation 2041 probably would shrink more in vacuum than in air. It becomes doubtful that the shrinkage data in vacuum would be altered by pre-drying the specimens when one considers the heating cycle employed for all tests. The specimens were placed in the furnace, heated to 1000F, and held at this temperature overnight (approximately 18 hr) under active vacuum. Heatup to 2200F was then accomplished the following day in about 3 hr, also under active vacuum. Consequently, it is believed that essentially all of the moisture was removed from the system before the temperature reached a critical point, thus eliminating any adverse effect on the specimens.

X-ray diffraction data were obtained for typical specimens subjected to the 2200F exposure. These tests were qualitative in nature, but did provide an order of magnitude estimate of the extent of conversion from the gamma alumina form of ALON-C. Table 2-21 summarizes these results. It was apparent that the inhibitor suppressed the formation of alpha alumina, enhanced the formation of amorphous alumina (balance in each case assumed to be amorphous since no significant quantities of any other crystalline forms were detected), and minimized, or at least retarded the agglomeration of the submicron particles as indicated by the shrinkage data.

Electron micrographs (rub-out technique) of the 2-hr and 168-hr specimens exposed to 2200F under vacuum were taken. These are shown in Figures 2-37 and 2-38, respectively. The 2-hr exposure specimen showed no sintering. After

TABLE 2-19.

LINEAR SHRINKAGE OF MIN-K FORMULATION 2041 IN AIR
AT 2200F FOLLOWING 400C DRYING

Nominal Density pcf	Firing Time hr	Average Shrinkage, %*		
		Length	Width	Thickness
20	24	9.5	10.3	11.2
30	24	7.6	8.2	8.0

* Average of four specimens.

TABLE 2-20.

ESTIMATED LINEAR SHRINKAGE OF MIN-K FORMULATION 2041 IN AIR AT 2200F ISOTHERMAL

Nominal Density pcf	Firing Time hr	Average Shrinkage, %*		
		Length	Width	Thickness
20	2	5.1	5.5	5.4
20	24	9.5	10.3	11.2
20	168	10.0	11.3	20.2
30	2	4.0	4.5	3.1
30	24	7.6	8.2	8.0
30	168	7.7	9.1	11.4

* Average of four specimens

TABLE 2-21.

QUALITATIVE X-RAY DIFFRACTION ANALYSIS
OF MIN-K FORMULATION 2041 FOLLOWING 2200F EXPOSURE

Firing Time hr	Form and Amount of Alumina	
	Air	Vacuum
2	Trace of alpha, balance amorphous	Trace of alpha, balance amorphous
24	Moderate alpha (40-60%), balance amorphous	Trace of alpha, balance amorphous
168	Moderate alpha (40-60%), balance amorphous	Moderate alpha (40-60%). balance amorphous

FIGURE 2-37.

MIN-K FORMULATION 2041 AFTER 2 HR IN VACUUM @ 2200F
MAG: 27,500X

1 micron

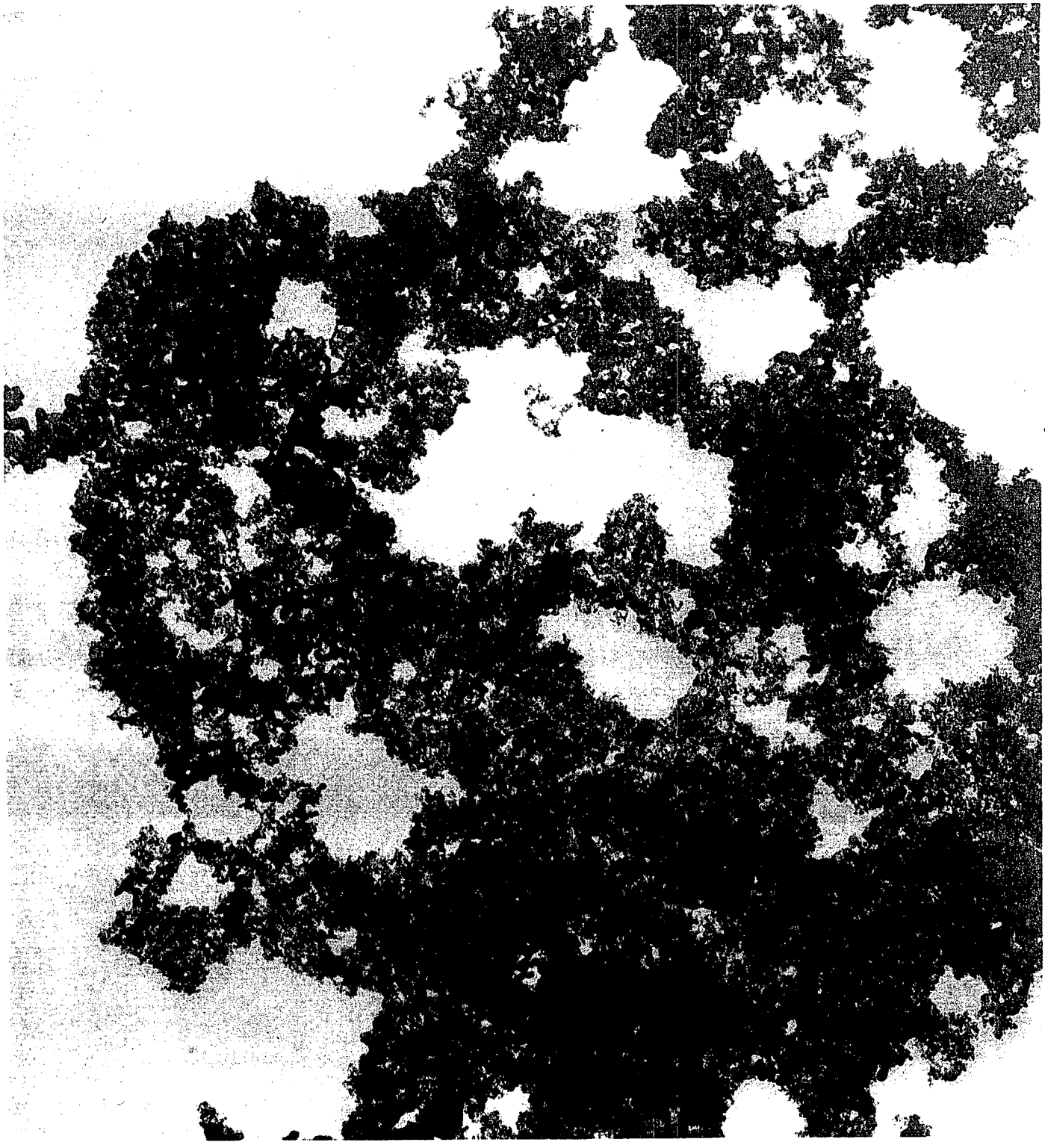

EMS 814-A

FIGURE 2-38.

MIN-K FORMULATION 2041 AFTER 168 HR IN VACUUM AT 2200F
MAG: 27,500X

1 micron

EMS 815-A

168 hr of exposure, sintering had definitely taken place. A comparison of Figure 2-38 with Figure 2-35 showed that the particles were approximately the same size. Thus, it would appear that the action of the inhibitor was one of retarding sintering (the specimen in Figure 2-35 had essentially no inhibitor), but that sintering would take place with time. Based on the earlier studies, it was concluded that the thermal conductivity of MIN-K Formulation 2041 in a gaseous media, would have been adversely affected as a result of the thermal exposure due to the particle sintering.

IV. TASK 3 - LOAD-BEARING INSULATION FOR 400 - 1800F SERVICE

INTRODUCTION

Task 3 was divided into two Subtasks. Subtask 3.1 was concerned with the development of a load-bearing insulation for lead-telluride service, or 1400F hot face, whereas Subtask 3.2 covered the effort to provide a thermally efficient load-bearing material for silicon-germanium systems up to 1800F hot face. The purpose of the load-bearing insulations is to support the heat source, as well as any preload which might be applied during the assembly of the generator. A brief description of each Subtask is as follows:

Subtask 3.1 - Load-Bearing Insulations for 400F to 1400F Service. A preliminary evaluation of high density MIN-K indicated that a product of approximately 35 pcf density would have a modulus of elasticity of between 15,000 and 25,000 psi with an increase in thermal conductivity of about 100 per cent over the normal 20 pcf density product. An examination of available ceramic insulation materials capable of carrying high loads showed that MIN-K would probably perform equally as well but at a lower density, and with a greater thermal efficiency. Therefore, it was intended to study various MIN-K formulations at 35 pcf density to achieve the optimum combination of modulus of elasticity and thermal conductivity.

Subtask 3.2 - Load-Bearing Insulations of Service up to 1800F. Phase I of this contract showed that Glasrock foamed silica at 25 pcf to 30 pcf density supported 200 psi at 1800F hot face with little or no crushing or relaxation. This product also had a relatively low thermal conductivity. Since it consisted solely of silica, however, it was believed that the addition of 5 to 15 per cent of an opacifier to the matrix would reduce the thermal conductivity. (It had already been shown during Phase I that at 1800F hot face, MIN-K cannot sustain any load without serious deformation.) Therefore, it was the intent of this Subtask to improve the thermal conductivity of Glasrock at 25 pcf density (nominal) without reducing its load-bearing capability at 1800F hot face.

SUBTASK 3.1 - LOAD-BEARING INSULATION FOR 400-1400F SERVICE

A load-relaxation evaluation of 20 pcf density MIN-K 2002 [1] showed that this material could not withstand excessive loading while at 1400F hot face conditions without a considerable amount of relaxation. After 2000 hr, the initial loading (up to 150 psi) had dropped about 50 per cent, while maintaining constant deflection. Since it would be advantageous to have a MIN-K formulation which would withstand relatively high static preloads (for fuel capsule support) without undue relaxation, high density MIN-K formulations, based on variations of MIN-K 2002, were evaluated for both thermal conductivity and load-relaxation.

168 hr of exposure, sintering had definitely taken place. A comparison of Figure 2-38 with Figure 2-35 showed that the particles were approximately the same size. Thus, it would appear that the action of the inhibitor was one of retarding sintering (the specimen in Figure 2-35 had essentially no inhibitor), but that sintering would take place with time. Based on the earlier studies, it was concluded that the thermal conductivity of MIN-K Formulation 2041 in a gaseous media, would have been adversely affected as a result of the thermal exposure due to the particle sintering.

IV. TASK 3 - LOAD-BEARING INSULATION FOR 400 - 1800F SERVICE

INTRODUCTION

Task 3 was divided into two Subtasks. Subtask 3.1 was concerned with the development of a load-bearing insulation for lead-telluride service, or 1400F hot face, whereas Subtask 3.2 covered the effort to provide a thermally efficient load-bearing material for silicon-germanium systems up to 1800F hot face. The purpose of the load-bearing insulations is to support the heat source, as well as any preload which might be applied during the assembly of the generator. A brief description of each Subtask is as follows:

Subtask 3.1 - Load-Bearing Insulations for 400F to 1400F Service. A preliminary evaluation of high density MIN-K indicated that a product of approximately 35 pcf density would have a modulus of elasticity of between 15,000 and 25,000 psi with an increase in thermal conductivity of about 100 per cent over the normal 20 pcf density product. An examination of available ceramic insulation materials capable of carrying high loads showed that MIN-K would probably perform equally as well but at a lower density, and with a greater thermal efficiency. Therefore, it was intended to study various MIN-K formulations at 35 pcf density to achieve the optimum combination of modulus of elasticity and thermal conductivity.

Subtask 3.2 - Load-Bearing Insulations of Service up to 1800F. Phase I of this contract showed that Glasrock foamed silica at 25 pcf to 30 pcf density supported 200 psi at 1800F hot face with little or no crushing or relaxation. This product also had a relatively low thermal conductivity. Since it consisted solely of silica, however, it was believed that the addition of 5 to 15 per cent of an opacifier to the matrix would reduce the thermal conductivity. (It had already been shown during Phase I that at 1800F hot face, MIN-K cannot sustain any load without serious deformation.) Therefore, it was the intent of this Subtask to improve the thermal conductivity of Glasrock at 25 pcf density (nominal) without reducing its load-bearing capability at 1800F hot face.

SUBTASK 3.1 - LOAD-BEARING INSULATION FOR 400-1400F SERVICE

A load-relaxation evaluation of 20 pcf density MIN-K 2002 (1) showed that this material could not withstand excessive loading while at 1400F hot face conditions without a considerable amount of relaxation. After 2000 hr, the initial loading (up to 150 psi) had dropped about 50 per cent, while maintaining constant deflection. Since it would be advantageous to have a MIN-K formulation which would withstand relatively high static preloads (for fuel capsule support) without undue relaxation, high density MIN-K formulations, based on variations of MIN-K 2002, were evaluated for both thermal conductivity and load-relaxation.

MIN-K 2002 at 20 pcf had a modulus of ealsticity of approximately 2050 psi. It was felt that a modulus of 15,000 to 25,000 psi would be desirable, reformulating as necessary to achieve the lowest thermal conductivity at the required density. It had also been established that 35 pcf was about the highest density which could be consistently fabricated, and that this density would yield a modulus generally within the desired range. Thus, with the density tentatively fixed, an evaluation of composition vs thermal conductivity was instituted.

Thermal Conductivity - Formulation Evaluations. The list of formulations devised for this evaluation, and the overall product density of each is given in Table 3.1-1. It will be noted that the fiber content was held constant throughout the evaluation. The purpose of the product densities below 35 pcf was to obtain a range of CAB-O-SIL M5 and TAM -5 TiO_2 densities within the sample series, and thus permit an evaluation of thermal conductivity based on each component separately.

Each of the products was evaluated for thermal conductivity at 800F mean temperature using the Rapid Meter apparatus per ASTM C-518-63T. Table 3.1-2 gives the results of this evaluation together with the CAB-O-SIL M5 and TAM -5 TiO_2 partial densities for each product. Items 1 through 6 of Table 3.1-2 were plotted as thermal conductivity versus CAB-O-SIL M5 density in Figure 3.1-1. Although an additional point or two would have been desirable in the 22 pcf CAB-O-SIL M5 density range, there was excellent correlation. It was apparent that the rate of conductivity increase took a sharp turn upward at about 22 pcf silica density. Relating back to the Task 2 studies where the electron microscope showed relatively few silica particles in contact with each other at a silica density of 15 pcf (MIN-K 2002), the number of particle-to-particle contacts probably increased rapidly above 22 pcf silica density. Thus, the rapid rise in conductivity would be attributed, to a large measure, to solid conduction through the CAB-O-SIL M5.

A plot of Items 7 through 12 of Table 3.1-2 as conductivity vs TiO_2 density at a constant silica density (18.5 to 19 pcf) is given in Figure 3.1-2. Although the spread of conductivity values was small, giving rise to greater possible error in interpretation, a distinct relationship appeared to exist. (MIN-K 2002 at 20 pcf cannot be plotted on this regression since its silica density is only 15 pcf.)

Based upon these thermal conductivity data, and the goal of a 35 pcf density product, one would maximize the silica density at approximately 22 pcf (to stay below the sharp break in the curve), and minimize the TiO_2 density at

TABLE 3.1-1

MIN-K FORMULATIONS FOR HIGH DENSITY THERMAL CONDUCTIVITY EVALUATIONS

Formulation No.	Composition, Weight %				Product Density pcf
	CAB-O-SIL M5	TAM -5 TiO_2	ASTROQUARTZ ½"G	MICROQUARTZ AA	
2002	75	16	5	4	20.0
2002	75	16	5	4	24.8
2002	75	16	5	4	30.7
2002	75	16	5	4	35.2
2003	67	24	5	4	28.0
2028	78	13	5	4	24.1
2029	80	11	5	4	30.4
2030	82	9	5	4	33.9
2032	71	20	5	4	26.5
2033	59	32	5	4	32.0

TABLE 3.1-2

THERMAL CONDUCTIVITY AND PARTIAL DENSITIES
OF HIGH DENSITY FORMULATIONS

Item	Formulation No.	Product Density pcf	CAB-O-SIL M5 Density pcf	TiO_2 Density pcf	Conductivity at 800F Mean Btu in./hr ft^2 °F *
1	2002	20.0	15.0	3.2	0.22(2)
2	2002	24.8	18.6	4.0	0.23(5)
3	2028	24.1	18.9	3.1	0.23(6)
4	2002	30.7	24.0	4.8	0.28(0)
5	2029	30.4	24.3	3.3	0.29(5)
6	2002	35.2	26.4	5.6	0.35(2)
7	2029	23.5	18.8	2.6	0.24(4)
8	2028	24.1	18.0	3.1	0.23(6)
	(Item 3 rewritten as Item 8. Test not repeated)				
9	2002	24.8	18.6	4.0	0.23(5)
	(Item 2 rewritten as Item 9. Test not repeated)				
10	2032	26.5	18.6	5.3	0.23(0)
11	2003	28.0	18.8	6.7	0.22(9)
12	2033	32.0	18.9	10.2	0.24(0)

* The third decimal place is presented in parenthesis for purposes of plotting the data. Because of accuracy limitations however, the third place is usually not quoted.

FIGURE 3.1-1.

THERMAL CONDUCTIVITY OF MIN-K FORMULATIONS
VS
CAB-O-SIL M5 DENSITY

800F Mean Temperature

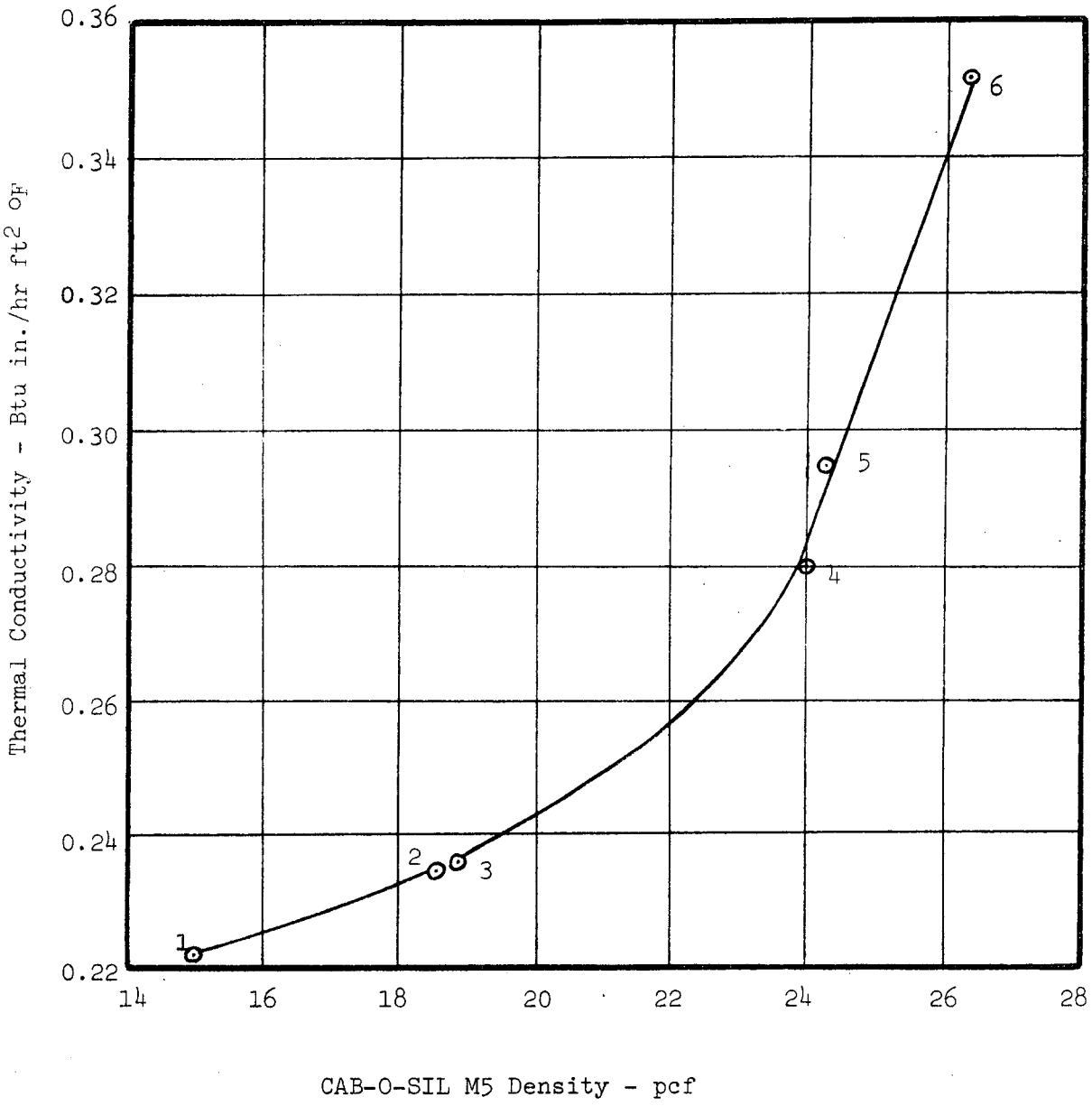

FIGURE 3.1-2.

THERMAL CONDUCTIVITY OF MIN-K FORMULATIONS
VS
TiO_2 DENSITY

(CAB-O-SIL Density = 19 pcf)

800 F Mean Temperature

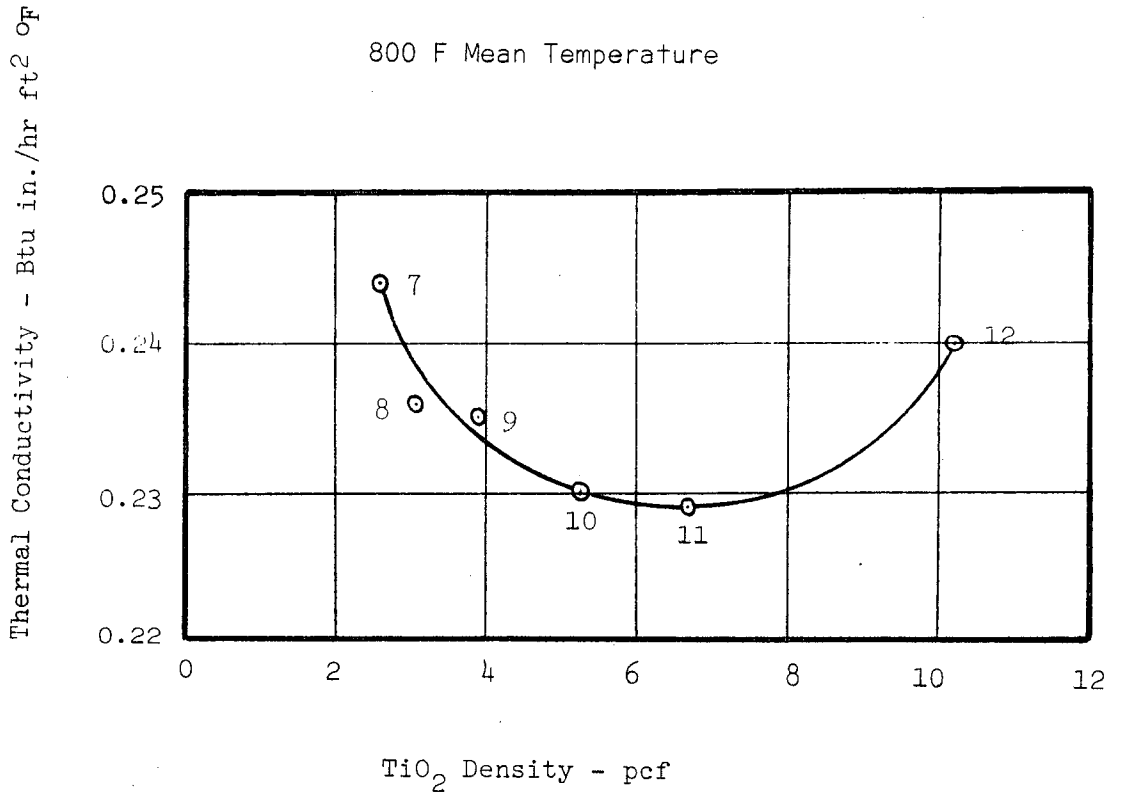

10 pcf, with the balance being fiber. Since the effect of added amounts of TiO_2 was small compared with similar increases in silica density (assuming that the TiO_2 does in fact turn upward as shown in Figure 3.1-2, a higher-than-optimum TiO_2 content could be tolerated. This analysis, however, disregarded the effect of either silica or titania density on the modulus of elasticity, which must be given prime consideration.

Modulus of Elasticity - Formulation Evaluations. To investigate the effect of silica density on the modulus of elasticity of the product, various formulations at a variety of densities were evaluated. Table 3.1-3 summarizes the materials tested. Four specimens (4½ x 4½ x 1) of each product were subjected to a stress-strain test at room temperature, and the modulus of elasticity was calculated based on the average of the four curves. This was then plotted vs $(\text{product density})^2 \times (\text{silica density})$ as shown in Figure 3.1-3. The function $(\text{product density})^2 \times (\text{silica density})$ was somewhat arbitrary, but was found to provide a reasonably good fit after several similar functions had been tried. Although a better function could probably have been determined, this appeared sufficient to indicate the effect of both product density and silica density on the modulus of elasticity of the product.

Based upon Figure 3.1-3, a 35 pcf block having a modulus of elasticity of 20,000 psi should have a silica density of 27 psi. This was very close to MIN-K 2002 at 35 pcf, and is probably within the normal density range (±1 pcf) anticipated for production fabrication (a 36 pcf block of MIN-K 2002 would have a modulus of elasticity of about 21,000 psi according to Figure 3.1-3). Therefore, all factors considered, MIN-K 2002 at 35 pcf appeared the best choice for load-bearing at 1400F. It was apparent that a significant tradeoff with thermal conductivity was necessary to achieve the degree of compression resistance desired: The thermal conductivity of this product at 35 pcf was still well below materials of similar strength, however.

Load-Relaxation Test Equipment and Procedure. The evaluation of the load-relaxation characteristics of MIN-K 2002 at 20 pcf density during Phase I was conducted by applying the load to a 4 x 4 x 1 in. specimen, noting the total deflection (specimen plus furnace), and, based upon prior furnace calibrations, calculating the specimen deflection. This deflection was then maintained throughout the test, while the load was reduced accordingly. The major sources of error in this procedure were the unknown creep rate of the furnace over the prolonged test period, and the necessity of a trial and error technique of determining the load necessary to achieve the original sample deflection.

TABLE 3.1-3

MATERIALS EVALUATED FOR MODULUS OF ELASTICITY

Point No.	Formulation No.	Product Density pcf	Modulus of Elasticity psi	(Product Density)^2 x (CAB-O-SIL Density)
1	2002	20.0	2,050	6,000
2	2028	25.0	4,800	12,200
3	2002	24.6	5,100	11,800
4	2002	29.8	8,950	20,300
5	2029	29.9	10,400	21,600
6	2002	35.0	17,700	32,200
7	2030	33.9	19,900	32,100
8	2002	38.7	28,700	43,500

FIGURE 3.1-3.

EFFECT OF MIN-K PRODUCT DENSITY AND CAB-O-SIL M5 DENSITY ON MODULUS OF ELASTICITY

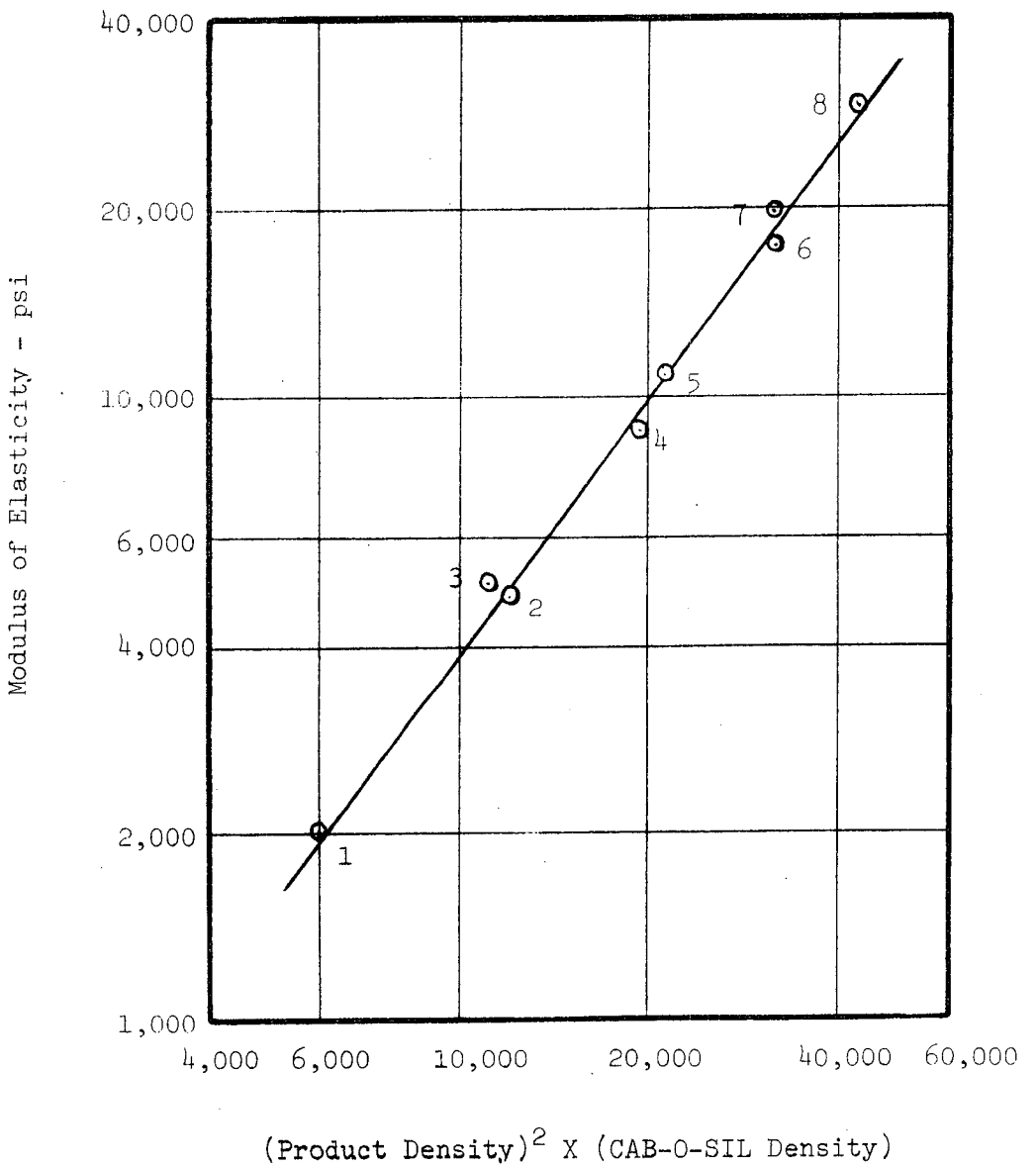

The test procedure for determining the load-relaxation characteristics of MIN-K 2002 at 35 pcf density was modified to reduce experimental error. Figure 3.1-4 is a schematic of this test rig. The specimen size was reduced to 2 x 2 x 1 in. This not only allowed greater test loads to be applied, but also permitted a direct measurement of the furnace deflection by placing the stem of a 0.001-in. increment dial gauge directly in contact with the 4 x 4 in. hot plate of the furnace (actual contact was made by a ceramic rod onto which the dial gauge stem rested). Two such gauges were placed at diagonally opposite corners, and adjacent to the specimen. The 1-in. wide heated area around the specimen was also covered with 35 pcf density MIN-K 2002 to maintain temperature uniformity across the specimen.

A 2 x 2 x 1-in. steel block was placed atop the specimen, while 3 x 1 x 3/4-in. bars were placed over the insulation surrounding the specimen. A thick, rigid steel bar was then placed diagonally across the 2 x 2 x 1-in. steel block (at 90 degrees to the diagonal line of the dial gauges measuring furnace deflection). Two dial gauges were then mounted on this upper bar to measure total deflection (specimen plus furnace).

Care was exercised during the assembly of each test so that the specimen was horizontal, the shaft transmitting the load was vertical, and that the shaft was centered on the specimen. Upon application of the load, if the two dial readings of total deflection differed by more than 0.010 in., the shaft was repositioned.

Hot and cold face specimen temperatures were measured with chromel alumel thermocouples laid in grooves cut into the specimen. The hot face temperature was held between 1390F and 1410F. Once set, the hot face temperature had a total variation of only 3 to 4F. Cold face temperatures averaged 160F, but ranged between 130F and 180F depending upon the individual specimen. The cold face temperature also had a very small total variation as a result of the on-off cycles of the heaters. However, during the course of some of the 500-hr tests, the cold face temperature drifted as much as 10F in a random manner. No attempt was made to control this temperature.

Stress-Strain Relationship at 1400F Hot Face. Following installation of the test specimen into the compression furnace, the heat was applied and temperature equilibrium was achieved under a "zero load" condition. As the test load was applied to each specimen, deflection readings were taken at 50 psi load increments up to the constant load scheduled for each particular specimen. Thus, a stress-strain relationship was developed at 1400F hot face. The prime difference between these tests and room temperature tests, however, was that the load at each increment had to be held constant for approximately 30 sec while the four dial readings were taken and recorded. During the room temperature tests, the load was increased continuously, and a single dial reading taken as it was moving slowly.

FIGURE 3.1-4.

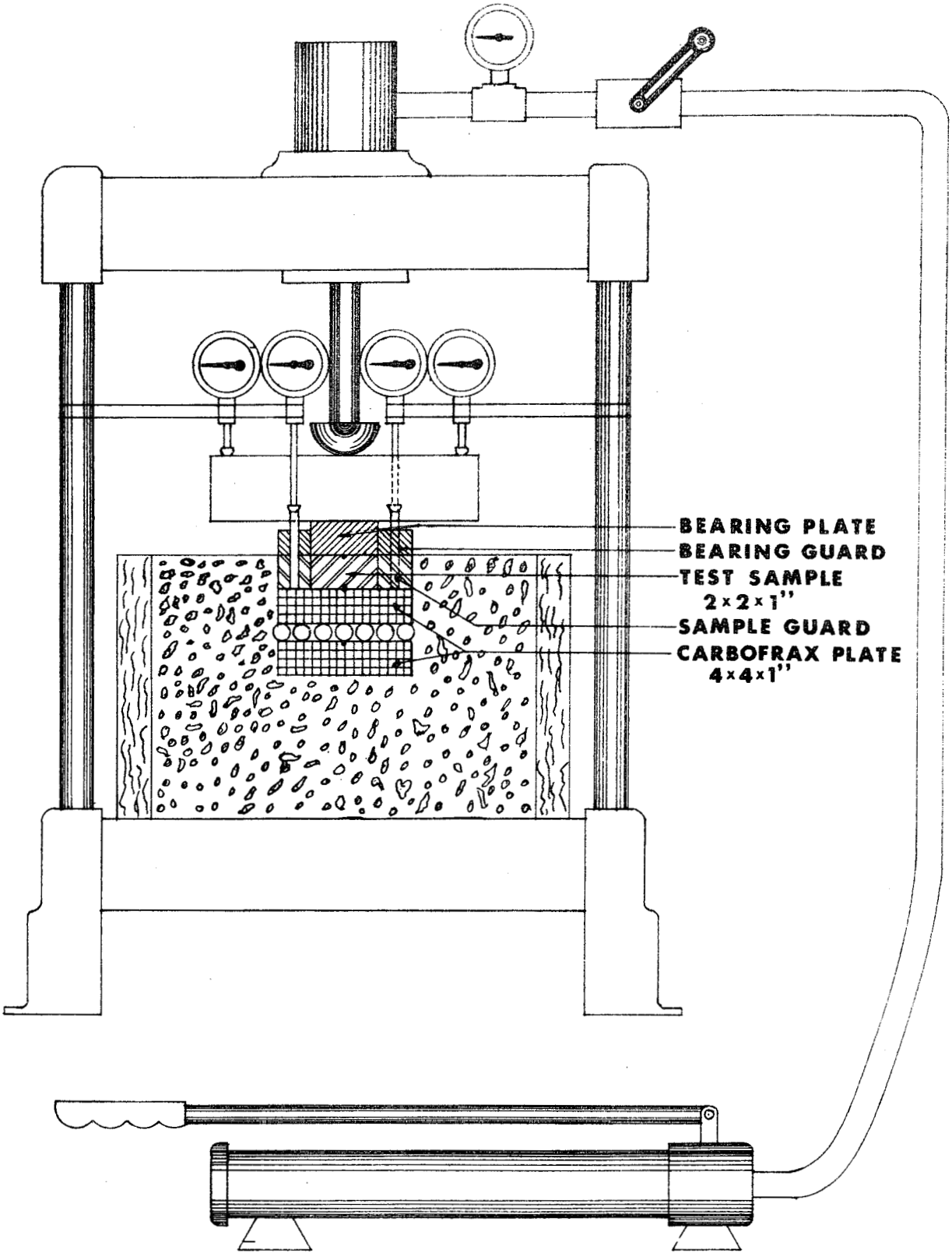

TYPICAL COMPRESSION—RELAXATION APPARATUS

Figure 3.1-5 presents both the room temperature and the 1400F hot face stress-strain relationships. The slopes of both were essentially the same although the hot face relationship more nearly passed through the zero-zero point on a straight line. This was probably due in part to the small preload (approximately 2 to 3 psi) applied to the hot face specimens at the "zero point" to insure a firm nesting of the hot and cold face thermocouples into the precut grooves in the specimen. No significance could be attached to the difference between the modulii of elasticity under hot face and room temperature conditions, and it was concluded that temperature had no effect upon this property of 35 pcf density MIN-K 2002. This confirmed earlier work by Martin Company, Nuclear Division (now Isotopes) that the compression modulus was independent of both temperature and extent of restraint (see Martin Co. Report No. MND-1369-45, dated January 1965, under Contract AT(30-1)-3169). Although the Martin Co. tests were conducted on MIN-K 1301, the submicron particulate structure of these materials is essentially the same.

It will be noted that the hot face tests were limited to 750 psi. This was considered to be well above the foreseeable load requirements, and it also approached the load limit (in pounds over a 4 x 4-in. area) of the heater assembly. Similarly, it represented a value well within the straight line portion of the stress-strain curve, thus providing a margin of safety. (The average stress-strain regression at room temperature began its slope change at 1100 psi, although several specimens indicated that this change might occur as low as 1000 psi.)

Deflection-Time Data. Following the stress-strain portion of the test, the maximum load scheduled for each specimen (100, 200, 300, 400, 500 or 750 psi) was applied and maintained for the remainder of the test. The specimen deflection was determined by the difference of the average of the two sets of dial readings (one set reading specimen plus furnace deflection, and one set reading furnace deflection). Loads were first applied to the specimens before 10:00 a.m. so that 6 hr of working time would be available for load adjustments necessitated by initial furnace creep. Subsequent dial readings and load adjustments were made at least once in the morning and once in the afternoon. Three to five specimens were tested at each load level, depending upon the variability of the data.

The average of the deflection-time data for each load level is plotted on a log-log scale in Figure 3.1-6. It was apparent that each average regression consisted essentially of two straight lines intersecting at between 15 and 30 hr. Although the tests were scheduled to run only for 500 hr, it was of interest to obtain some indication of the performance of the product for periods up to 10,000 hr. Consequently, it was necessary to determine the best mathematical expression for each regression. Admittedly, such an extrapolation was dangerous since it assumed that no further change in slope would occur.

FIGURE 3.1-5.

STRESS-STRAIN CHARACTERISTICS OF MIN-K 2002 AT 35 PCF

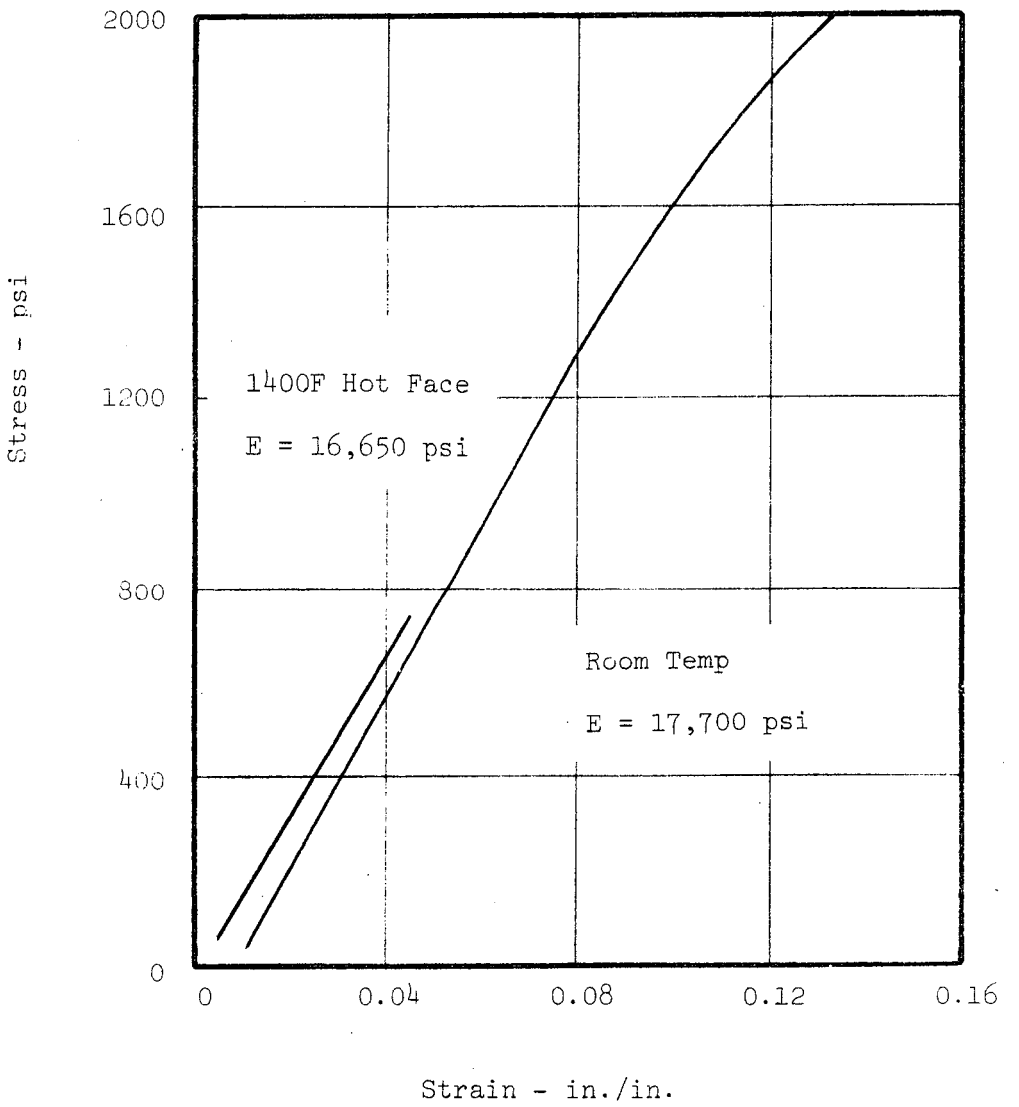

FIGURE 3.1-6.

EFFECT OF CONSTANT LOAD ON 35 PCF MIN-K 2002
AT 1400F HOT FACE

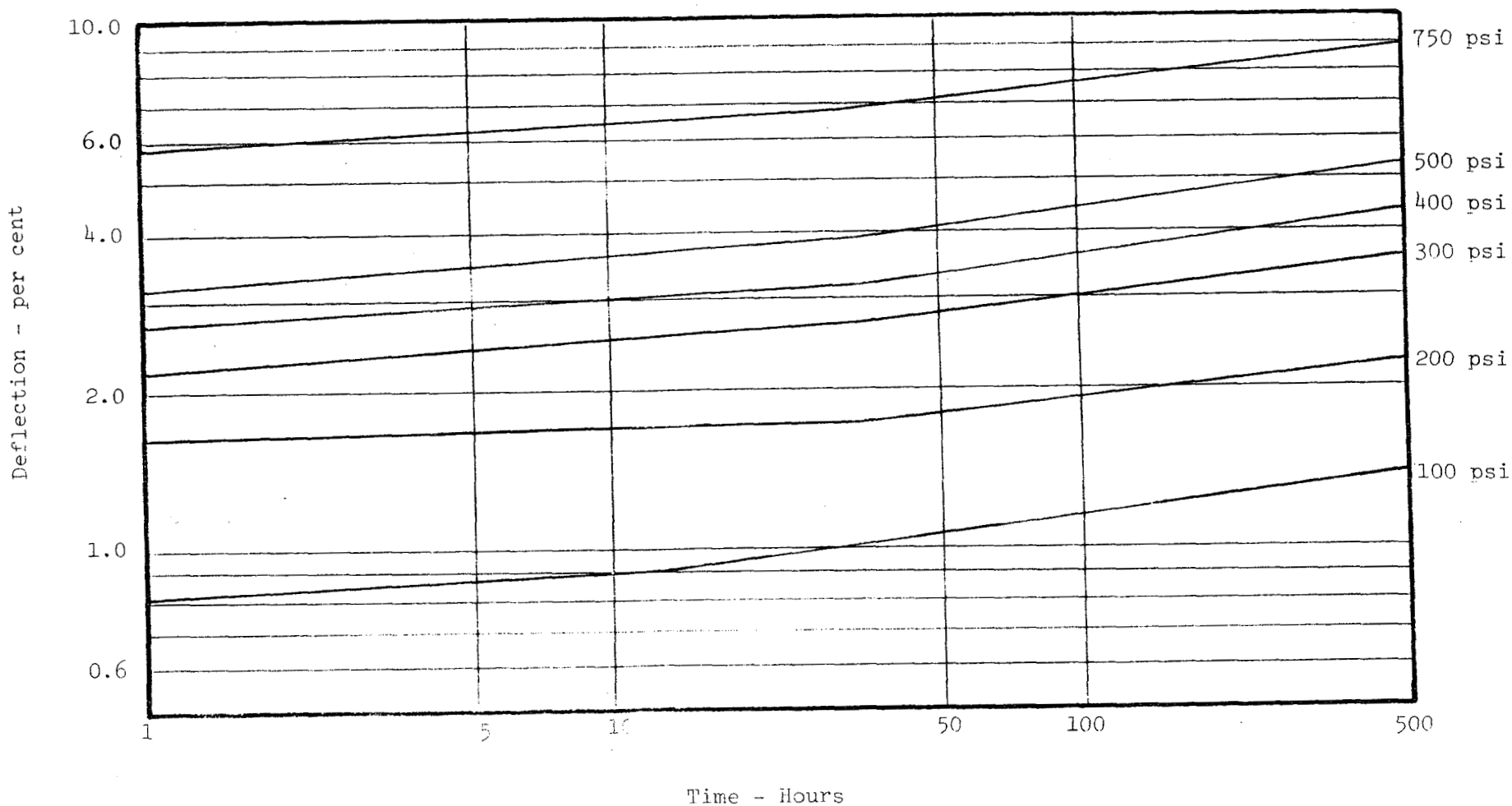

As a first attempt to achieve a mathematical relationship for each load level utilizing all of the data for each test specimen, an equation of the form

$$\log Y = A + B \log T + C (\log T)^2 \qquad (1)$$

where: Y = per cent deflection
T = time in hours

was used. In general, a high degree of correlation was attained with only several exceptions from a total of 24 sets of data. The equation constants were then used to extrapolate the deflection (Y) for times up to 10,000 hr. As anticipated, the Y values exceeded 100 per cent when the time approached 10,000 hr due to the time squared function in equation (1). Since these extrapolations carried no practical significance, they were not included in this report.

Subsequently, a straight line equation was assumed,

$$\log Y = A + B \log T \qquad (2)$$

and the first few data points eliminated from the analysis (the last data point to be eliminated was at T = 6 hr and the first to be included was at T = 22 hr). This may be justified on the basis that only the data at the higher values of time should control the extrapolation, and that the number of points excluded was small compared with the total. The equation constants, the index of determination, and the standard deviation of residuals for each specimen are given in Table 3.1-4. The index of determination represents the per cent of the variability of log Y that is explained by log T, whereas the standard deviation of residuals is the variability remaining in log Y not explained by the regression on log T. Only in the case of specimens 110C and 110D, both at 100 psi constant loading, did the index of determination drop below 95 per cent. Unexplained deviation from the curve at this low pressure could be expected since this region of specimen stress-strain is in the area where a curvilinear function may exist to a small degree.

Each equation was then plotted and extrapolated to 10,000 hr. The average relationship for each set of data, i.e., 100 psi, 200 psi, etc., was obtained by averaging the numerical values of deflection within each set at several intervals of time. These average curves are shown in Figure 3.1-7. It should be noted that between load levels of 100, 200, 300, 500 and 750 psi, there was only one

TABLE 3.1-4

EQUATION CONSTANTS FOR EACH 35 PCF MIN-K 2002 SPECIMEN
TESTED UNDER CONSTANT LOAD AND AT 1400F HOT FACE

Equation: Log Y = A + B Log T

Constant Load psi	Specimen ID	Constants A	Constants B	Index of Determination %	Standard Deviation of Residuals
100	102I	-0.209	0.140	98.6	0.0051
	110C	-0.239	0.045	78.9	0.0080
	110D	-0.253	0.065	66.2	0.0170
	110E	-0.200	0.136	97.5	0.0074
200	104D	0.316	0.065	99.0	0.0046
	107C	0.100	0.102	98.7	0.0039
	107H	0.156	0.066	98.4	0.0028
	110B	0.156	0.091	95.2	0.0068
300	104E	0.261	0.090	98.2	0.0030
	107B	0.305	0.103	99.1	0.0032
	110A	0.226	0.134	99.1	0.0043
	110F	0.241	0.135	99.4	0.0047
400	104F	0.367	0.095	98.5	0.0034
	107A	0.339	0.124	98.8	0.0045
	107G	0.250	0.125	99.5	0.0031
	104A	0.441	0.102	99.7	0.0019
	107I	0.212	0.124	99.3	0.0036
500	104G	0.414	0.102	99.6	0.0022
	104I	0.456	0.110	99.3	0.0031
	107F	0.440	0.112	99.7	0.0020
	110G	0.546	0.107	99.3	0.0034
750	107E	0.722	0.089	99.8	0.0013
	104H	0.709	0.096	99.8	0.0015
	107D	0.608	0.118	99.4	0.0028

FIGURE 3.1-7.

DEFLECTION VS TIME FOR 35 PCF MIN-K 2002 UNDER CONSTANT LOADS

1400F Hot Face

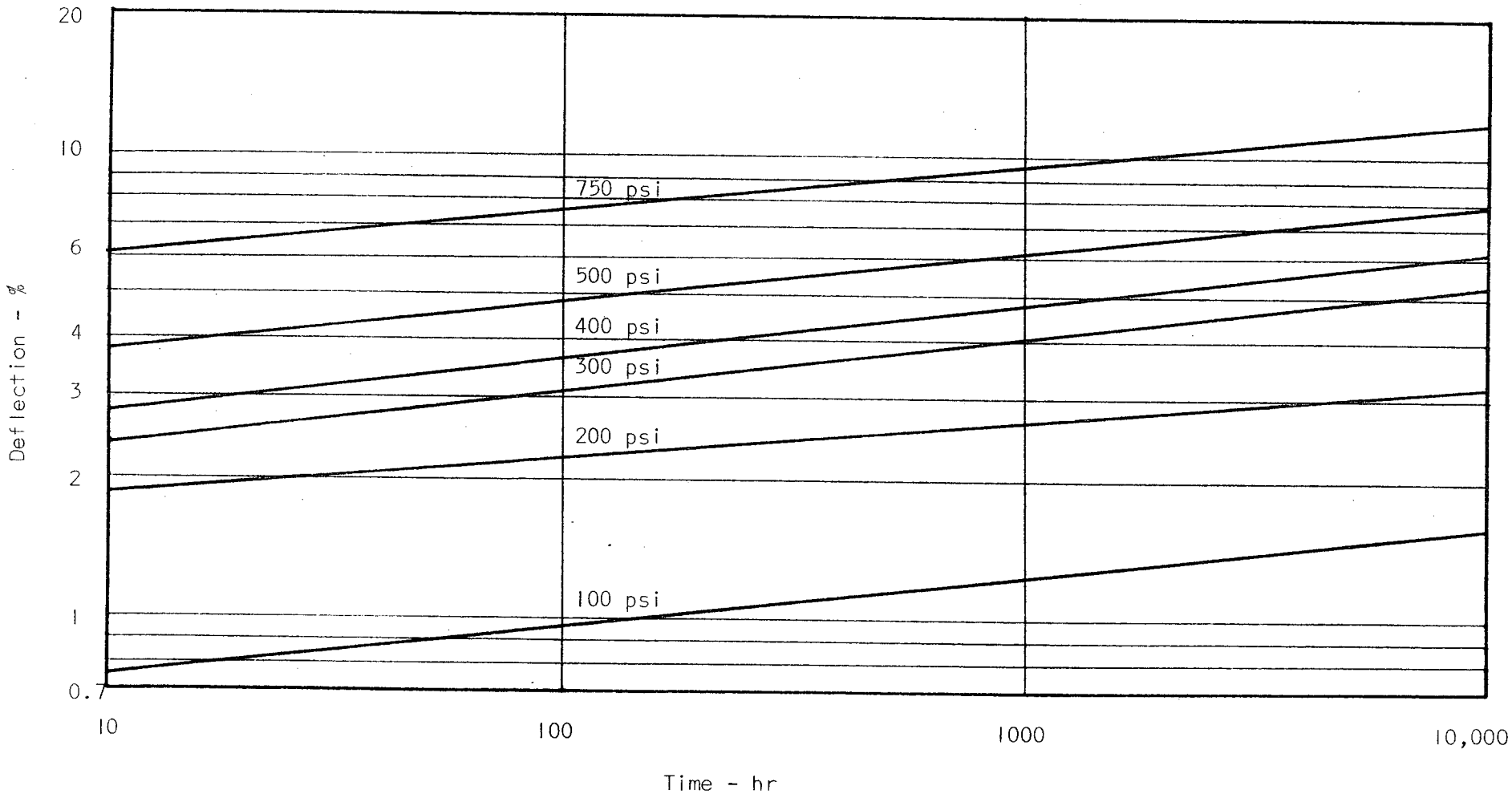

instance where overlapping occurred between individual relationships of two adjacent levels of load. (The highest individual relationship at the 200 psi level overlapped the lowest individual relationship at the 300 psi level between time equals 10 and 100 hr.) The maximum and minimum relationships at the 400 psi level overlapped their adjacent levels by a significant amount, however. These are summarized in Table 3.1-5. Some overlapping was anticipated, however, because of the high modulus of elasticity of 35 pcf MIN-K 2002, and the ±0.5 pcf density tolerance maintained on the test specimens. Although by normal standards the density tolerance was small, the effect of density on the modulus of elasticity was shown to be very significant. The average relationships shown in Figure 3.1-7 appeared reasonable, however, and were used in subsequent calculations, in spite of the apparent slope misfit for the 200 psi level.

Load-Relaxation Determination. The ultimate goal of this investigation was to determine the extent of the load-relaxation of the insulation once it had been compressed to a certain initial load, and subsequently maintained at a constant deflection. Such a condition would be encountered when the insulation was used as the heat source support where a preload was applied during assembly of the generator, and all relative dimensions were subsequently held constant for the life of the generator. It was known that the insulation would relax with time, but the direct measurement of this relaxation, or decrease in stress through the insulation was a relatively difficult trial and error experiment when testing the specimen at operating temperature.

To determine the relaxation of the insulation, the actual measured specimen deflection at time = 0 for a given load level was extended as a horizontal line across Figure 3.1-7. The intersection of this line with the sloping constant load regressions constituted the stress at that particular time which the insulation would be exerting on the closed generator system. (To facilitate this conversion from deflection to relaxation, Figure 3.1-7 was re-plotted in terms of log deflection vs log load at 10, 100, 1000, and 10,000 hr. This plot is not shown.)

The average measured time zero intercept was used since the intercepts calculated from equation (2) did not include the initial 6 hr of data. Table 3.1-6 compares the average measured values with the calculated equation constants for each load level. It was interesting to note that at 750 psi, the two values are the same, indicating that the break in the time-deflection curve may disappear at the higher loads.

The results of the conversion from a deflection-time relationship to a relaxation-time relationship are shown in Figure 3.1-8. All of these curves appeared satisfactory except for the 200 psi initial load relationship, which indicated a 220 psi specimen stress after 10 hr of loading. A problem of this

TABLE 3.1-5

MAXIMUM AND MINIMUM DEFLECTION VALUES FOR EACH LOAD LEVEL
AT 10 AND 10,000 HR

MIN-K 2002 @ 35 pcf and 1400F Hot Face

Load Level psi	Deflection, %			
	10 hr		10,000 hr	
	Minimum	Maximum	Minimum	Maximum
100	0.65	0.85	0.88	2.2
200	1.6	2.4	2.6	3.8
300	2.2	2.6	4.2	6.0
400	2.2	3.4	5.1	7.1
500	3.2	4.5	6.5	9.3
750	5.3	6.5	11.8	12.5

TABLE 3.1-6

MEASURED AND CALCULATED TIME ZERO INTERCEPTS (DEFLECTIONS)

MIN-K 2002 @ 35 pcf and 1400F Hot Face

Load Level psi	Deflection @ Time Zero, %	
	Average Measured Value	Average Calculated Value
100	0.70	0.60
200	1.68	1.53
300	2.02	1.81
400	2.36	2.10
500	3.07	2.92
750	4.78	4.78

FIGURE 3.1-8.

STRESS VS TIME AT CONSTANT DEFLECTION FOR VARIOUS INITIAL LOADS

MIN-K 2002 at 35 pcf
1400F Hot Face

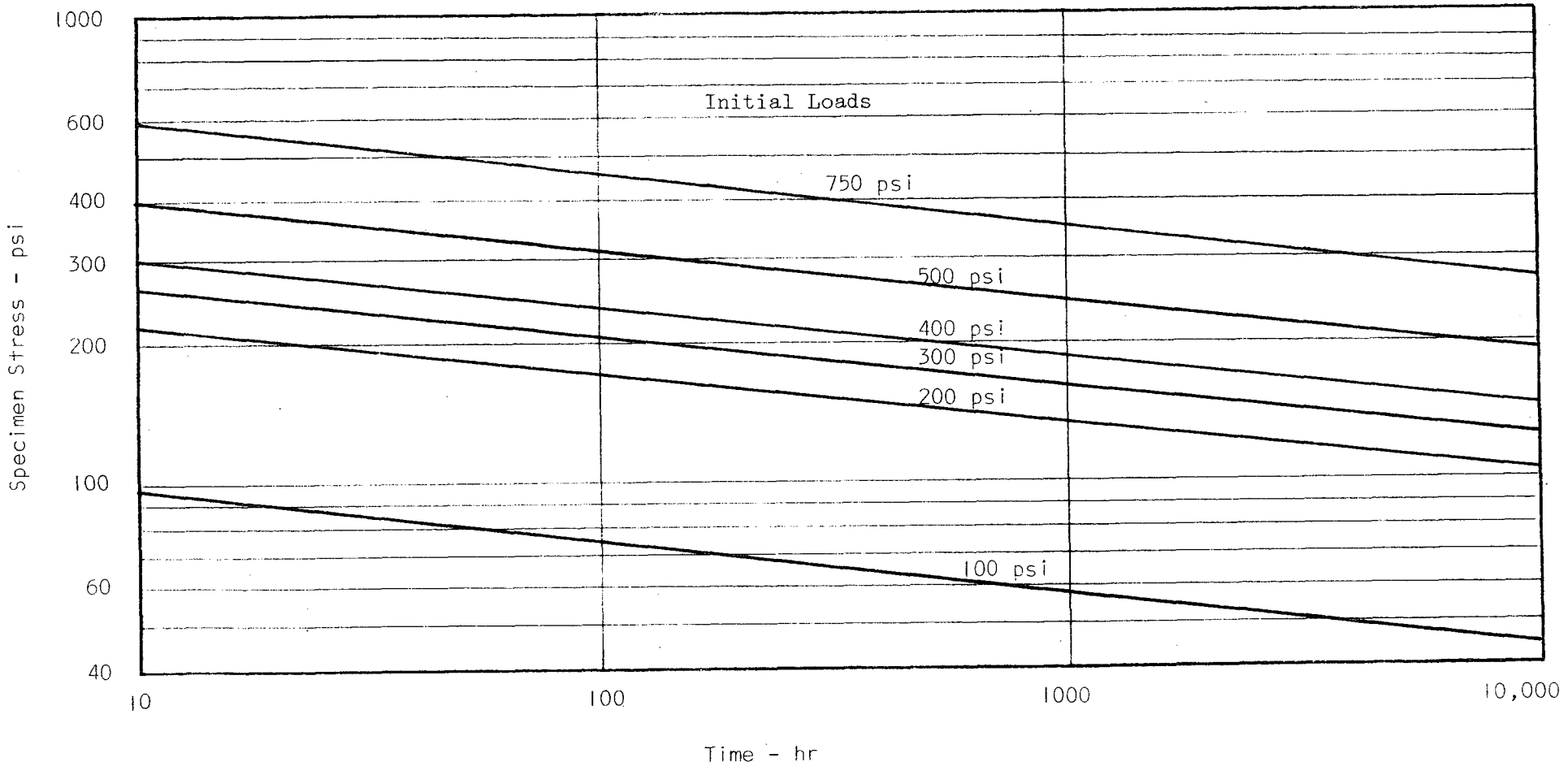

nature could have been anticipated, however, due to the apparent slope misfit shown in Figure 3.1-7 following the extrapolation of the basic data to 10,000 hr.

Figure 3.1-8 was then converted to its final form of per cent of initial load vs time as shown in Figure 3.1-9. The 200 psi initial load curve was not converted for the reason indicated previously. Similarly, the 100 psi initial load curve was not converted because it also did not conform to the same regression as did the 300 to 750 psi initial load regressions. This mismatch probably related back to the fact that the stress-strain relationship of 35 pcf MIN-K 2002 for loads up to 100 psi may be slightly curvilinear. Had it been plotted, however, it would have ranged from 97 per cent of initial load at 10 hr, to 44 per cent of initial load at 10,000 hr. The spread of data at 10,000 hr for the regression plotted in Figure 3.1-9 was approximately ±5 per cent (i.e., the per cent of initial load for 300 to 750 psi initial loads varied from about 34 per cent to 44 per cent).

Summary of Analysis. The largest single source of potential error in the above analysis was the extrapolation of the data from 500 hr to 10,000 hr. It assumed that there was no further change in slope of the deflection-time curve as was noted at about 15 hr. This was probably a reasonable assumption, however, since Phase I [1] load-relaxation tests on 20 pcf MIN-K 2002 (at considerably lower pressure, and by a slightly different technique) resulted in a straight line relationship up to 2000 hr. Thus, although there was reason to believe that the extrapolation was valid, it must be considered indicative only.

It was mentioned at the outset of this Subtask that the Phase I effort indicated that MIN-K 2002 at 20 pcf density would relax to about 50 per cent of its initial load for initial loads up to 150 psi after 2000 hrs. It can be seen from Figure 3.1-9 that the 35 pcf MIN-K 2002 also relaxes to about 47-48 per cent of its initial load after 2000 hrs. Although this consistency of results between two widely different product densities lends credence to the data, it would appear that little change in the load relaxation characteristics has been made as a result of the density increase. However, it should be stressed that the 20 pcf density product should not be loaded above 150 psi, whereas the 35 pcf density product will tolerate initial loads up to 750 psi. Thus, even with the same per cent load relaxation rate, the higher density product has a considerable higher load carrying and load retention (in actual pounds or psi) capability than the lower density product.

Thermal Conductivity. The thermal conductivity of MIN-K 2002 at 35 pcf was determined by the Guarded Hot Plate technique in air and argon between 500F and 1200F mean temperature. Figure 3.1-10 presents the data points and the probable area into which each average curve would fall had a large number of specimens been tested. The area of the conductivity curve in air was obtained by drawing

FIGURE 3.1-9.

LOAD-RELAXATION WITH TIME FOR 35 PCF MIN-K 2002

1400F Hot Face

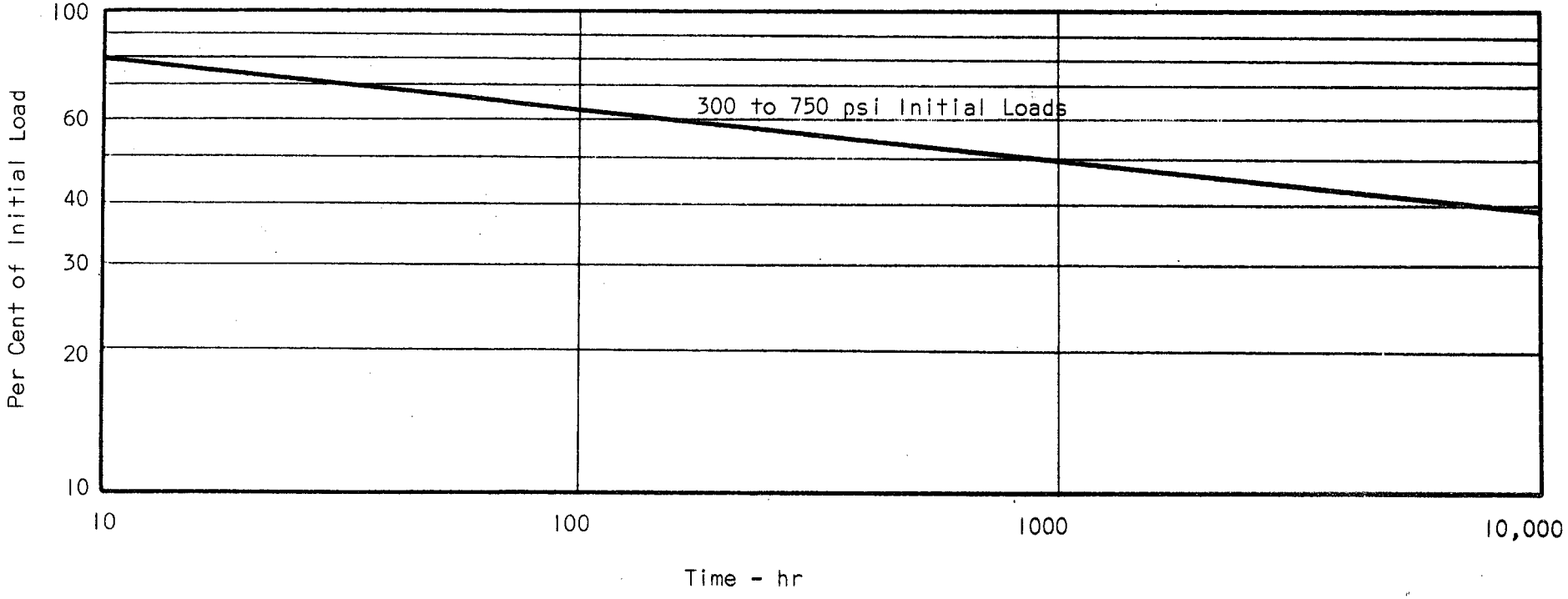

FIGURE 3.1-10.

THERMAL CONDUCTIVITY OF 35 PCF
MIN-K 2002 IN AIR AND ARGON

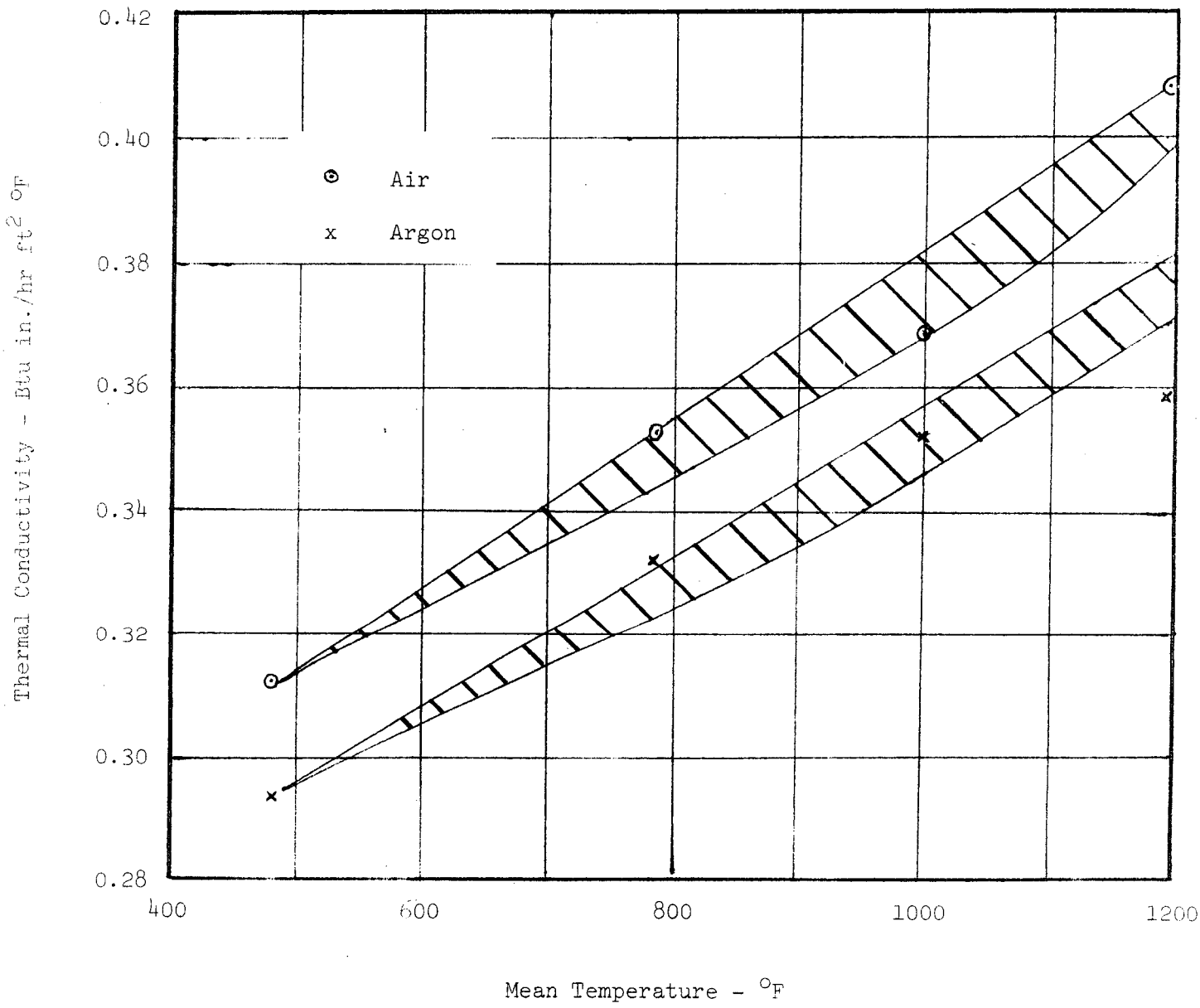

the "maximum" and "minimum" curves through the air data points. The area of the conductivity curve in argon considered not only the data points, but also the parallel relationship between air and argon values discussed previously for 20 pcf MIN-K 2002. The magnitude of the difference between the upper and lower limits of each area is well within normal experimental error. Similarly, points outside the areas do not deviate from the area by more than the potential experimental error. These data were generated by Dynatech Corp., Cambridge, Mass.

SUBTASK 3.2 - LOAD-BEARING INSULATION TO 1800F

Introduction. Phase I of AT(29-2)-2661 [1] concluded that GLASROCK 25, a 25-30 pcf density foamed silica product made by Glasrock Products, Inc., was best suited for load-bearing applications up to 200 psi at 1800F hot face. This conclusion was reached not only because of the product's ability to withstand this load with no measurable permanent set (and hence, no relaxation), but also because of its relatively low thermal conductivity and low density compared with other ceramic materials of comparable compressive strength. The nature of the product also lent itself to possible thermal opacification (through the addition of particulate opacifiers such as those used in the MIN-K formulations) to further enhance its insulating value. Therefore, Glasrock Products, Inc., Atlanta, Georgia, was subcontracted under Phase II of this contract to investigate the manufacturing techniques required to add various thermal opacifiers to this product without significantly altering its compressive strength, and to assist in the evaluation of such new products.

The planned program consisted of three parts. The first part covered the introduction of the four candidate opacifiers (described later) into the foam matrix, and the subsequent evaluation of the resulting products for cold crushing strength, thermal stability in air and vacuum at 1800F (isothermal), X-ray analysis to determine cristobolite content, Rapid Heat Meter thermal conductivity evaluation at 800F mean temperature, permanent set under 200 psi load at 1800F hot face after 1 wk, and chemical analysis to determine opacifier content.

Part 2 of the program repeated Part 1 using the two best opacifiers (based upon the physical properties determined in Part 1), but at two different levels of opacifier content to establish the effect of opacifier content on the physical properties.

Part 3 was scheduled to determine the normal variation in physical properties which could be anticipated in the production of the optimum opacified product. Part 3 was not undertaken for reasons which will become evident.

The manufacturing techniques and the process modifications necessary to introduce opacifiers into the product are contained in the Glasrock Products, Inc. Final Report, and presented as Appendix B. With the exception of the conclusions, physical property data, and other general observations, the details of the manufacture will not be discussed in the main body of this report.

Part 1 - Candidate Opacifiers. The candidate opacifiers were:

a. TiO_2 - -5μ HG TiO_2 supplied by TAM Division, National Lead Company

b. Cr_2O_3 - Charles Pfizer Company

c. ZrO_2 - TAM Division, National Lead Company

d. $ZrSiO_4$ - TAM Division, National Lead Company

These materials were chosen for evaluation based on their apparent stability at elevated temperatures, their known ability to block radiation transmission, and their availability.

Although the grade or average particle size of each candidate was chosen based upon the manufacturer's literature, it was desirable to determine the particle size distribution of each to assess further its suitability as an opacifier. Previous work (1) had shown that a 1.5 to 2.5 micron particle size was optimum for the anticipated service temperatures.

The particle size distributions were determined using a Coulter Counter. This instrument operates on the principle which involves the determination of the volume of each particle while suspended in an electrolyte, and the counting of all particles within the limits of 0.6 microns and 180 microns (spherical diameter). A typical analysis would involve 20,000 to 40,000 particles, thus providing a statistically accurate sample description. Data reduction was computerized to yield information in tabular and graphical form, both as differential and cumulative percentages, and with weight and number distribution.

Table 3.2-1 summarizes the particle size distribution of the four candidate opacifiers. Expanding the optimum desired size range from 1.5 to 2.5 microns, to 1 to 3 microns, the distribution data can be regrouped to give an indication of which material might be the best from a particle size standpoint. This is shown in Table 3.2-2. On this basis, one would expect the TiO_2 and the $ZrSiO_4$ to perform about equally, whereas the Cr_2O_3 and ZrO_2 would be less efficient. However, since each material has its own opacification efficiency, the relative performance of each based on thermal conductivity tests must be the final criterion.

Part 1 - Manufacture. Fifteen per cent by weight (dry basis) was selected as the opacifier content for the first series of experimental formulations. The slurries were cast into 20-in. long by 15-in. high by 4-in. wide slabs which were subsequently slit into thinner sections (approximately 1 in.) for product evaluations. When slit, the position of the individual pieces relative to the

TABLE 3.2-1

PARTICLE SIZE DISTRIBUTION OF CANDIDATE OPACIFIERS FOR GLASROCK 25 FOAMED SILICA

Equiv. Spherical Diameter microns	Weight, %			
	TiO_2	Cr_2O_3	ZrO_2	$ZrSiO_4$
< 1	0	2	18	0
1 - 2	19	23	24	45
2 - 3	53	34	24	29
3 - 4	20	25	20	15
4 - 6	7	15	12	11
> 6	1	1	2	0

TABLE 3.2-2

PARTICLE SIZE DISTRIBUTION OF CANDIDATE OPACIFIERS
PRESENTED IN TERMS OF OPTIMUM SIZE RANGE

Size Range Microns	Weight, %			
	TiO_2	Cr_2O_3	ZrO_2	$ZrSiO_4$
1 - 3	72	57	48	74
Balance	28	43	52	26

original casting was noted to establish product uniformity trends. Thus comparisons were made between specimens at the top and bottom of the original casting, as well as between the center and outer sections.

The introduction of the opacifiers into the slurry definitely necessitated changes in the manufacturing procedure as noted in Appendix B. Indications were that 15 per cent was the maximum opacifier content which could be tolerated. The pore structure of each of the four products was not as uniform as in the standard unopacified product. Internal cracks were evident after the slabs were slit, and several pours never reached the firing stage due to slumping in the plaster molds.

Sufficient material was available from each formulation, however, to permit product evaluation. Since these samples represented the "first screening", no attempt was made to solve the manufacturing problems at this time.

Part 1 - Density. Since the opacified product should retain as much of the strength as possible exhibited by the unopacified product, an attempt was made to increase the density of the product by the amount of opacifier added (15 per cent). Theoretically, this would represent a 29-30 pcf product. Overall density control, however, was not as close as desired as shown in Table 3.2-3, which presents the average of five determinations. With the exception of the zircon specimens, however, the density within a given casting appeared to be quite uniform. Similarly, the five individual determinations were all acceptably close to their average.

Part 1 - Cold Crushing Strength. The effect of the opacifiers on the cold crushing strength of the blocks was very evident as shown in Table 3.2-4. The zirconia values were an average of five tests, whereas the remaining values were averages of three tests. Similarly, the effect of location within the casting is shown. Only the zirconia product showed a significant difference between locations, although density and opacifier content evaluations could not explain this difference.

To some extent, the loss of cold crushing strength of the chromia and the zirconium silicate specimens was attributed to the low density of the product (see Table 3.2-3). However, it was also suspected that the presence of 15 per cent opacifier physically or chemically affected the strength.

Part 1 - Thermal Stability. Table 3.2-5 presents the average linear shrinkage of the products after 168 hr (1 wk) at 1800F (isothermal) in air. The values represent an average of eight 3 x 2 x 1-in. specimens, four tested at Glasrock Products, Inc. and four at the Johns-Manville Research & Engineering Center.

TABLE 3.2-3

DENSITY OF OPACIFIED GLASROCK 25 SPECIMENS - PART I

Opacifier	Specimen Location	Product Density pcf
ZrO_2	top	27.8
	bottom	28.2
TiO_2	top	29.2
	bottom	29.6
$ZrSiO_4$	top	25.6
	bottom	27.1
Cr_2O_3	top	24.8
	bottom	25.0

TABLE 3.2-4

COLD CRUSHING STRENGTH OF OPACIFIED GLASROCK 25 - PART I

Opacifier	Specimen Location	Crushing Strength psi
ZrO_2	top	603
	bottom	789
TiO_2	top	366
	bottom	346
$ZrSiO_4$	top	181
	bottom	187
Cr_2O_3	top	84
	bottom	71
none		500 - 750

TABLE 3.2-5

THERMAL STABILITY OF OPACIFIED GLASROCK 25 - PART I

(168 hr at 1800F in air)

Opacifier	% Average Linear Shrinkage
ZrO_2	0.31
TiO_2	0.04
$ZrSiO_4$	0.08
Cr_2O_3	0.05

There was excellent agreement between the two groups of data. The thermal stability in air of all specimens appeared to be satisfactory.

To evaluate the thermal stability of these products in vacuum at 1800F (isothermal), four specimens of each product were placed into individual ceramic tube furnaces which were connected by a manifold to a common vacuum system. Upon achieving the desired temperature (with continuous evacuation during heatup), it was noted that 15 microns was the minimum pressure which could be achieved within the four tubes. Isolating each tube separately, it was found that the specimens containing chromia were outgassing rapidly. Similarly, the specimens containing zircon were also outgassing although to a lesser degree (maximum vacuum attainable was 4 microns). The zirconia and titania specimens, on the other hand, were readily pumped to approximately 1 micron. Upon isolation of these tubes from the vacuum pump, the pressure rise within these furnace chambers was extremely slow, indicating little or no outgassing from the zirconia or titania. The chromia and zircon specimens were then isolated from the vacuum system for the remainder of the test (168 hr) and allowed to achieve equilibrium pressure ($>$ 100 microns). The other two sets of specimens were pumped continuously and maintained at approximately 1 micron. Within the accuracy of measurement ($\pm$0.002 in.) none of the specimens showed any linear shrinkage as a result of this exposure.

Part 1 - Chemical Analysis. The chemical analysis results (by convential wet analysis techniques) are given in Table 3.2-6. The analysis was run only for the particular opacifier in question, and the balance was considered to be silica. The distribution of the opacifier within the cast slabs was excellent as shown by the 0.2 per cent maximum variation between the top, middle, and bottom portions of the slab. The average opacifier content compared closely with the intended amount of 15 per cent.

Part 1 - Thermal Conductivity. The thermal conductivity of the four products is summarized in Table 3.2-7. Two specimens of each product were tested, and as anticipated from the density and chemical analysis determinations, the variation in conductivity between specimens was small.

Also presented in Table 3.2-7 are the "partial densities" of opacifier and silica based upon the chemical analysis. To examine the relationship between thermal conductivity and silica density, these parameters were plotted as shown in Figure 3.2-1. A distinct correlation appeared to exist, as was also shown to be the case with high density MIN-K (see Subtask 3.1). It appeared, therefore, that the silica density was the dominant factor, and that the difference in opacification efficiency which one might expect between opacifiers would not become evident.

Part 1 - Permanent Set. Four zirconia and two titania specimens (4 x 4 x 1 in.) were subjected to 1800F hot face and a constant load of 200 psi for 168 hr.

TABLE 3.2-6

CHEMICAL ANALYSIS OF OPACIFIED GLASROCK SPECIMENS - PART I

Opacifier	Opacifier Content, %			
	Top	Middle	Bottom	Average
ZrO_2	14.4	14.4	14.3	14.4
TiO_2	14.2	14.4	14.4	14.3
$ZrSiO_4$	14.4	14.4	14.4	14.4
Cr_2O_3	15.9	15.8	15.8	15.8

TABLE 3.2-7

THERMAL CONDUCTIVITY AND DENSITY OF OPACIFIED GLASROCK SPECIMENS
PART I

Sample No.	Opacifier	Density, pcf			Conductivity @ 800F*
		Product	Opacifier	Silica	Btu in./hr ft^2 $^\circ$F
1	ZrO_2	28.0	4.00	24.0	1.28
2	ZrO_2	28.0	4.00	24.0	1.26
3	TiO_2	29.6	4.23	25.4	1.28
4	TiO_2	29.4	4.21	25.2	1.26
5	$ZrSiO_4$	27.2	3.92	23.3	1.15
6	$ZrSiO_4$	27.1	3.90	23.2	1.14
7	Cr_2O_3	25.0	3.95	21.1	1.01
8	Cr_2O_3	24.6	3.89	20.7	0.99

*Nominal mean temperature - actual ranged between 770F and 805F

FIGURE 3.2-1.

THERMAL CONDUCTIVITY VERSUS SILICA DENSITY OF GLASROCK AT 15 PER CENT OPACIFICATION LEVEL

PART I

(770F - 805F Mean Temperature)

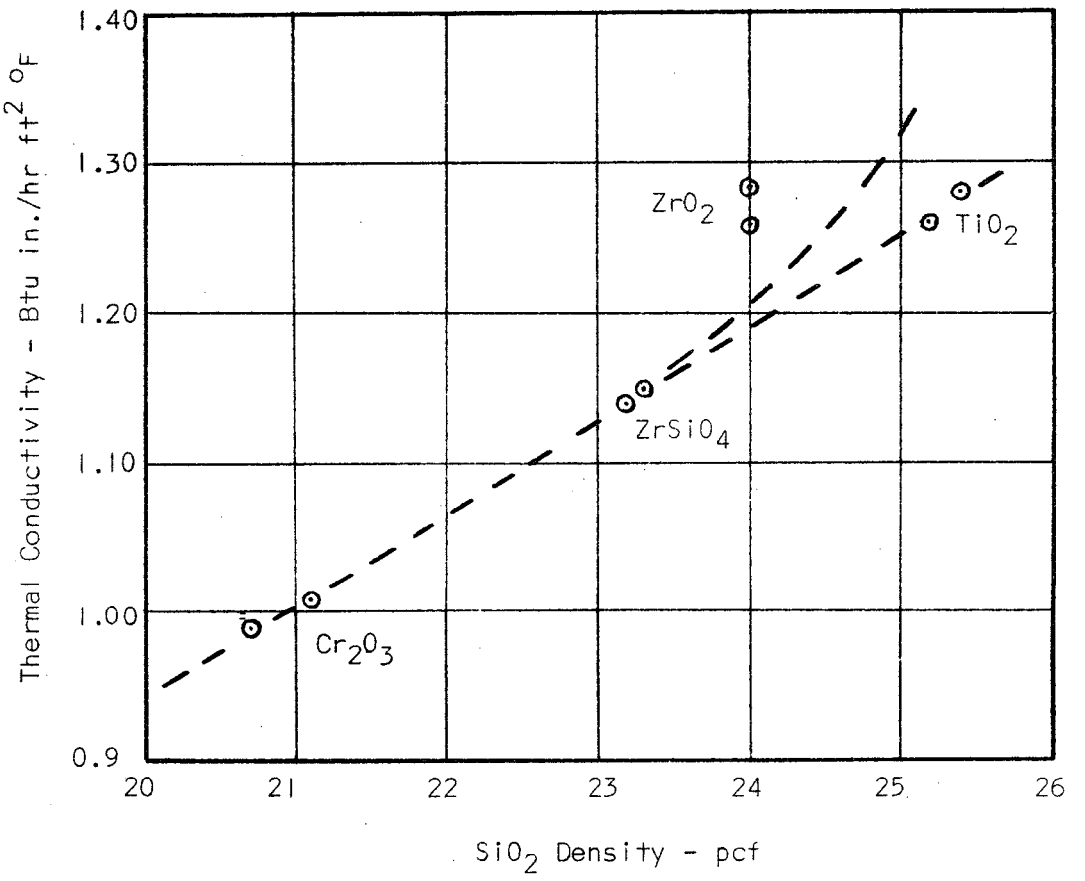

Table 3.2-8 shows the permanent set of each specimen (thickness direction) in terms of inches. Although the zirconia specimens had twice the cold crushing strength of the titania specimens, the zirconia specimens had a greater tendency to creep under 200 psi constant load. The chromia and zircon products were not evaluated since their cold crushing strength was already below 200 psi.

Part 1 - Conclusions. Zircon and chromia were eliminated from subsequent consideration as candidate opacifiers due to their outgassing tendency, and their highly detrimental effect upon the cold crushing strength. Titania, although relatively low in cold crushing strength, showed less creep or permanent set under constant load than zirconia. It also was the lightest of the opacifiers, and hence, would opacify more efficiently on a weight basis. Fifteen per cent zirconia, however, did not alter the ultimate crushing strength and thus should be given additional consideration. It also provided fewer manufacturing problems than the titania.

Part 2 - Manufacture. The manufacture of Glasrock silica foam containing 5 and 10 per cent (nominal) ZrO_2 was conducted in the same manner as the previous product containing 15 per cent ZrO_2. No basic difficulties were encountered, and it was estimated that the pore size was slightly smaller and more uniform as a result of the lower opacifier content. Comments by the manufacturer indicated that the lower additive content appeared to have less effect upon the unfired characteristics of the foamed slab (internal sag, drying cracks, etc.) than the original 15 per cent level. Consequently, less control over slurry properties such as per cent solids and pH would be required under production conditions.

Similar success was not achieved with the 5 and 10 per cent TiO_2 products. Although the 15 per cent TiO_2 product was successfully manufactured and evaluated, the first run of the 10 per cent TiO_2 product resulted in a complete loss of all usable material due to excessive cracking and crazing of the product. The 5 per cent TiO_2 specimens also cracked and crazed, but a judicious choice of test samples permitted the product evaluation to be conducted.

Subsequently, three more 10 per cent titania batches and one each at the 15 and 5 per cent titania levels were tried. In two cases, 60 per cent of the fired slab contained cracks, while the remaining three batches were discarded due to excessive slumping during the drying stage.

The manufacturing process was then radically changed such that in place of the 18-hr mixing of titania with the slurry (in a large ball mill without the grinding balls), a 30-min mixing cycle was substituted, using the grinding balls. This resulted in an excellent slab, free from internal cracks and voids. A repeat of this run also resulted in a sound slab, although it did not totally survive the shipment from Atlanta, and appeared to have less uniformity of pore structure than its immediate predecessor.

TABLE 3.2-8

PERMANENT SET OF OPACIFIED GLASROCK SPECIMENS - PART I

(1800F Hot Face, 200 psi, 168 hr)

Sample	Permanent Set (Thickness Direction) in.
ZrO_2 - 1	0.006
ZrO_2 - 2	0.005
ZrO_2 - 3	0.017
ZrO_2 - 4	0.010
ZrO_2 - Average	0.010
TiO_2 - 1	0.003
TiO_2 - 2	0.003
TiO_2 - Average	0.003

The complete physical property evaluation of the Part 2 candidate formulations was limited to the 5 and 10 per cent zirconia, and the 5 per cent titania materials. The 10 per cent titania formulations were evaluated for thermal conductivity only.

Part 2 - Density. The density of the 5 per cent TiO_2 and the 5 and 10 per cent ZrO_2 opacified products is summarized in Table 3.2-9. In general, the product density was considered satisfactory. Maximum uniformity was obtained with the 5 per cent TiO_2 product, while the major variation in the ZrO_2 products occurred in the thermal stability specimens, which also were the smallest of the test specimens.

Part 2 - Cold Crushing Strength. The effect of 5 and 10 per cent ZrO_2 and 5 per cent TiO_2 on the cold crushing strength of the product is summarized in Table 3.2-10. A comparison with previous tests on the 15 per cent opacified products showed that the reduction in ZrO_2 content had little effect (695 psi vs 730 psi) on the average crushing strength at room temperature. This should be anticipated since the strength was already in the 500-750 psi range of the standard unopacified product. The reduction in TiO_2 content from 15 per cent to 5 per cent, however, resulted in a significant increase in strength (355 psi to 600 psi). Thus, it would appear that the TiO_2 at the 15 per cent level did have a physical or chemical effect upon the silica structure, even though none was obvious. It will be noticed that the average silica density of these three products, the factor which probably controls the strength of the product, was between 25 and 30 pcf (normal for the unopacified product).

Part 2 - Chemical Analysis. The chemical analysis of three experimental products is given in Table 3.2-11. Four specimens were analyzed from various parts of a slab. The results indicated good uniformity, and, with the possible exception of the 10 per cent ZrO_2 product, that the target opacifier contents were achieved with reasonable success.

The analysis of these specimens was conducted by X-ray emission spectrography utilizing a lithium tetraborate fusion technique. Two grams (2.000g) of -100 mesh sample were fused with 10.0000g $Li_2B_4O_7$ in a platinum crucible. The homogeneous melt was cast on a hot aluminum plate and allowed to solidify in the form of a glass button. The bottom surface of the button was wet ground and polished on a metallographic wheel fitted with a No. 320 grit paper. The X-ray intensities of zirconium (ZrK alpha) and of titanium (TiK alpha) were measured according to appropriate X-ray spectrographic techniques, and compared with the respective intensities of standard buttons of known composition prepared from spectrographically pure oxides in exactly the same manner. The accuracy of this technique had been established at ± 0.1 per cent (i.e., 8.8 ± 0.1 per cent).

TABLE 3.2-9

PRODUCT DENSITY OF OPACIFIED GLASROCK SPECIMENS - PART 2

	Average Density, pcf		
	5% ZrO_2	10% ZrO_2	5% TiO_2
Slabs before cutting*	28.1	29.4	29.3
Conductivity samples (2) (12 x 12 x 1 in.)	28.1	29.7	29.2
Permanent Set (4) (4 x 4 x 1 in.)	28.0	29.1	29.2
Thermal Stability (4) (3 x 2 x 1 in.)	29.2	27.6	29.3
Probable Average**	28.2	29.3	29.3

* Number and size varied depending upon degree of breakage during shipment.
**Added weight given to the larger samples.

TABLE 3.2-10

COLD CRUSHING STRENGTH OF OPACIFIED GLASROCK - PART 2

Opacifier	Average Cold Crushing Strength, psi (4 Tests)
5% ZrO_2	736
10% ZrO_2	726
5% TiO_2	600

TABLE 3.2-11

OPACIFIER CONTENT OF GLASROCK SPECIMENS - PART 2

Opacifier	Opacifier Content, %			
	Top	Middle	Bottom	Avg
ZrO_2	4.4	4.6	4.6	
	4.6			4.6
ZrO_2	8.8	8.8	8.8	
			8.8	8.8
TiO_2	5.1	5.1	5.1	
	5.1			5.1

Part 2 - Thermal Stability. The thermal stability of the opacified Glasrock specimens (3 x 2 x 1-in. in size) is given in Table 3.2-12. Each value represents an average of the length, width, and thickness of three specimens subjected to 1800F for 168 hr. No significant difference in shrinkage was found either between specimens, or between measurement direction of a particular specimen. Thermal stability of all specimens was considered satisfactory.

Part 2 - Permanent Set. Four 4 x 4 x 1-in. specimens of each Glasrock formulation were subjected to 1800F hot face and a constant load of 200 psi for 168 hr. Table 3.2-13 shows the permanent set of each specimen (thickness direction) in terms of inches resulting from the load. A comparison of these data with those presented for the 15 per cent opacified products showed that the TiO_2 content had little or no effect upon the load-carrying capability of the product. Conversely, the average permanent set of the ZrO_2 products was definitely related to the ZrO_2 content (0.005 in., 0.008 in., and 0.010 in. for the 5, 10 and 15 per cent products, respectively). This was somewhat unfortunate in light of the manufacturing problems connected with the TiO_2 products. At this point, ZrO_2 was the prime opacification candidate, but its presence in the silica matrix appeared to affect the long-term load-carrying capability.

Part 2 - Thermal Conductivity. The thermal conductivity of all opacified Glasrock specimens is presented in Table 3.2-14. Also shown is the total product density, opacifier density (by analysis), and silica density (by difference). The exception to this is specimens 15, 16, 17, and 19 which were not analyzed for opacifier content.

Specimens 15 and 16 represented the first successful manufacture of the 10 per cent titania formulation (opacifier ball-milled into slurry 30 min). These two specimens were also the first to show a significant improvement in thermal conductivity below the conductivity-silica density relationship described in Figure 3.2-1. Specimen 17 represented a "duplication" of Specimens 15 and 16 using the same manufacturing technique. The thermal conductivity, however, was not duplicated. Specimens 18 and 19 represent retests of Specimens 10 and 16, respectively, to confirm that the conductivity equipment was not the cause of the sudden drop in conductivity with Specimens 15 and 16.

To complete the study of the effect of the opacifiers on the thermal conductivity of Glasrock, a series of unopacified specimens ranging in density from 18.2 pcf to 30.4 pcf was also tested in the Rapid Heat Meter apparatus at 800F mean temperature. The results of these tests are shown in Table 3.2-15.

Figure 3.2-2 is a comparison of all data in Table 3.2-14 and Table 3.2-15 on a thermal conductivity vs product density basis. It was apparent that the data fell into two distinct groups: opacified and unopacified specimens. The most recent 10 per cent titania formulations showed the most scatter around the

TABLE 3.2-12

THERMAL STABILITY OF OPACIFIED GLASROCK SPECIMENS - PART 2

(168 hr at 1800F)

Opacifier	Average* Linear Shrinkage, % Air	Vacuum
5% ZrO_2	0.23	0.09
10% ZrO_2	0.44	0.08
5% TiO_2	0.26	0.20

* Average of three specimens each measured for length, width, and thickness shrinkage.

TABLE 3.2-13

PERMANENT SET OF OPACIFIED GLASROCK SPECIMENS - PART 2

(168 hr, 1800F hot face, 200 psi)

Sample	Permanent Set (Thickness Direction) in.
5% ZrO_2 - 1	0.005
- 2	0.005
- 3	0.007
- 4	0.003
- Average	0.005
10% ZrO_2 - 1	0.006
- 2	0.009
- 3	0.004
- 4	0.011
- Average	0.008
5% TiO_2 - 1	0.000
- 2	0.005
- 3	0.004
- 4	0.002
- Average	0.003

TABLE 3.2-14

THERMAL CONDUCTIVITY AND DENSITY OF
ALL OPACIFIED GLASROCK SPECIMENS - PARTS 1 AND 2

Specimen No.	Opacifier Amount and Type	Density, pcf			Conductivity @ 800F* Btu in./hr ft^2 ^{o}F
		Product	Opacifier	Silica	
1	5% ZrO_2	28.0	1.3	26.7	1.24
2	5% ZrO_2	27.8	1.3	26.5	1.24
3	10% ZrO_2	30.2	2.6	27.6	1.34
4	10% ZrO_2	29.4	2.6	26.8	1.29
5	15% ZrO_2	28.0	4.0	24.0	1.28
6	15% ZrO_2	28.0	4.0	24.0	1.26
7	5% TiO_2	29.2	1.5	27.7	1.38
8	5% TiO_2	29.0	1.5	27.5	1.36
9	15% TiO_2	29.6	4.2	25.4	1.28
10	15% TiO_2	29.4	4.2	25.2	1.26
11	15% $ZrSiO_4$	27.2	3.9	23.3	1.15
12	15% $ZrSiO_4$	27.1	3.9	23.2	1.14
13	15% Cr_2O_3	25.0	4.0	21.0	1.01
14	15% Cr_2O_3	24.6	3.9	20.7	0.99
15	10% TiO_2	27.7	2.8**	24.9	1.09
16	10% TiO_2	27.7	2.8**	24.9	1.03
17	10% TiO_2	27.1	2.7**	24.4	1.36
18	15% TiO_2	29.4	4.2	25.2	1.25
19	10% TiO_2	27.7	2.8**	24.9	1.04

* Nominal mean temperature - actual ranged between 770F and 805F

**Estimated

TABLE 3.2-15

THERMAL CONDUCTIVITY AND DENSITY OF
UNOPACIFIED GLASROCK SPECIMENS - PART 2

Specimen No.	Product Density, pcf	Conductivity @ 800F* Btu in./hr ft^2 ^{o}F
1	30.4	1.40
2	29.3	1.33
3	28.4	1.35
4	28.6	1.40
5	27.3	1.31
6	27.3	1.32
7	25.4	1.25
8	25.2	1.24
9	18.2	0.95
10	18.3	1.04

*Nominal mean temperature - actual ranged between 770F and 805F.

FIGURE 3.2-2.

THERMAL CONDUCTIVITY - PRODUCT DENSITY
RELATIONSHIP FOR OPACIFIED AND
UNOPACIFIED GLASROCK
PARTS 1 AND 2

(770F - 805F Mean Temperature)

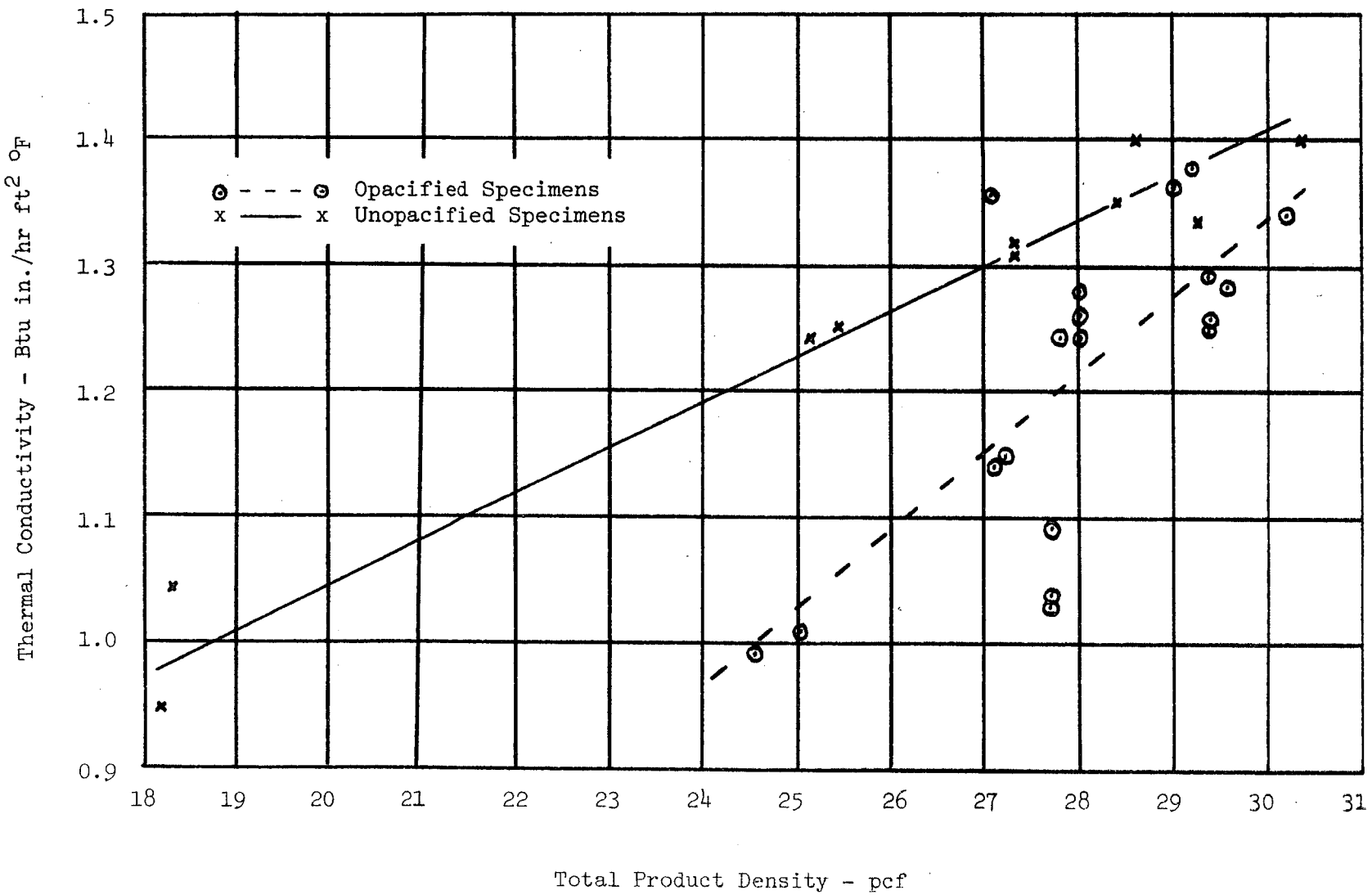

average regression. In general, however, it was concluded that the opacified products were more efficient than the unopacified product on a product density basis, although the regressions appeared to intersect somewhere above 30 pcf density (the actual existence of a difference in slope could be questioned).

Figure 3.2-3 represents a comparison of the same data on the silica density basis. This is probably a more realistic comparison since it must be assumed that the silica density controls the load-bearing characteristics. On this basis, it was not reasonable to draw a distinction between the two sets of data. The slope of the regression in Figure 3.2-3 lies between the slopes of the two regressions in Figure 3.2-2 (although closer to that of the unopacified regression), indicating that the slope difference depicted in Figure 3.2-2 may not actually exist. Based on Figure 3.2-3, however, it was difficult to justify further effort toward opacifying Glasrock 25.

Parts 1 and 2 - General Discussion. The cause for the apparent ineffectiveness of the opacifiers was not investigated in detail under this program. However, it can be speculated that it is related to the relative indices of refraction of opacifier and silica, and the physical location of the opacifier particles within the product. The opacifiers chosen for consideration are "scatterers" rather than "reflectors", and as such, their ability to opacify is a function of their high refractive index, or more specifically, the ratio of their refractive index to that of their immediate surroundings.

Glasrock is cellular in structure, and hence, it is not unreasonable to assume that most, if not all of the opacifier particles were partially or totally embedded in the silica cell wall. The advantage of their high index of refraction may therefore be negated considerably since their effectiveness must now be measured in terms of the refractive index of silica rather than of air (or space). For example, amorphous silica has a refractive index of approximately 1.5, while rutile titania has a refractive index of 2.6. In air, titania acts as an excellent opacifier; in silica, the ratio of the titania and silica indices may not be significantly different from the ratio of the silica and air indices.

This is a convenient hypothesis which would explain not only why the opacifiers in general did not improve the thermal conductivity of Glasrock, but also the reason for the greater spread of data for the opacified specimens (extent to which the particles were embedded in the cell wall). To the extent that this hypothesis has validity, however, it is undoubtedly over-simplified.

A second and more apparent difference between the 10 per cent titania specimens which differed significantly in thermal conductivity, although similar in composition, was the cell size and wall thickness of the specimens. A thin section from each specimen was prepared and magnified 50X. Photomicrographs of these sections are presented in Figures 3.2-4 and 3.2-5.

FIGURE 3.2-3.

THERMAL CONDUCTIVITY VS SILICA DENSITY FOR
OPACIFIED AND UNOPACIFIED GLASROCK
PARTS 1 AND 2

(800F Mean Temperature)

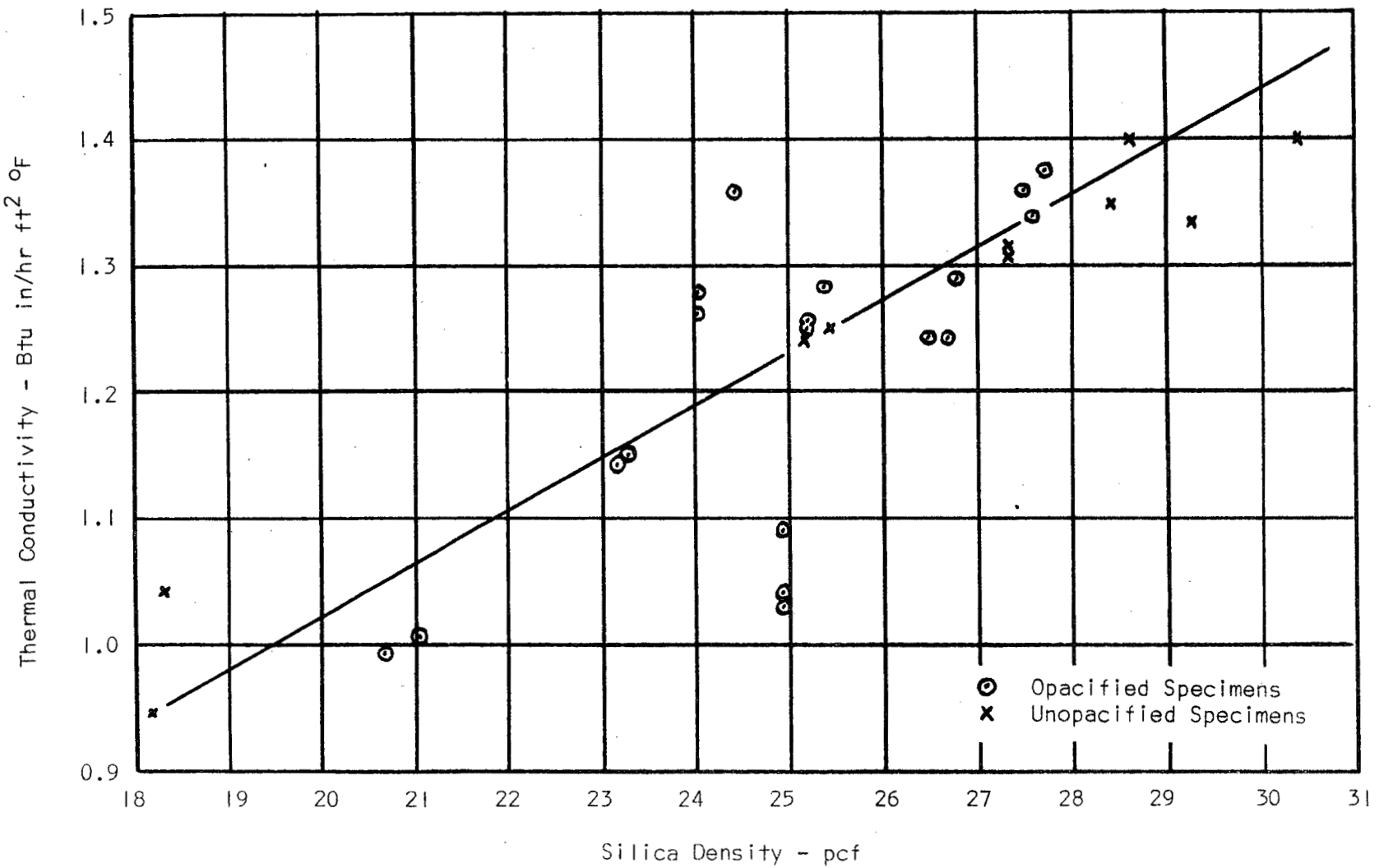

FIGURE 3.2-4.

THIN SECTION OF 10 PER CENT TITANIA OPACIFIED GLASROCK
HAVING A LOW THERMAL CONDUCTIVITY

MAG: 50X

100 microns

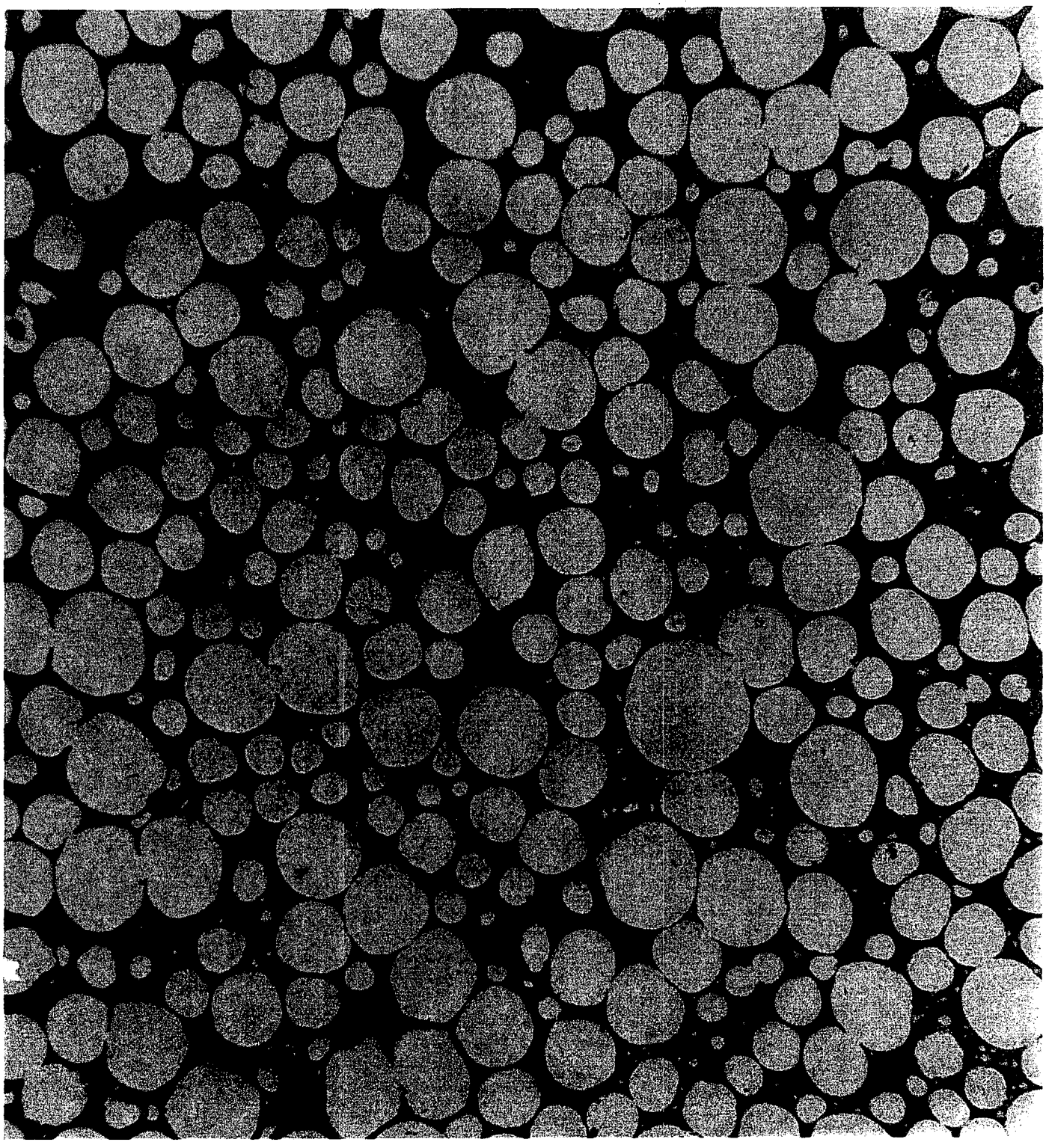

NEG E-3831A

FIGURE 3.2-5.

THIN SECTION OF 10 PER CENT TITANIA OPACIFIED GLASROCK
HAVING A HIGH THERMAL CONDUCTIVITY

MAG: 50X

100 microns

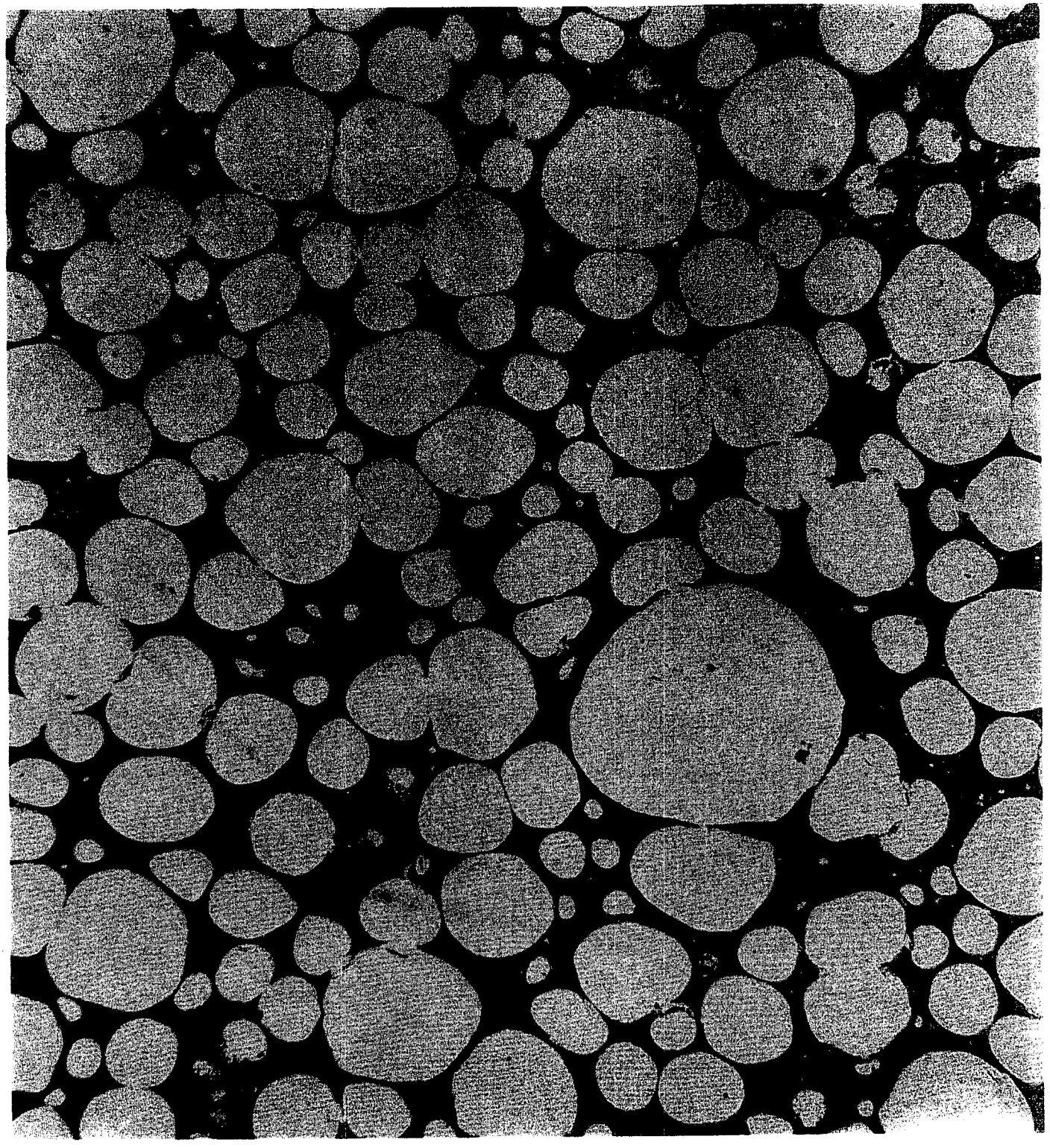

NEG E-3832A

The difference in the pore size is immediately evident. Random measurements of the pores (which appear as bubbles) indicated that the specimen having the lower conductivity (Figure 3.2-4) had an average pore size of about 0.2 mm with a maximum size of about 0.5 mm. The other specimen (Figure 3.2-5) had an average pore size of about 0.3 mm with a maximum size of about 0.7 mm. Similar measurements of the wall thickness indicated 0.07 mm and 0.1 mm for the low and high conductivity material, respectively. The wall thickness measurements are obviously less reliable, however, since wall thickness was considerably more difficult to define.

These thin sections were also studied under a polarizing microscope at 500X magnification using transmitted light. This permitted the observation of the titania particles. This study indicated that the particles were well distributed throughout the walls of both specimens. Assuming an average titania particle size of 2 microns, essentially all of the particles would be entirely embedded in the 70 and 100 micron average wall thicknesses.

Thus, it appears that cell size, and possible cell wall thickness exert a major influence on the thermal conductivity of the Glasrock. The larger the cells, the fewer the number of interruptions to radiation afforded by the cell walls. Similarly, the thicker the walls, the less devious would be the path of heat flow by solid conduction. The latter factor, however, is probably considerably less important. This cell size theory does not invalidate the original speculation that the effectiveness of the titania as an opacifier is diluted to its presence in a silica matrix. However, cell size probably represents the major cause of the spread in conductivity values between "similar" specimens.

A recheck (unaided eye) of the various unopacified specimens tested indicated that the cell size was quite uniform for samples within a given density range. The difference noted in the thin sections presented above was also evident qualitatively with the unaided eye. Thus, it appears that the presence of these "foreign" titania particles within the silica slurry, resulted in an uncontrolled foaming action, and a subsequent variation in cell size. Until this can be more closely controlled, it would be difficult to determine the true effectiveness of the opacifier.

Part 3 - Introduction. In view of the problems connected with the manufacture of an opacified Glasrock product, together with the possible minimal improvement in thermal conductivity which might be achieved with considerable additional work, the efforts to opacify Glasrock foam silica were dropped. Instead, the unopacified product was studied further for thermal conductivity, permanent set under various constant loads, and stress-strain relationship.

Part 3 - Load-Bearing Capability of Unopacified Glasrock. Since the normal production density range of the GLASROCK 25 product is 25 to 30 pcf, unopacified specimens representing these approximate density limits were evaluated separately. Test loads ranged from 500 psi down to 200 psi in 100 psi increments. The specimens, 2 x 2 x 1 in., were tested for up to 500 hr under constant load. The measure of performance was the permanent set imparted to the specimen as a result of the load. Since Glasrock is a relatively rigid ceramic, it was considered that any significant permanent set constituted a failure.

It was intended that the tests be conducted at 1800F hot face, thus simulating service conditions. However, frequent heater failures and long replacement delivery times, necessitated that the last part of the test series be conducted at room temperature. A comparison of room temperature and 1800F hot face results at the 300 psi load level, however, indicated that the permanent set was no greater at 1800F than at room temperature, and that it may be even slightly less. Thus, the room temperature tests were considered sufficiently indicative of product performance to justify their conductance.

Table 3.2-16 is a description of all of the specimens tested. It will be noted that the permanent set was determined twice: "as tested", and "after scraping". Failure of Glasrock under compressive load resulted in a crushing of the cellular structure, and a subsequent accumulation of silica dust on the surface of the specimen. To establish just how much of the specimen was crushed as a result of the load, it was necessary to remove this layer of compacted dust.

It became apparent that significant crushing of the specimens occurred at loads greater than 200 psi, as shown by the difference in the thickness measurements after test. It was also noted that loose dust could be blown from the surface of the 30 pcf specimens after the 200 psi test, while no dust was evident on the 25 pcf specimens.

The existence of a measurable amount of silica dust initially constituted an arbitrary indication of failure to sustain the applied load. It was considerably more difficult, however, to catalogue a permanent set of up to 7 mils. Due to the ever-present loose particles of silica on the surface, repetitive measurements have shown that a plus or minus 0.002 in. thickness measurement variation might exist. However, the extent to which a 0.005 to 0.010 in. permanent set constitutes a failure can only be judged with a specific set of service conditions and requirements.

It is interesting to note that the 30 pcf (nominal) specimens consistently had a higher average permanent set than the 25 pcf (nominal) specimens at the

TABLE 3.2-16

PERMANENT SET OF 25 AND 30 PCF UNOPACIFIED GLASROCK SILICA FOAM - PART 3

Specimen No.	Specimen Density pcf	Compressive Load psi	Test Time hr	Permanent Set, in. As Tested	Permanent Set, in. After Scraping	Thermal Conditions
25C-1	25.2	500	23-1/2	0.011	0.020	1800F hot face
25C-2	25.1	500	24	0.032	0.050	1800F hot face
30C-1	28.2	500	3/4	0.028	---	1800F hot face
30C-2	29.9	500	24	0.010	0.020	1800F hot face
25C-3	24.9	400	197	0.020	0.027	1800F hot face
25C-4	25.0	400	164	0.014	0.017	1800F hot face
30C-3	30.4	400	270	0.017	0.021	1800F hot face
30C-4	30.3	400	271	0.030	0.042	1800F hot face
25C-5	25.0	300	354	0.017	0.020	1800F hot face
25C-7	24.9	300	504	0.009	0.014	1800F hot face
30C-5	29.1	300	336	0.009	0.013	1800F hot face
30C-6	28.3	300	500	0.021	0.030	1800F hot face
30C-7	29.1	300	503	0.012	0.015	1800F hot face
25-0-1	25.6	300	504	0.009	0.013	cold
25-0-2	25.1	300	504	0.008	0.011	cold
30-0-1	27.2	300	504	0.025	0.038	cold
30-0-2	28.1	300	504	0.014	0.025	cold
25-0-3	25.2	200	504	0.002	0.002	1400F hot face
25-0-4	25.0	200	504	0.002	0.002	1400F hot face
25-0-5	25.1	200	504	0.002	0.002	cold
25-0-6	25.0	200	504	0.002	0.002	cold
25-0-7	25.0	200	502	0.002	0.002	cold
30-0-3	27.9	200	504	0.007	0.007	cold
30-0-4	28.9	200	504	0.005	0.005	cold
30-0-5	27.6	200	502	0.004	0.005	cold
30-0-6	29.1	200	502	0.002	0.005	cold
30-0-7	27.8	200	502	0.002	0.005	cold

200 psi stress level. This may indicate that the lower density material is more "resilient", or that the cell walls tend to yield under load rather than fracture as in the case of the 30 pcf material. Intuitively, however, one might not expect such a difference in performance with a relatively small difference in density.

Part 3 - Stress-Strain of Unopacified Glasrock. The stress-strain characteristics of unopacified Glasrock were determined on 2 x 2 x 1-in. specimens both before and after the prolonged 200 psi loading. As before, the specimens were separated into the two nominal density groups representing the normal production limits. Three fresh specimens at each density, and the ten specimens previously subjected to the 500-hr permanent set evaluation were tested with a 1000-lb Tinius-Olsen test machine. This machine applies the load mechanically rather than hydraulically and therefore load application can be stopped instantaneously at any desired level. This feature was utilized for these tests at 12.5 psi load increments to facilitate the strain readings. Although the strain dial had 0.001 in. divisions, the readings were estimated to 0.00025 in. The hesitations at each load increment were limited to several seconds.

Figure 3.2-6 presents the stress-strain relationships for the four groups of specimens. The existence of two distinct slopes for each group is probably an indication of a surface consolidation, although one would probably expect such a phenomenon to be strain-dependent rather than stress-dependent. Each break in the regression occurred between 90 and 100 psi stress.

As expected, the fresh 30 pcf specimens (curve A) were slightly stronger than the fresh 25 pcf specimens (curve B). Similarly, the constant load of 200 psi resulted in irreversible internal damage, thus weakening slightly the 25 pcf specimens (curve C). However, the extent to which this took place for the 30 pcf specimens (curve D) was somewhat unexpected. Table 3.2-17 summarizes the modulus of elasticity for each group of specimens at the 0-100 psi and 100-200 psi stress levels.

As a further check of the effect of sustained loading on the subsequent stress-strain relationships, Table 3.2-18 shows the average permanent set of each group of specimens following the stress-strain test. This was determined two ways: immediately following the release of the load while the specimen was still in the compression fixture, and thickness measurements (external of the test fixture) before and after test. Although the two measurement techniques did not agree exactly, they both indicated the relative effect of the specimen history.

FIGURE 3.2-6.

STRESS-STRAIN OF UNOPACIFIED GLASROCK
AT 25 AND 30 PCF DENSITY - PART 3

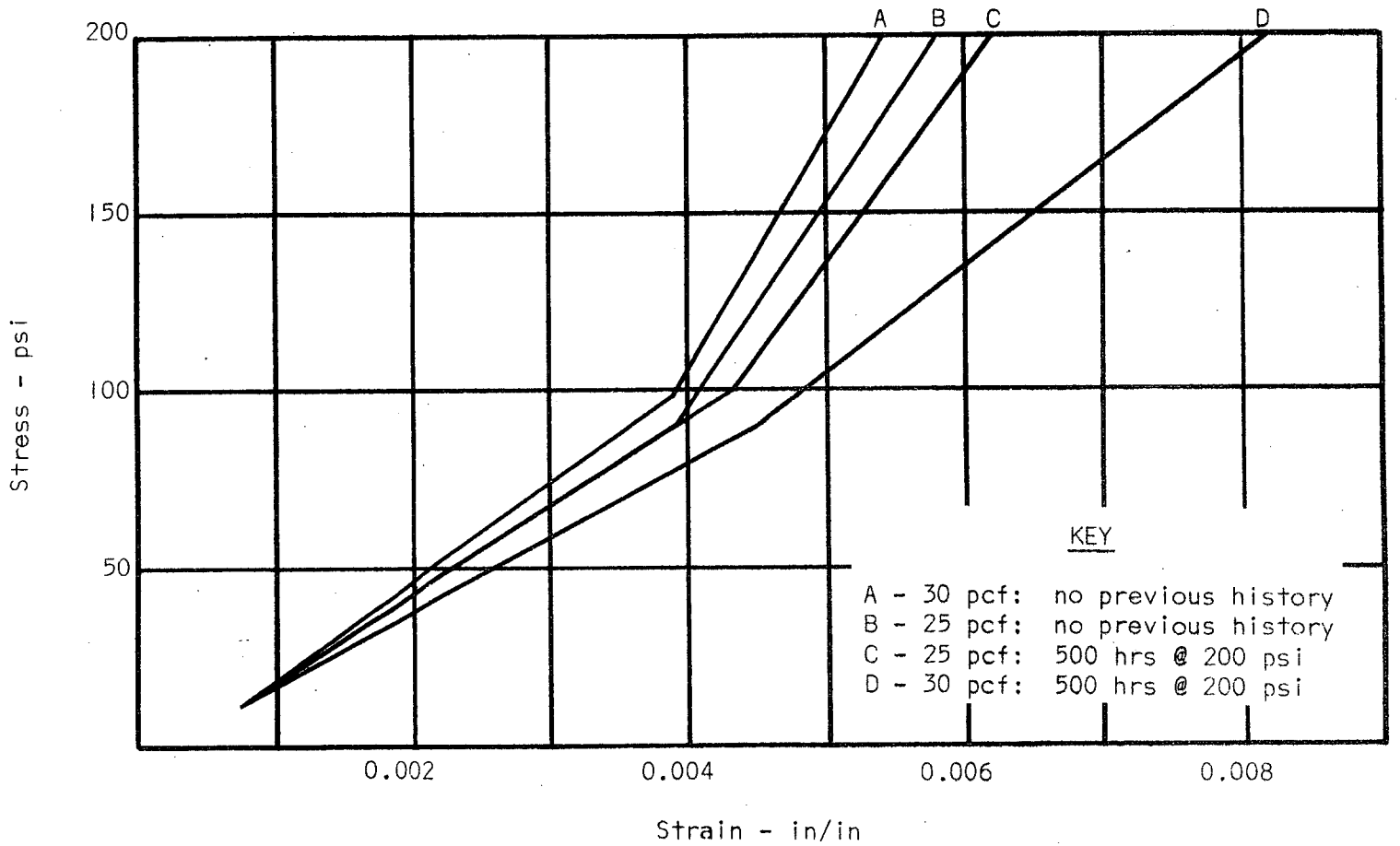

TABLE 3.2-17

MODULII OF ELASTICITY FOR UNOPACIFIED GLASROCK
BEFORE AND AFTER SUSTAINED 200 PSI LOADING

PART 3

Nominal Density psi	Previous History	Modulus of Elasticity, psi	
		0-100 psi Stress	100-200 psi Stress
25	none	25,000	57,500
25	500 hr @ 200 psi	25,000	51,000
30	none	27,500	67,500
30	500 hr @ 200 psi	20,800	30,000

TABLE 3.2-18

PERMANENT SET OF UNOPACIFIED GLASROCK SPECIMENS
FOLLOWING THE STRESS-STRAIN EVALUATION

PART 3

Nominal Density psi	Previous History	Average Permanent Set, in. In Fixture	Average Permanent Set, in. External to Fixture*
25	none	< 0.0005	0.001
30	none	0.0005	0.001
25	500 hr @ 200 psi	0.001	0.002
30	500 hr @ 200 psi	0.003	0.004

* Thickness measured to nearest 0.001 in.

Part 3 - Cyclic Loading up to 200 psi. Two 25 pcf (nominal) and two 30 pcf (nominal) specimens having no stress history, were subjected to cyclic loadings to determine if the sudden change in slope of the stress-strain curve was related to the permanent set, and if the material followed the same relationship after several cycles as it did on the first cycle (as shown in Figure 3.2-6). Each cycle was separated by a 15-sec period of zero load. All strain and permanent set measurements were taken in the test fixture. The cycles were:

1. Up to 75 psi in 12.5 psi increments
2. Up to 125 psi in 12.5 psi increments
3. Up to 175 psi in 25 psi increments
4. Up to 200 psi in 25 psi increments

All four specimens had the same stress-strain relationship, they followed quite closely the 25 pcf relationship (curve B of Figure 3.2-6), and they appeared to deviate only slightly from this relationship on successive cycles. The permanent set also appeared to increase slightly after each cycle, although it achieved only 0.0005 in. after the final cycle. Thus, if any significant progressive changes did occur either in the relationship or the permanent set, the measuring devices were of insufficient accuracy to detect them.

Part 3 - Thermal Conductivity of Unopacified Glasrock. Three 12 x 12 x 1-in. specimens of unopacified Glasrock were selected for thermal conductivity evaluation in the ASTM C-182 High Temperature Calorimeter apparatus for Insulating Firebrick. The specimens of 27.3, 27.4, and 29.0 pcf density were chosen to represent an average density about midway between the 25 to 30 pcf limits normally encountered in production. The average density was 27.9 pcf. The specimens were tested together in series and instrumented such that for given hot and cold face temperatures of the apparatus, three conductivity values at three different mean temperatures could be obtained simultaneously. The hot face temperature was controlled at three levels between 1000F and 1800F, thus giving a total of nine conductivity values ranging between 300F and 1600F mean temperature. Table 3.2-19 presents the pertinent data from this test series, while Figure 3.2-7 is a plot of the conductivity data vs the mean temperature.

The deviation of the data from a straight line regression was remarkably small. Similarly, the value of 1.38 Btu in./hr ft^2 ^{o}F at 800F mean temperature was in excellent agreement with the 1.36 value shown in Figure 3.2-3 at 28 pcf silica density.

Two of these specimens were then tested by Dynatech Corp. in both air and vacuum. These values are also plotted on Figure 3.2-7. The air values closely paralleled

TABLE 3.2-19

THERMAL CONDUCTIVITY OF UNOPACIFIED GLASROCK
AS DETERMINED BY ASTM C-182

PART 3

Equipment Temperatures, °F		Specimen Δ T	Specimen	Thermal Conductivity
Hot Face	Cold Face	°F	Mean Temp, °F	Btu in./hr ft^2 °F
1048	118	270	913	1.46
		291	633	1.26
		370	303	1.02
1403	138	350	1228	1.69
		393	856	1.42
		522	399	1.09
1809	168	440	1589	1.94
		498	1120	1.60
		702	519	1.17

FIGURE 3.2-7.

THERMAL CONDUCTIVITY OF UNOPACIFIED GLASROCK 25 SILICA FOAM
UP TO 1600F MEAN TEMPERATURE - PART 3

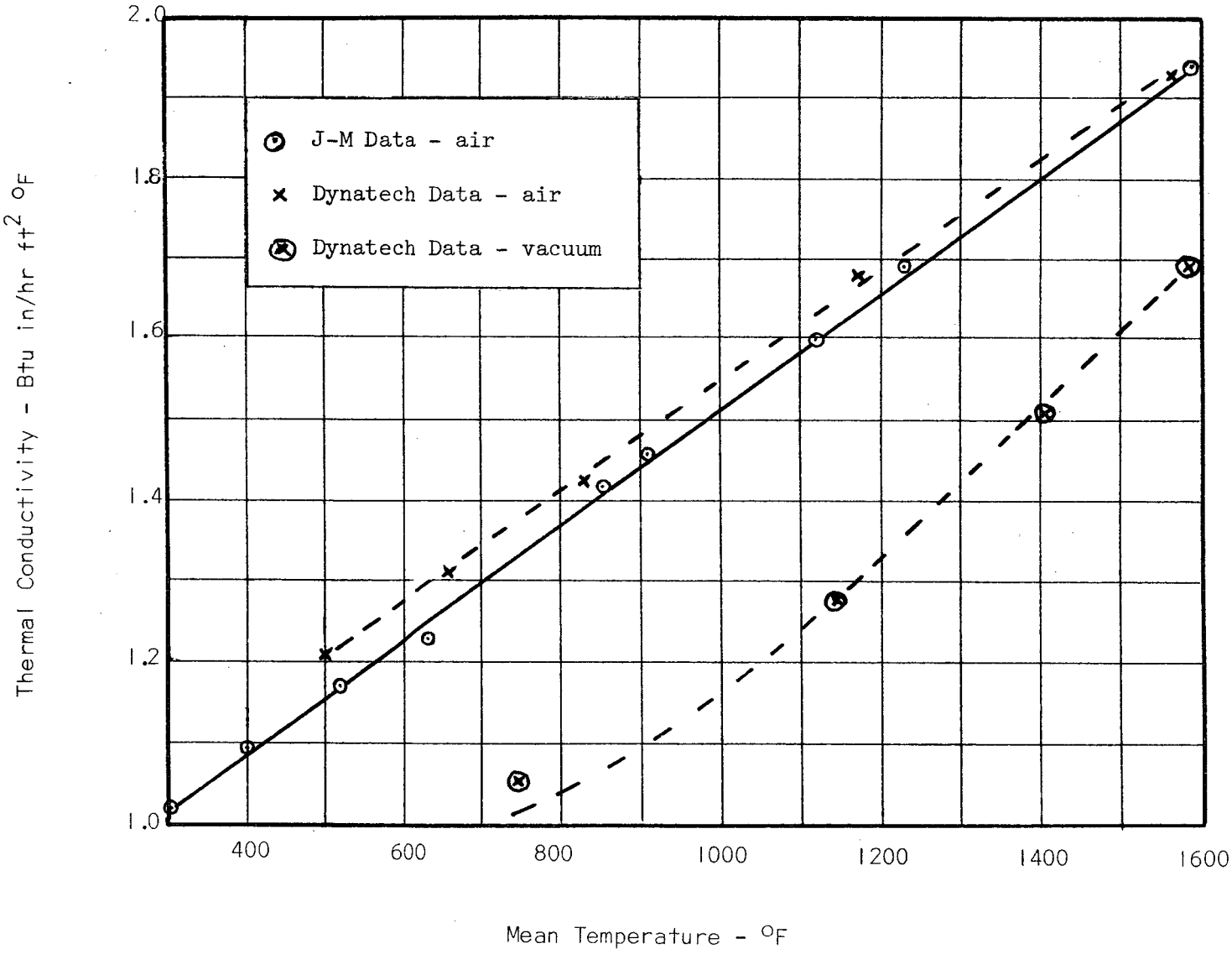

those obtained by Johns-Manville. Any differences between the two curves should be attributed to experimental differences. No pervious vacuum data has been published for comparison purposes, although there is no reason to question the current values.

V. CONCLUSIONS

A. PHASE I, TASK 5 - DETAILED EVALUATION

1. MIN-K 1999, 2002, and 2020 appeared to have the same thermal conductivity vs density relationships in air and argon atmospheres.

2. These products are expected to have the same relationship in vacuum as well, but thermal conductivity test procedures must be refined before consistent and acceptable data can be obtained.

3. Extended thermal exposure of MIN-K 1999, 2002, and 2020 to their respective service conditions appeared to have no effect upon the thermal conductivity of these products when re-evaluated in air and argon. Although the same is expected to be true for the conductivity in vacuum, verification was not possible with the existing conductivity testing porcedure.

B. PHASE II, TASK 2 - MATERIAL RESEARCH AND DEVELOPMENT

1. The useful temperature limit of submicron sized particles compacted together into a MIN-K structure, as determined by the shrinkage of the molded product, appeared to be considerably below the generally accepted useful temperature limit of a dense body of the same composition.

2. The tendency for submicron ALON-C particles in the compressed state to sinter to a larger, but limiting size, with a resulting pore size of 0.1 to 0.5 microns was tentatively attributed to Van der Waal's forces. The pore size increase was of sufficient magnitude to yield a body which no longer had the low thermal conductivity in a gaseous media characteristic of MIN-K. The conversion of the ALON-C from the gamma to the alpha form was also thought to contribute to the sintering process.

3. The sintering of the particles could be retarded by the use of a shrinkage inhibitor such as K_2SO_4. However, indications were that sintering could not be prevented over a long period of time at 2200F.

4. ALON-C, which was the most stable of the low density submicron particles appeared to be servicable only up to about 2000F. Above this temperature, particle sintering within the body took place which eliminated the MIN-K thermal conductivity effect.

5. The development of a reasonably lightweight MIN-K product useful to 2200F did not appear possible with the submicron materials currently available on the market.

C. PHASE II, TASK 3 - LOAD-BEARING INSULATION FOR 400 - 1800F SERVICE

SUBTASK 3.1 - LOAD-BEARING INSULATIONS FOR 400 TO 1400F SERVICE

1. The modulus of elasticity of high density MIN-K Formulations is a function of both the product density and the CAB-O-SIL M5 density.

2. MIN-K 2002 at 35 pcf had a modulus of elasticity of about 17,200 psi (average of hot face and room temperature tests), which fell within the 15,000 to 25,000 psi target for the program.

3. The thermal conductivity of MIN-K Formulations is also strongly dependent upon the CAB-O-SIL M5 density, particularly above 20 to 22 pcf.

4. The desired modulus of elasticity could only be achieved with a significant increase in thermal conductivity. Typical values for 35 pcf density MIN-K 2002 at 800F mean temperature were 0.35 Btu in/hr ft^2 ^oF in air, and 0.33 Btu in/hr ft^2 ^oF in argon.

5. Constant load tests at 1400F hot face resulted in a family of deflection vs time curves at each constant load. These data, extrapolated to 10,000 hrs and subsequently replotted in terms of per cent of initial load vs time, indicated that 40 per cent of the initial load (between 300 and 750 psi) would be retained after 10,000 hr if the initial deflection were held constant.

6. Initial loads above 750 psi and below 300 psi may not follow the same relationship of per cent of initial load vs time due to a possible curvilinear stress-strain relationship at either loading extreme.

LOAD-BEARING INSULATIONS OF SERVICE UP TO 1800F

1. The presence of opacifying particles, and titania in particular, in the Glasrock silica slip appeared to result in an inconsistent

pore size within the finished product, and a general reduction in product strength.

2. The thermal conductivity, on the average, of the opacified product was no better than the unopacified product when compared on an equivalent silica density basis.

3. Typical thermal conductivity values for unopacified Glasrock silica foam at an average density of 27.9 pcf were 1.52 Btu in/hr ft^2 ^oF in air and 1.16 Btu in/hr ft^2 ^oF in vacuum at 1000F mean temperature.

4. Unopacified Glasrock foam silica sustained 200 psi for prolonged periods at 1800F hot face with minimal permanent set (and hence minimal load relaxation). Higher loads resulted in excessive crushing of the fused silica cellular structure.

5. The stress-strain relationship of Glasrock between zero and 200 psi appeared to consist of two distinct straight lines. Between zero and 100 psi the modulus of elasticity averaged 26,250 psi, while between 100 psi and 200 psi it averaged 62,500 psi.

VI. REFERENCES

1. J. O. Collins, "Develop 1800F-400F Fibrous-Type Insulation For Radioisotope Power Systems", AEC Contract AT(30-1)-3633, Phase I, Final Report, Report No. ALO 3633-7, October 2, 1967.

2. R. L. Coble, "Sintering Crystalline Solids. I. Intermediate and Final State Diffusion Models, "J. Appl. Phys., 32, 787 (1961).

3. W. D. Kingery, Introduction to Ceramics. John Wiley & Sons, Inc., New York, 1960, pp 241, 370.

4. J. A. Hedvall, "Sintering and Reactivity of Solids, "Ceramic Age, February 1955, p 13.

5. Kingery, p 373

6. Kingery, p 241

7. A. E. Paladino and R. L. Coble, "Effect of Grain Boundaries on Diffusion Controlled Processes in Aluminum Oxide, " J. Am. Ceram. Soc., 46, 133 (1963).

8. D. L. Johnson and I. B. Cutler, "II, Initial Sintering Kinetics of Alumina," J. Am. Ceram. Soc., 46, 545 (1963).

9. W. J. Smothers and H. J. Reynolds, "Sintering and Grain Growth in Alumina," J. Am. Ceram. Soc., 37, 591 (1954).

10. Kingery, p 353

11. D. L. Johnson and I. B. Cutler, "Diffusion Sintering: I, Initial Stage Sintering Models and Their Application to Shrinkage of Powder Compacts," J. Am. Ceram. Soc., 46, 541 (1963).

12. G. C. Kuczynski, "Self-diffusion in Sintering of Metallic Particles," Trans. AIME, 185, 169(1949).

13. W. D. Kingery and M. Berg, "Study of the Initial Stages of Sintering Solids by Viscous Flow, Evaporation-Condensation, and Self-diffusion," J. Appl. Phys., 26, 1205 (1955).

14. J. E. Burke, "Role of Grain Boundaries in Sintering," J. Am. Ceram. Soc., 40, 80 (1957).

15. R. L. Coble, "Initial Sintering of Alumina and Hematite," J. Am. Ceram. Soc., 41, 55 (1958).

16. G. C. Kuczynski, "Sintering of Crystalline Oxides," Modern Developments in Powder Metallurgy; Proceedings of the International Powder Metallurgy Conference, New York, N. Y., June 14-17, 1965. Volume I - Fundamentals and Methods, P 332.

17. L. C. F. Blackman, "Lattice Defects and the Sintering of Oxides," The Industrial Chemist, December 1962, p 620.

18. P. W. Clark and J. White, "Some Aspects of Sintering," Trans. Brit. Ceram. Soc., 49, 305 (1950).

19. P. W. Clark, J. H. Cannon, and J. White, "Further Investigation on Sintering of Oxides," Trans. Brit. Ceram. Soc., 52, 1 (1953).

20. C. S. Morgan and L. L. Hall, "Effect of Isostatic Pressure on Sintering," J. Am. Ceram. Soc., 50, 382 (1967).

21. A. A. Ammar and D. W. Budworth, "Pressure Sintering of NaCl and Other Ionic Materials," Trans. Brit. Ceram. Soc., 66, 93 (1967).

22. Kingery, p 581

23. C. Herring, "Diffusional Viscosity of a Polycrystalline Solid," J. Appl. Phys., 21, 437 (1950).

24, Kingery, p 582.

25. M. J. O'Hara, "Sintering Kinetics of Composite Compacts of Alumina," Tech. Progress Rept. prepared for the Atomic Energy Commission under Contract AT(11-1)-1122, Dept. of Ceramic Engineering, University of Utah, Salt Lake City, August 31, 1966, p 81.

26. E. J. Felten, "Hot Pressing of Alumina Powders at Low Temperatures," J. Am. Ceram. Soc., 44, 381 (1961).

27. R. Chang and C. G. Rhodes, "High-Pressure Hot-pressing of Uranium Carbide Powders and Mechanisms of Sintering of Refractory Bodies," J. Am. Ceram. Soc., 45, 379 (1962).

28. Kingery, pp 167, 227, 340.

29. A. J. Dekker, Solid State Physics. Prentice-Hall, Inc., Englewood Cliffs, New Jersey, 1957, p 160.

30. Kingery, pp 72, 394.

31. W. A. Weyl, "Atomistic Interpretation of the Mechanism of Solid State Reactions and of Sintering," Ceramic Age, November, 1952, p 36.

32. Kingery, pp 335, 364, 370, 377.

33. N. C. Kothari, "The Effect of Particle Size on Sintering Kinetics in Alumina Powder," J. Nucl. Mati., 17, 43 (1965).

34. D. Lewis and M. W. Lindley, "Enhanced Activity and the Characterization of Ball-Milled Alumina," J. Am. Ceram. Soc., 49, 49 (1966).

35. D. R. Wilder and E. S. Fitzsimmons, "Further Study of Sintering Phenomena," J. Am. Ceram. Soc., 38, 66 (1955).

36. J. L. Burke, "Further Discussion on Sintering Mechanisms, Grain Growth, and Grain Boundaries," Paper presented at Ceramic Seminar, Rutgers University, January 9, 1965.

37. G. V. Cullen, et al, "Hot-Pressing of MgO Aggregates" J. Am. Ceram. Soc., 50, 688 (1967).

38. C. G. Barlow, "The Granulation of Powders," The Chemical Engineer, July/August 1968.

39. Blackman, December 1962, p 624; January 1963, p 24.

40. Kuczynski, p 332.

41. R. L. Green, "Continued Discussion on the Role of Water Vapor in High Temperature Ceramic Processes," Paper presented at Ceramic Seminar, Rutgers University, November 21, 1964.

42. O. Winkler, "Conditions for Effective Vacuum Sintering and Their Realization in Practice," Powder Met., 12, 1958, p 114.

43. F. E. Wagstaff, S. D. Brown, and I. B. Cutler, "Influence of H_2O and O_2 Atmospheres on the Crystallization of Vitreous Silica," Phys. Chem. Glasses, 5, 76 (1964).

44. R. W. Lee, "On the Role of Hydroxyl in the Diffusion of Hydrogen in Fused Silica," Phys. Chem. Glasses, 5, 35 (1964).

45. R. Brueckner, "Influence of Hydroxyl Content on the Density and the Diffusion Mechanism in Vitreous Silica," Glastech Ber., 38, 153 (1965).

46. M. Green, K. R. Jennings, J. W. Linnet, and D. Schofield, "Recombination of Atoms at Surfaces - Part 7; Hydrogen Atoms at Silica and Other Similar Surfaces," Tech. Rept. prepared for U. S. Air Force under Contract AF61(514)-1117 Inorganic Chemistry Laboratory, Oxford University, England, February 1960.

47. Y. Moriya, "Vacuum Sintering of Quartz Powder and Phase Transformation of Quartz," Vacuum, 11, 158 (1961).

48. M. O. Warman and D. W. Budworth, "Effects of Residual Gas on the Sintering of Alumina to Theoretical Density in Vacuum," Trans. Brit. Ceram. Soc., 66, 265 (1967).

49. R. L. Coble, "Sintering Alumina: Effects of Atmospheres," J. Am. Ceram. Soc., 45, 123 (1962).

50. Blackman, December 1962, p 620; January 1963, p 23.

51. Weyl, p 31.

52. Smothers and Reynolds, p 588.

53. J. T. Jones, P. K. Maitra, and I. B. Cutler, "Role of Structural Defects in the Sintering of Alumina and Magnesia," J. Am. Ceram. Soc., 41, 353 (1958).

54. H. P. Cahoon and C. J. Christensen, "Sintering and Grain Growth of Alpha-Alumina," J. Am. Ceram. Soc., 39, 337 (1956).

55. I. B. Cutler, C. Bradshaw, C. J. Christensen, and E. P. Hyatt, "Sintering of Alumina at Temperatures of 1400°C and Below," J. Am. Ceram. Soc., 40, 134 (1957).

56. M. O. Warman and D. W. Budworth, "Criteria for the Selection of Additives to Enable the Sintering of Alumina to Proceed to Theoretical Density," Trans. Brit. Ceram. Soc., 66, 253 (1967).

57. C. A. Bruch, "Sintering Kinetics for the High Density Alumina Process," Bull. Am. Ceram. Soc., 41, 799 (1962).

58. J. R. Keski, "Effects of Manganese Oxide on the Sintering of Alumina," Tech. Progress Rept. prepared for the Atomic Energy Commission under Contract AT(11-1)-1122, Dept. of Ceramic Engineering, University of Utah, Salt Lake City, August 31, 1966, p 1.

59. J. R. Keski and I. B. Cutler, "Effect of MnO on Sintering of Alumina," J. Am. Ceram. Soc., 48, 653 (1965).

60. C. W. Hewson and W. D. Kingery, "Effect of MgO and $MgTiO_3$ Doping on Diffusion-Controlled Creep of Polycrystalline Alumina," J. Am. Ceram. Soc., 50, 218 (1967).

61. J. W. Nelson and I. B. Cutler, "Effect of Oxide Additions on Sintering of Magnesia," J. Am. Ceram. Soc., 41, 406 (1958).

62. G. K. Layden and M. C. McQuarrie, "Effect of Minor Additions on Sintering of MgO," J. Am. Ceram. Soc., 42, 89 (1959).

63. H. J. S. Kriek, W. F. Ford, and J. White, "Effect of Additions on the Sintering and Dead-burning of Magnesia," Trans. Brit. Ceram. Soc., 58, 1 (1959).

64. R. Pampuch, "Contribution to the Problem of Sintering Pure Oxides with Additives," Bull. Soc. Franc. Ceram., 46, 3 (1960).

65. P. F. Eastman and I. B. Cutler, "Effect of Water Vapor on Initial Sintering of Magnesia," J. Am. Ceram. Soc., 49, 526 (1966).

66. R. J. Anderson, "Effects of Water Vapor on the Sintering of MgO," Trans. Faraday Soc., 60, 930 (1964).

67. R. O. Peterson, "Effect of Water Vapor on the Initial Sintering of Calcia," Tech. Progress Rept. prepared for the Atomic Energy Commission under
C Contract AT(11-1)-1122, Dept. of Ceramic Engineering, University of Utah Salt Lake City, August 31, 1966, p 41.

68. E. P. Hyatt, C. J. Christensen, and I. B. Cutler, "Sintering of Zircon and Zirconium Oxide with the Aid of Certain Oxides," Am. Ceram. Soc. Bul., 36, 307 (1957).

69. J. P. Roberts, J. Hutchings, and C. Wheeler, "Sintering and Diffusion Studies of Zinc Oxide," Trans. Brit. Ceram. Soc., 55, 75 (1956).

70. S.Goldsztaub, et al, "Effect of Vacuum on the Sintering Temperature," Sciences et Industries Spatialis, November-December 1966, p 52-56.

VII. APPENDIX A

COMPOSITION OF MIN-K 1999, 2002, AND 2020

Material	Weight, per cent		
	1999	2002	2020
Submicron Silica (CAB-O-SIL M5)	75	75	75
Silica Fiber (MICRO-QUARTZ)	8	4	--
Silica Fiber (MICRO-QUARTZ Prefired 1800F, 2 hr)	--	--	4
Quartz Staple Fiber (ASTROQUARTZ 1/4 in.)	1	--	--
Quartz Staple Fiber (ASTROQUARTZ 1/2 in.)	--	5	5
Opacifier (TAM -5μ TiO_2)	16	16	16

APPENDIX B

DEVELOPMENT OF LOAD BEARING THERMAL INSULATION

FINAL REPORT

U.S. Atomic Energy Commission
Sub Contract 3900-2
Prime Contract AT(29-2)-2661
Formerly AT(30-1)-3633

December 9, 1968

P. B. Lassiter
Director of Research
Glasrock Products, Inc.
2210 Marietta Blvd., N.W.
Atlanta, Georgia 30318

TABLE OF CONTENTS

Title	Page
List of Tables	2
Abstract	3
Scope	4
Introduction	5
Procedure	6
Authorized Additional Work Under Part II	15
Results	16
Conclusions	20
Appendix I	21
Appendix II	23

LIST OF TABLES

Table	Page
Table I	8
Table II	10
Table III	13
Table IV	14
Table V	17
Table VI	18

ABSTRACT

Fused silica (SiO_2) foams were prepared with varying amounts of titania (TiO_2), zirconia (ZrO_2), zircon ($ZrSiO_4$) and chromia (Cr_2O_3) opacifiers in an attempt to produce an insulating material having properties equal to or better than Glasrock Products, Inc.'s 25 pound density fused SiO_2 foam. Specimens were prepared in the laboratory by Glasrock and tested by Glasrock Research and Johns-Manville Research and Engineering Center. All four opacifiers were to some degree successfully integrated into the fused SiO_2 foam. However, chromia (Cr_2O_3) and zircon ($ZrSiO_4$) were eliminated because they lowered the strength and out-gassed at 1800°F in vacuum. Titania (TiO_2) and zirconia (ZrO_2) had at best marginal effects on thermal conductivity. In all cases the effect of adding opacifiers was considered to be unreliable because of difficulties in their successful introduction into the standard manufacturing process.

SCOPE

This report covers the preparation and testing of fused SiO_2 foam with opacifying agents as described in Parts 1 and 2 of the subject sub-contract plus authorized additional work and covers work done during the period February 12, 1968, to November 30, 1968.

INTRODUCTION

Sub-contract 3900-2 was initiated to develop and to make a preliminary evaluation of low thermal conductivity insulation capable of operating at 1800°F hot face for use in radioisotope thermoelectric power generators. The intent of the program was to reduce the thermal conductivity of Glasrock Foam 25 through the addition of opacifying agents, without compromising the load bearing characteristics of the present product. In order to accomplish this, it was recognized that other properties such as density and thermal expansion, etc., might be altered to some degree.

The prime contract, AT-(29-2)-2661 formerly AT (30-1)-3633, was between the U.S. Atomic Energy Commission and Johns-Manville Research and Engineering Center, Manville, New Jersey.

PROCEDURE

PART I.

The four (4) opacifiers were used as received from Johns-Manville Corp. who purchased them from the various suppliers.

The opacifiers used were the following:

TiO_2	-	HG TiO_2 - 5 μ TAM Division, National Lead Co.
$ZrSiO_4$	-	Superpax, TAM Division, National Lead Co.
ZrO_2	-	Opax, TAM Division, National Lead Co.
Cr_2O_3	-	#7099 oxide, Charles Pfizer & Co.

The amount of opacifiers added was 15% on a dry basis, i.e., 85% fused SiO_2, 15% opacifier.

Several methods were tried using small batches in an effort to find the best way of introducing opacifiers into the standard procedure for making Glasrock Foam 25. The methods tried included the following:

1. Making a slip of the opacifier and mixing the opacifier slip with the fused SiO_2 slip.
2. Adding the dry powder and foaming agent to the fused SiO_2 slip and mixing.
3. Adding the dry opacifiers to the fused SiO_2 slip and adding additional water.

In the process of making small experimental batches, it became obvious that the pH-viscosity relationship of the slip had a significant effect on the properties of the foamed mix. At that time a study of pH vs. viscosity was made in the following manner.

1. Dry opacifiers were added to fused SiO_2 slip in a one quart polyethylene jar. 85% fused SiO_2 to 15% opacifier (dry basis) was used.
2. Water content of the mixture was adjusted to 18.1%.
3. pH was adjusted over a range of values (See Table I) by the addition of reagent grade concentrated Hydrochloric Acid and mixing for 10 to 15 minutes.
4. pH was measured with a Corning, model 7, pH meter with automatic temperature compensator.
5. Viscosity was measured with a Brookfield viscometer Model LVF, using a speed of 12 r.p.m. and a number 2 spindle.

Table I lists the pH-viscosity relationships obtained.

After standing overnight, it was found that the pH and viscosity values had changed drastically. At that time it was decided to use the following procedure in casting the various foam blocks, based on the experience gained from additive introduction and pH-viscosity relationships:

1. Add fused SiO_2 slip to the lab ball mill. (No mill balls were in mill.)
2. Add dry opacifiers and sufficient water to attain approximately 80% solids and roll overnight to insure proper mixing.
3. Adjust viscosity-pH at the time of preparing the foamed mix, i.e., just before pouring in the molds.

Casting of Test Specimens (15% Opacifier Content)

The final properties of the mix were determined on a trial and error basis based primarily on experience and knowledge of mixes which would make suitable foam.

The required amount (15% opacifier - 85% fused SiO_2) of the opacifier was added to the fused silica slip and rolled overnight in a large ball mill without grinding balls. The next morning

TABLE I

pH-Viscosity Relationship for 85% Fused SiO_2-15% Opacifier Slips

Zircon

HCl Added	Viscosity CPS	pH
none	375	4.4
1 drop	305	3.6
3 drops	295	3.5
3 drops	290	3.2
3 drops	310	2.9
3 drops	345	2.7

Cr_2O_3

HCl Added	Viscosity CPS	pH
none	276	3.8
2 drops	245	3.4
1 drop	245	3.2
3 drops	258	2.9
3 drops	275	2.6

TiO_2

HCl Added	Viscosity CPS	pH
none	285	4.9
3 drops	235	4.3
3 drops	225	2.8
3 drops	245	3.8
3 drops	255	3.0

ZrO_2

HCl Added	Viscosity CPS	pH
none	off scale	
4 drops	off scale	
6 drops	off scale	

the pH of the slip-opacifier was adjusted to the proper viscosity pH range for each additive.

Table II shows casting conditions of the slips.

Sufficient foaming agent was added to give the desired fired density. The batch was cast in plaster molds. After the standard casting time in the molds, the blocks were dried in air at room temperature for 24 hours and then in a dryer at 250°F for 24 hours. The specimens were then fired at 2000°F for 16 hours.

Test specimens were cut from fired blocks and tested for density, thermal stability, and cold crushing strength. As specified in the contract, specimens were prepared as above and supplied to the prime contractor for their part of the testing.

The specimens for density and cold crushing strength were cut approximately 2" x 2" x 2". The dimensions were measured with a caliper-type scale with a micrometer attachment accurate to 0.001". The specimens were weighed on a laboratory balance, accurate to 0.1 grams. The densities were reported in pounds per cubic foot, obtained with appropriate conversion factors.

The specimens were tested for cold crushing strength in a universal testing machine with automatic loading rate. The breaking load was obtained from a gauge, reading to the nearest 25 pound graduation.

TABLE II

Casting Conditions of Fused SiO_2-Opacifier Slips at Time of Foaming (Part I)

	% Solids	pH
ZrO_2	80	3.4
$ZrSiO_4$	79	4.8
Cr_2O_3	77	4.0
TiO_2	80	4.3

The specimens for thermal stability were cut approximately 3" x 2" x 1" and fired for 168 hours in a gas fired laboratory kiln with automatic temperature control to $\pm$ 15°F. The dimensions before and after firing were measured with the caliper-type scale.

PART II.

Based on the results obtained in Part I, Cr_2O_3 and $ZrSiO_4$ were eliminated because of low strength obtained in the cold crushing tests and out-gassing under vacuum at 1800°F. Experience gained in Part I, involving the addition of opacifiers, indicated that 15% opacifier-85% fused SiO_2 was approaching the maximum amount of additive which could be introduced without seriously affecting the standard manufacturing process. Therefore, it was decided to proceed in Part II with TiO_2 and ZrO_2 additives in amounts of 5 and 10% by weight. Weights were based on the dry weight of the fused silica, i.e., 5 and 10% additive to 95 and 90% fused silica respectively.

The established procedures from Part I were followed as closely as possible in Part II; however, some minor adjustments were necessary because of the differing effects of lower concentrations on the pH and viscosity of the fused silica foaming process. As in Part I, these minor changes in standard procedure were determined on a trial and error basis and were based primarily on experience and knowledge of mixes which would make suitable foam.

Specimens of 5% and 10% ZrO_2 and 5% TiO_2 were prepared and shipped to the prime contractor for testing.

Table III indicates the casting conditions used in Part II. Considerable difficulty was experienced in making the 10% TiO_2 specimens. Table IV gives a summary of data on TiO_2 additive batches made in Parts I and II. Note that only the first (15% TiO_2) and the last (10% TiO_2 ball milled) produced suitable specimens in opacifier concentrations higher than 5%. Testing of the 10% TiO_2 ball milled batch at the prime contractor's facility indicated a significant lowering of the K value. It was decided at that time to proceed with an additional batch of 10% TiO_2 ball milled into another lot of fused SiO_2 slip. At the time Glasrock was independently working with fused SiO_2 slips of higher purity than normal, i.e., 99.8% + SiO_2. These slips had produced significantly stronger specimens in both high density and foamed fused silica bodies. Consequently, one of these higher purity slips was chosen for a further attempt at making the 10% TiO_2 in hopes of improving strength as well as conductivity and at the same time gain experience in reliability of ball milling in the opacifiers with respect to property improvement. Sufficient quantities of high purity sand were purchased and fused by Glasrock. Specimens of 10% TiO_2 with this higher purity slip were prepared according to earlier described

TABLE III

Casting Conditions of Fused SiO_2-Opacifier Slips at Time of Foaming (Part II)

	% Solids	pH
5% ZrO_2	82.6	3.3
10% ZrO_2	80.8	3.3
5% TiO_2	83.2	3.1
10% TiO_2	84.9	3.4

TABLE IV

Summary of TiO_2 Mixes

% TiO_2	15	5	10	10	10	15	10	5	10*
Size of Batch (lbs.)	268	232	244	244	246	23	22	21	246
Lot of TiO_2	1	2	2	2	3	3	3	3	3
Lot of Slip	1	1	1	2	2	2	2	2	3
pH	4.28	3.1	3.1	3.3	3.4	3.25	3.15	2.55	3.4
Viscosity**	377	20 sec.	22 sec.	17 sec.	17 sec. 240 cps.	18 sec.	17 sec.	18 sec.	17 sec. 198 cps.
Color	Yellow	Orange	Orange	Orange	Orange	Orange	Orange	Orange	Yellow
Degree of Cracking	0	0	90%	60%	60%	--	--	--	0
Slumping	50%	0	0	0	0	100	100	100	0

* TiO_2 ball milled into slip.

** Cps. viscosities measured with Brookfield Viscometer.
Sec. viscosities measured with # 4 Zahn Cup.

procedures and furnished to the prime contractor for testing.

Authorized Additional Work Under Part II.

At the request of the prime contractor, four regular production 25 pcf fused SiO_2 foam block of 25-30 pcf density were selected by the production personnel at Glasrock's Summerville, South Carolina, foam plant and shipped to the prime contractor for tests to determine the effect of density on thermal conductivity. In addition, since no block less than 25 pcf were found in production inventory, an attempt was made to prepare two 18" x 12" x 3" block of 100% fused silica in two different densities between 20 and 25 pcf. These attempts were made according to standard production procedures for Glasrock Foam #25. However, since 25 pcf is approximately the lowest density which can be reliably produced by standard procedures on 100% SiO_2 foam, only one of the lightweight batches produced a foam block suitable for testing. The density of this block was nominally 18 pcf. Sufficient specimens for thermal conductivity tests were prepared from this block and shipped to the prime contractor. The purpose of these specimens was to determine the effect of density on conductivity in 100% fused SiO_2 foams.

RESULTS

PART I

Properties obtained in Part I are reported in Table V. Of the four opacifiers tested at 15% concentration, $ZrSiO_4$ and Cr_2O_3 seriously reduced the cold crushing strength as compared to standard Glasrock Foam #25. Thermal stabilities of all four additive compositions were at an acceptable level. In no case was cristobalite formation on firing a problem.

Bulk densities were in the expected range as corrected for differences in opacifier specific gravity. Variations in bulk density from the top of the block to the bottom were negligible. Based on the data reported in Table V, ZrO_2 and TiO_2 were chosen for testing in Part II. Opacifier concentrations of 5% and 10% of these two additives were used instead of10% and 20% as called for in the original contract because of difficulties in being able to add more than 15% opacifier to the fused SiO_2 foaming system.

PART II

Properties obtained in Part II are reported in Table VI. Testing of the 10% TiO_2 was not done because of difficulty in obtaining suitable specimens until late in Part II. At that time, it was decided to suspend laboratory work since tests by the prime contractor indicated that opacifier additions were not having

TABLE V

Properties of 85% Fused SiO_2-15% Opacifier Compositions Made Under Part I

Opacifier	ZrO_2	$ZrSiO_4$	Cr_2O_3	TiO_2
Bulk Density (pcf)				
Top	27.8	25.6	24.8	29.1
Bottom	28.1	27.1	25.0	29.6
Linear Shrinkage (%)				
1" dimension	0.244	0.163	0.120	0.000
2" dimension	0.294	0.190	0.090	0.013
3" dimension	0.325	0.017	0.042	0.027
Cold Crushing Strength (psi)	700	200	85	320
% Cristobalite Content	1.1	None	2.0	1.0

TABLE VI

Properties of Fused SiO_2-Opacifier Compositions Made Under Part II

Opacifier	5% ZrO_2	10% ZrO_2	5% TiO_2	10% TiO_2
Bulk Density (pcf)	28.8	30.4	29.2	--
Linear Shrinkage (%)				
1"	.309	.457	.074	--
2"	.136	.499	.242	--
3"	.232	.374	.265	--
Cold Crushing Strength (psi)	736	726	600	--
% Cristobalite	1.7	1.9	3.2	--

significant effects on thermal conductivity. Bulk densities, linear shrinkages, cold crushing strengths, and per cent cristobalite for the specimens other than 10% TiO_2 were within expected ranges.

Difficulties with 10% TiO_2

As indicated in Table IV, the following variables were tested:

1. Size of batch
2. Lot of TiO_2
3. Lot of fused SiO_2
4. pH
5. Viscosity

While no definite conclusions can be drawn from these data, several possibilities exist which could explain the difficulties encountered.

1. Ball milling as a means of dispersing additives is necessary for reliable results.
2. Differences existed in either the TiO_2 or fused SiO_2 slip, or both.
3. Small batches are not reliable.

Another factor which could have influenced the results with 10% TiO_2 is an unknown factor which is occasionally encountered in the production of 100% fused SiO_2 foam and produces similar defects, i.e., severe slumping in the molds or excessive cracking after firing.

CONCLUSIONS

Although suitable specimens were prepared in the laboratory from all the required opacifier additives, their overall effect in reducing thermal conductivity without serious loss of strength was at best marginal. Density had almost as much effect as opacifiers (See appendix II). In addition some difficulty was experienced in reliably introducing these opacifiers into the standard manufacturing procedures for Glasrock Foam 25. Consequently, it was decided that the desired objectives could not be attained within the scope of this contract.

APPENDIX I

Test Procedure for % Cristobalite

The following procedure was used to determine the cristobalite content of the various specimens at the Georgia Tech Engineering Experiment Station. Cristobalite contents were measured in terms of the percentage cristobalite diffraction intensity relative to Georgia Tech Engineering Experiment Station's A-4 "100%" cristobalite standard. To this end, the relation of cristobalite diffraction intensities to the amounts of cristobalite present in cristobalite-fused silica mixtures were studied with the aid of a set of standard samples. The "100%" cristobalite sample, A-4, was prepared by firing a rod of slip-cast fused silica for 60 hours at 2500°F. It was crushed to 325 mesh and mixed with similarly sized fused silica to produce standard samples containing various known percentages of A-4. The actual cristobalite content of A-4 has yet to be accurately determined; hence, all cristobalite measurements were reported in terms of the percentage diffraction intensity relative to A-4 as 100%; therefore, all estimates are conservative.

Test samples for cristobalite content determinations were crushed to 325 mesh so that they would exhibit no preferred orientation due to overly large particles, and all samples were packed onto a frosted glass slide to help maintain random orientation of the powder for a standard "roughness" of the sample surface. Repacking studies

show that when this procedure is used the variations from sample to sample, due to preferred orientation and to surface roughness, are quite small. In addition, no variation in intensity with packing density has been found.

Scans of from 18° to 25° (2θ) using copper radiation are sufficient for measurement of the (101) cristobalite reflection ($2\theta = 21.98^{\circ}$). However, this reflection occurs (in the diffraction traces) atop the broad "hump" characteristic of amorphous silica, and great care must be exercised in eliminating from both the standard and sample diffractometer traces those portions of the spectra which do not constitute the cristobalite (101) reflection intensity.

The integrated intensity was used, as it was, to a first approximation, independent of the crystalline sizes and the residual inhomogeneous strains in the crystals. The integrated intensity was a most convenient index since it was directly proportional to the percentage of A-4 in the standard samples at least over the range 0.5 to 20.0% of A-4. It should also be noted that the problem of the overlapping of $K\alpha_1$ and $K\alpha_2$ lines was avoided when integrated intensities are used.

At the present state of development, the cristobalite content can be reliably determined if the sample contains more than 0.2% cristobalite. It has been standard practice to report the interval expected to contain the cristobalite content of a test material at the 95% confidence level.

APPENDIX II

Rapid Heat Meter Thermal Conductivities
of Standard Glasrock Fused SiO_2
of Varying Densities

$T = 300^{o}F$

Density PCF	Mean Temp. ^{o}F	Thermal Conductivity BTU in./hr ft^2 ^{o}F
18.6	787	0.95
18.6	791	1.04
25.2	783	1.24
25.5	783	1.25
27.3	779	1.32
27.3	782	1.31
28.9	778	1.40
28.4	769	1.35
29.2	783	1.33
30.5	780	1.40